(NASA-CR-165177) HIGH-DENSITY FUEL COMBUSTION AND COOLING INVESTIGATION Final Report, Oct. 1977 - Aug. 1980 (Aerojet Liquid Rocket Co.) 114 p HC A06/MF A01 CSCL 21B G3/25

N81-16177

Unclas 41258

HIGH-DENSITY FUEL COMBUSTION AND COOLING INVESTIGATION

Final Report

By

R. J. LaBotz
D. C. Rousar
H. W. Valler

AEROJET LIQUID ROCKET COMPANY

Prepared For

NATIONAL AERONAUTICS AND SPACE ADMINISTRATION

NASA-Lewis Research Center

Contract NAS 3-21030

NASA CR 165177

FOREWORD

The work described herein was performed at Aerojet Liquid Rocket Company under Contract NAS 3-21030. The NASA Project Manager was Ned Hannum of the NASA-Lewis Research Center. The ALRC Program Manager was Larry Bassham, the Operations Project Manager was Rich LaBotz, and the Project Engineer was Don Rousar and, subsequently, Harry Valler.

The technical period of performance for this program was from October 1977 through August 1980.

The authors wish to acknowledge the contributions of the following ALRC personnel:

Jack Ito - Injector Design Analysis and Test Data Performance Analysis.

Jim Fang - Acoustic Cavity and Stability Test Data Analysis.

Bill Lawver - Igniter Design and Test Data Analysis.

Kin Wong - Mechanical Design of Hardware.

Gene Hron - Hardware Fabrication.

Blake Cathroe - Igniter Testing and Calorimetric Flow Calibration.

Cliff Crossman - Injector and Calorimeter Testing.

Dick Ewen - Thermal Design and Test Data Analysis

TABLE OF CONTENTS

TABLE OF CONTENTS (cont.)

LIST OF TABLES

LIST OF FIGURES

LIST OF FIGURES (CONT.)

I. INTRODUCTION

A. BACKGROUND

Development of an economical space transportation system necessitates that the propulsion system be completely reusable, have long life, be high-performing, and use low-cost propellants. Recent vehicle studies indicate that the most desirable propellants are LOX/hydrogen and LOX/high-density fuel, generally hydrocarbons. Engines for the Single-Stage-To-Orbit (SSTO), Liquid Rocket Booster (LRB), and Orbit Transfer Vehicle (OTV) will have to operate at higher chamber pressures than previous engines to meet the packaging and performance requirements for these vehicles. Although basic combustion and heat transfer data presently exist for LOX/hydrogen over wide ranges of operating conditions, there is very little fundamental combustion and heat transfer data for the LOX/hydrocarbon propellant combinations. The technology base established by previous LOX/ hydrocarbon engines, i.e., H-I, F-I and Titan I, was at performance and pressure levels below those required by the new engines. In addition the combustion stability margin required in the new applications is considerably greater than that of the previous LOX/hydrocarbon engines.

B. PROGRAM SCOPE

The High-Density Fuel Combustion and Cooling Investigation, Contract NAS 3-21030, was initiated in October 1977. The purpose of the program was to provide the analysis, design, fabrication, and testing of several engine configurations in order to investigate the ignition, combustion, stability, and thermal characteristics of LOX/RP-1 propellants. The different engine configurations tested include the following: 1) 8274 and 13790 kPa (1200 and 2000 psia) chamber pressure injectors with like-doublet and pre-atomized triplet elements; 2) cooled and uncooled acoustic resonators; and 3) uncooled graphite chambers and water-cooled chambers ranging in length from 27.9 to 37.5 cm (11 to 15 in.). Two of the four water-cooled chambers had axial coolant slots. The other two water-cooled chambers had circumferential coolant slots and are referred to as calorimeter chambers. A high-pressure LOX/RP-1 igniter was also designed and developed to provide ignition. Combustion and heat transfer data were obtained over a chamber pressure range of 6895 to 13790 kPa (1000 to 2000 psia) and a mixture ratio range of 2:4.

II. SUMMARY

The objective of this contract was to determine the combustion and heat transfer characteristics of LOX/RP-1 propellants in the 1000 and 2000 psia chamber pressure range. This was accomplished through the design, fabrication, and testing of injectors of two different patterns. Testing was conducted with both uncooled chambers and cooled calorimeter chambers over a range of pressures and mixture ratios. The nominal design requirements and test conditions are given in Table I.

A LOX/RP-1 torch spark igniter was designed and demonstrated as part of this program. Prior to its use in the injector testing, the igniter was evaluated for reliability and operating characteristics in igniter-only testing. A total of 69 such tests were conducted, with ignition being achieved in 55 of the tests. The non-ignitions occurred early in the test program and were the result of electrical problems. After these problems were resolved, the igniter test program concluded with 36 consecutive successful ignitions.

The thrust chamber testing was conducted in 2 parts: an injector test series and a calorimeter chamber test series. Four injectors were fabricated for the injector test series. These consisted of two different patterns (a pre-atomized triplet [PAT] and a transverse like-on-like [TLOL] for each of two chamber pressure points (8274 kPa and 13790 kPa; 1200 psia and 2000 psia). The initial test series which addressed hardware checkout, combustion stability, and performance, progressed from short-duration firings with uncooled hardware and adjustable tune acoustic resonators to long-duration firings with the 2 NASA-supplied water-cooled chambers. Test durations up to 30 sec with multiple mixture ratio points were included in this series. Other test variables included chamber pressures ranging from 7170.5 to 13514 kPa (1040 to 1960 psia), fuel temperatures of 283° to 394°K (50° to 250°F), and chamber lengths of 27.9 and 37.5 cm (11 and 15 in.).

The injector performance test series was followed by calorimetric testing. The calorimeter test series consisted of 2 long-duration calorimetric chamber tests at 13790 kPa (2000 psia) with heated fuel and the PAT injector. These tests were multiple operating point tests and provided steady-state data over a mixture ratio range of 1.9 to 2.8. Heat flux data were obtained at 34 axial locations on these tests.

The measured injector performance ranged from 95 to 97.5% ERE (energy release efficiency) depending on the injector pattern and operating conditions. Analysis of the performance data indicated the primary loss mechanism to be low mixing efficiency. The PAT pattern was stable under all operating conditions. However, there were several instances of spontaneous 1-T instability encountered with the TLOL pattern. The overall chamber heat loads produced by the PAT and TLOL patterns were nearly identical and showed a strong linear dependence on mixture ratio. The difference in total heat load between the 27.9 cm (11 in.) and 37.5 cm (15 in.) chamber configurations was

TABLE I. - DESIGN REQUIREMENTS AND TEST CONDITIONS

° Oxidizer:	Liquid Oxygen (MIL-P-25508A)
° Fuel:	RP-1 (MIL-P-25576)
° Vacuum thrust, N (ε = 400:1)	88,964 (20,000 lbs)
° Nozzle throat diameter, cm:	6.25 (2.46 in.) (Uncooled & calorimeter chambers) 6.60 (2.60 in.) (NASA water cooled chambers)
° Thrust chamber diameter, cm:	12.19 (4.80 in.)
° Nozzle area ratio (ε = 400:1, 90% bell truncated to):	8
° Chamber pressure, kPa:	13790 (2000 psia)
° Mixture ratio (O/F):	2.8
° Safety factor:	1.5 times maximum operating pressure
° Overall Energy Release Efficiency:	>98%
° Range of Test Conditions:	
° Chamber pressure:	8274 to 13790 kPa (1200 to 2000 psia)
° Mixture ratio (O/F):	2.2 to 3.2
° Thrust chamber wall temperature °K:	700-811 (800 - 1000°F)
° Fuel Temperature, °K:	283-394 (50-250°F)

II, Summary (cont.)

substantially greater than anticipated. The bare wall calorimeter chamber data showed that local heat fluxes were below those predicted near the injector and 70% greater than those predicted in the throat. Although the calorimeter chamber was blackened by the testing, the heat transfer data, combined with the very light to nonexistent sooting near the injector, gave no indication of the existence of a soot thermal barrier.

III. FINDINGS AND RECOMMENDATIONS

A. FINDINGS

1. Combustion Stability

The 13790 kPa (2000 psia) pre-atomized triplet (PAT-2000) was tested extensively, proving stable under all operating conditions. The 8274 kPa (1200 psia) and 13790 kPa (2000 psia) transverse like-on-like injectors (TLOL-1200 and TLOL-2000) exhibited spontaneous 1-T (first tangential) instabilities. The TLOL-1200 injector was stabilized by retuning the uncooled resonator but was spontaneously unstable in 1-T when tested with a cooled resonator which had a slightly different configuration than the uncooled resonator. The TLOL-2000 injector exhibited consistent spontaneous 1-T instabilities which eventually destroyed the unit. No bomb testing to evaluate stability margin was undertaken during the program. The PAT-1200 injector was not tested.

All injectors tested were stable in the chug mode as had been predicted. The sensitivity of the PAT-2000 injector to 1-L instability which had been forecast during the design phase was not observed in the test data.

2. Performance

A performance goal of 98% energy release efficiency (ERE) was established for this program. The PAT injector achieved approximately 97% ERE and the TLOL injector approximately 97.5% ERE with hot fuel (in excess of 367°K [200°F]) and a chamber length (L') of 37.5 cm (15 in.). With ambient fuel or a short chamber, the performance was reduced by 1 to 2%.

The hot fuel (representative of regenerative operating conditions) improved the vaporization and consequently the combustion efficiency. Further improvements in performance will require improved intra-element mixing.

Other conclusions relative to performance are as follows:

a. The mixing efficiency (E_m) is not significantly improved with either increased chamber length or heated fuel for either injector pattern.

b. The mixing efficiency of the TLOL-1200 is approximately 82% compared with the 73% mixing efficiency of the PAT-2000; the corresponding mixing performance losses are 2% and 3% respectively.

c. The TLOL-1200 and PAT-2000 fuel droplet vaporization rates appeared to be lower than initially predicted at the forward end of the combustor. This resulted in both lower performance and longer sensitive time lags than initially predicted by analytical combustion models.

d. The PAT injector has a more uniform fuel drop size distribution about the mass median than the TLOL. This resulted in both faster PAT vaporization performance gain with added chamber length and reduced high frequency combustion gain than demonstrated by the TLOL.

3. Ignition

Ignition of the main engine propellants by the LOX/RP-1 igniter was 100% reliable. However, operation of the igniter itself was erratic due to problems such as changes in igniter valve sequencing, spark extinguishment by LOX/high pressure, and plugged orifices.

4. Chamber Heat Flux

Hot-fire testing of the water-cooled NASA chambers and the water-cooled calorimetric chamber have shown the following:

a. The heat transfer data obtained on this program exhibit very little scatter, have a high degree of internal consistency, and are repeatable.

b. Chamber heat flux is a strong linear function of mixture ratio, with low mixture ratios giving low fluxes.

c. The difference in total heat load between the 27.9 cm (11 in.) and 37.5 cm (15 in.) L' chambers was significantly greater than had been predicted.

d. The measured heat fluxes in the regenerative combustion chamber were substantially lower than predicted while throat heat fluxes were substantially higher than predicted. Several possible explanations have been identified for the difference between the analytical heat flux predictions and the experimental results.

e. The thermal data gave no evidence of carbon deposition creating a thermal barrier on the chamber wall.

5. Leakage

Early in the test program, leakage was a major problem area. A number of changes were made during the course of the program to resolve this problem area. The two most effective changes involved: (1) replacing the hard, glass-filled Teflon seals with softer virgin Teflon seals and (2) using shims, back-up rings, and reduced bolt torque to minimize flange distortion.

B. RECOMMENDATIONS

1. Combustion Stability

The inherent stability of the PAT-2000 injector was demonstrated on this program. A logical next step would be to assess its dynamic stability with bomb testing. The TLOL pattern was found to be in a marginal condition and was intermittently stable. A more extensive stability assessment of the TLOL pattern with additional changes in cavity tuning would establish whether the pattern could be stabilized. It would also provide data for improving the accuracy of the analytical stability model.

2. Performance

The primary performance loss mechanism for both the PAT and TLOL patterns was found to be poor mixing. The next logical activity in developing a high-pressure LOX/RP-1 technology base would be to establish the design features required in an injector to achieve good mixing under these operating conditions without sacrificing combustion stability or compatibility. Single element cold-flow and single element hot-fire tests would be recommended as the basic experimental tool for this activity. This is an important first step in developing a high mixing efficiency pattern. If the intra-element mixing is optimized, injector mixing performance will be high regardless of inter-element pattern interactions. This experimental work should be run in parallel with an analytical activity directed at the development of a mixing model using the data from this effort and previous experimental programs.

Historically the stoichiometric flame temperature has been used as the driving temperature in droplet vaporization rate analyses. Some of the performance, stability, and injector end heat transfer data from this program are explainable using a reduced driving temperature near the injector. The validity of using a reduced driving temperature should be further assessed both analytically and experimentally.

Specific recommendations are as follows:

a. Test the PAT-1200 injector to determine whether significant performance differences occur over the range of 8274 - 13790 kPa (1200 - 2000 psia). This will help establish whether the measured performance differences between the TLOL-1200 and PAT-2000 injectors reported herein are due to pattern differences or to differences in Pc level. The combustion instabilities encountered with the TLOL-2000 injector eliminate the TLOL patterns from a chamber pressure effect study.

b. In order to achieve high injector performance efficiency, optimize the cold-flow intra-element mixing efficiency (E_m) of the PAT injection element.

c. To further maximize injector performance, optimize the spray overlap to enhance the inter-element mixing efficiency of the PAT injector pattern element interaction.

d. Conduct additional uni-element PAT hot-fire tests in the photographic chamber with the above hydraulically optimized element to calibrate the extent to which combustion effects degrade the mixing efficiency achieved in cold flow.

e. Via uni-element cold flow, develop injection elements which produce the most uniform droplet size distributions possible.

f. Develop a tractable mixing model using data from the literature as well as data being generated in the above activities.

3. Ignition

The primary sources of problems in the LOX/RP-1 spark-activated torch igniter were the power supply and peripheral test stand hardware. Some problems were also encountered with leaks past the spark plug and broken ceramic. Even though the spark plugs employed on this program had not been designed for high-pressure service, they were used because the very long delivery times for high-pressure plugs are inconsistent with the program schedule and would have created a time delay problem. An integral high-pressure spark plug and exciter with closely coupled reproducible response valves would likely yield the desired igniter reliability.

4. Chamber Heat Flux

Data obtained on this program have uncovered several areas in which additional heat transfer work is recommended. Both the higher than anticipated throat heat fluxes and lack of significant sooting accentuate a difficult cooling problem and must be better understood. The goals of the recommended work would be, 1) to determine whether the current results are valid only for the hardware designs employed on this program or are more generally applicable and, 2) to establish the design and operating factors which influence the heat flux and sooting. With these broad goals the following specific recommendations are made.

a. Repeat the calorimeter chamber tests with different injector patterns to establish the dependence of sooting, axial heat flux

profiles, and throat heat flux on injector pattern. At least one of the patterns tested should be designed to avoid any possibility of unburned propellants impinging on the converging wall, burning, and giving rise to high throat heat fluxes.

b. The heat flux data obtained on this program imply substantial heat flux reductions are achievable with film cooling. A new injector with a separately controlled fuel film cooling ring should be tested with the calorimeter chamber and data obtained with various amounts of film cooling. This experimental work should be coupled with a parallel analytic effort which correlates the data with existing film cooling models. The effects of wall zone chemistry on soot deposition could also be assessed as part of this effort.

c. A new calorimeter chamber with a much steeper converging angle should be fabricated and tested to establish whether the throat heat flux can be reduced by stabilizing the boundary layer with higher acceleration.

d. A systematic study should be undertaken of the factors influencing soot deposition. Data should be obtained under controlled conditions of wall mixture ratio, mass flux, wall material, and wall temperature. An analytical model of the soot deposition process should be hypothesized and developed in conjunction with the experimental program.

5. Leakage

High-pressure assemblies require interface flanges with adequate stiffness to minimize unloading of the seals when the assembly is pressurized. Sealing is also improved by the use of large cross-section seals which tolerate greater flange distortion than smaller cross-section seals. Sealing surfaces should be recessed or protected with a lip to minimize damage during handling.

IV. TECHNICAL DISCUSSION

This section of the report is organized into three major subsections: (1) Hardware Design and Fabrication; (2) Hot-Fire Testing; and (3) Test Results and Supporting Analysis.

A. HARDWARE DESIGN AND FABRICATION

The hardware fabricated by ALRC for this program was designed to meet the requirements of Table I. A brief discussion of each of the major components follows.

1. Injector

The basic design and fabrication of the four injectors fabricated on this program differed only in the injector pattern itself. The injector assemblies consisted of three major components: injector body, injector face, and resonator. The particular design used for these injectors is of the same basic type as that used successfully by Aerojet on a number of previous programs. The design employs a machined concentric ring manifold, a face made of photoetched platelets, and a separate detachable acoustic resonator. This configuration was selected because 1) it is versatile in terms of accepting different patterns and pattern replacement, 2) the manifold hydraulics have been well characterized, and 3) it allows use of both cooled and uncooled resonators. Use of a common design also had obvious cost benefits in both design and fabrication. Descriptions of the individual subcomponents follow.

a. Injector Body

The injector body, shown in Figures 1 and 2, contains the propellant manifold passages, a central igniter port, the acoustic cavity interface, the thrust takeout interface, and provisions for instrumentation. It is fabricated from five separately machined parts: the central core, the oxidizer distribution ring, the outer flange, the igniter sleeve, the fuel distribution plate, and the fuel cover-plate. All parts are made from 304L stainless steel and are joined by welding.

b. Injector Face

As noted previously, two types of injector elements were used on this program: the pre-atomized triplet (PAT) and transverse like-on-like (TLOL). With these elements, four different injector face patterns were designed and fabricated: the PAT-1200, the PAT-2000, the TLOL-1200, and the TLOL-2000. The 8274 kPa (1200 psia) and 13790 kPa (2000 psia) patterns of each type were identical except for the differences in element size which were necessary to accommodate the differences in flowrate and pressure drop. The individual injector faces were made from a stack of nickel platelets which had

Figure 1. LOX/RP-1 Injector Body, Backside

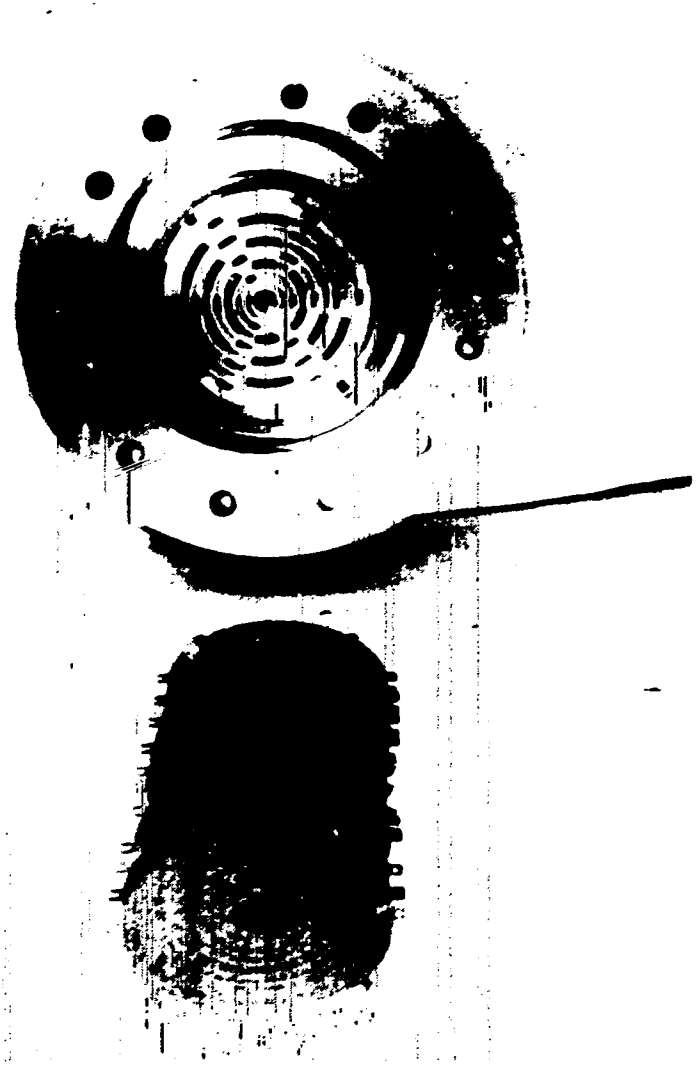

Figure 2. LOX/RP-1 Injector Body, Face Side

the pattern photoetched into them. A typical platelet stack is shown in Figure 3. Following photoetching, the individual platelets were diffusion-bonded to form a monolithic faceplate. At this point, the bonded platelet stacks were flow-checked to ascertain that they had the desired hydraulic characteristics. After the flow checks, the platelet stacks were joined to the manifolds by diffusion-bonding, followed by a redundant E-B weld. None of the injectors had any provision for film cooling or contained a special low mixture ratio row of elements around its outer periphery.

(1) Transverse Like-On-Like Pattern (TLOL)

Previous experience with LOX/RP-1 propellants and recent analyses indicated that a TLOL element (like impinging doublets) is the best choice in terms of combustion stability and is acceptable from the standpoint of performance. The pattern layout is shown on Figure 4, and the element cross section is shown on Figure 5. The name "Transverse" has been applied to this like- on-like element because the flow passages which supply the injection orifices are parallel to the injector face, i.e., transverse to the chamber flow direction. Both fuel and oxidizer fans are oriented radially. Pairs of unlike fans are oriented edge-on (planar). The TLOL pattern consists of 132 elements arranged on a 7-ring manifold. The space at the center portion of the injector is for the igniter.

(2) Pre-Atomized Triplet Pattern (PAT)

The design philosophy adopted for the second injector pattern was that it should have a higher performance potential than the TLOL pattern even though this might result in a higher risk from the standpoint of combustion stability.

Past experience had indicated that higher performance could be anticipated with unlike impinging elements because of their high mixing efficiencies. Three specific types of unlike impinging elements were considered for the second pattern: conventional F-O-F triplets, splash plate unlike doublets, and a pre-atomized triplet (PAT) which incorporates two fuel splash plate elements and one oxidizer X-doublet element. Of these three, the PAT element was selected because it was considered to have the highest probability of achieving the high performance level of EDM-drilled triplets while circumventing some of the stability disadvantages. The PAT consists of two fuel splash plate orifices which impinge on one centrally located oxidizer X-doublet orifice. The splash plate and X-doublet orifices as well as typical element cross sections are shown in Figure 6. The PAT pattern layout is shown on Figure 7. The splash plate elements form fans of fuel droplets at acute angles to the injector axis (30-45°). The X-doublet elements form axially directed fans of oxidizer droplets. The PAT pattern contained 120 elements.

Figure 3. LOX/RP-1 Injector Platelets

P_c = 13790 kPa (2000 psia)

O/F = 2.80

$\dot{W}_{ox}$ = 17.64 kg/sec (38.9 lb/sec)

$\dot{W}_f$ = 6.30 kg/sec (13.9 lb/sec)

ΔP_{ox} = 2427 kPa (352 psia)

ΔP_f = 2248 kPa (326 psia)

D_{ox} = 0.145 cm (0.057 in.)

D_f = 0.094 cm (0.037 in.)

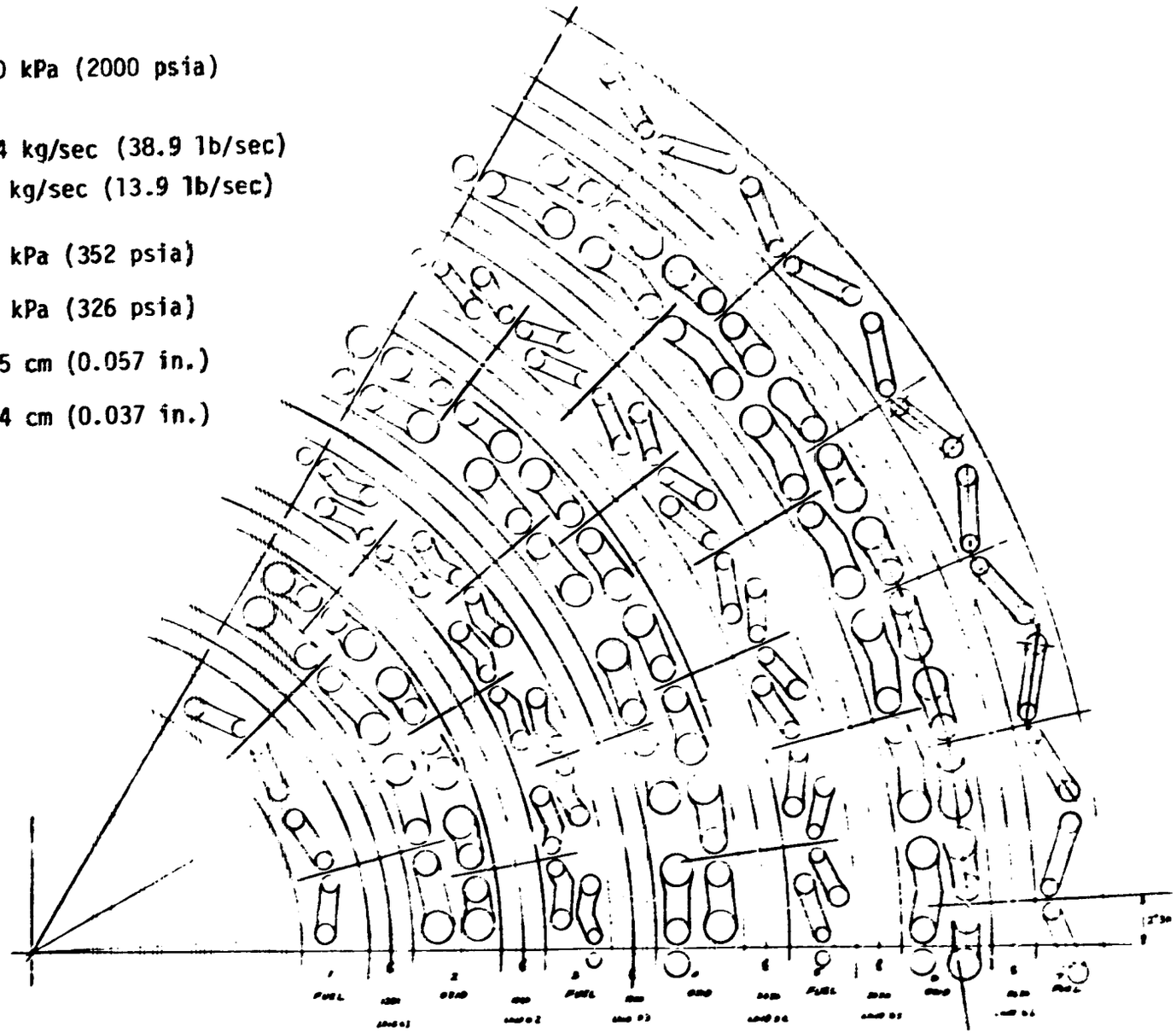

Figure 4. Transverse Like-on-Like Injector Pattern Layout

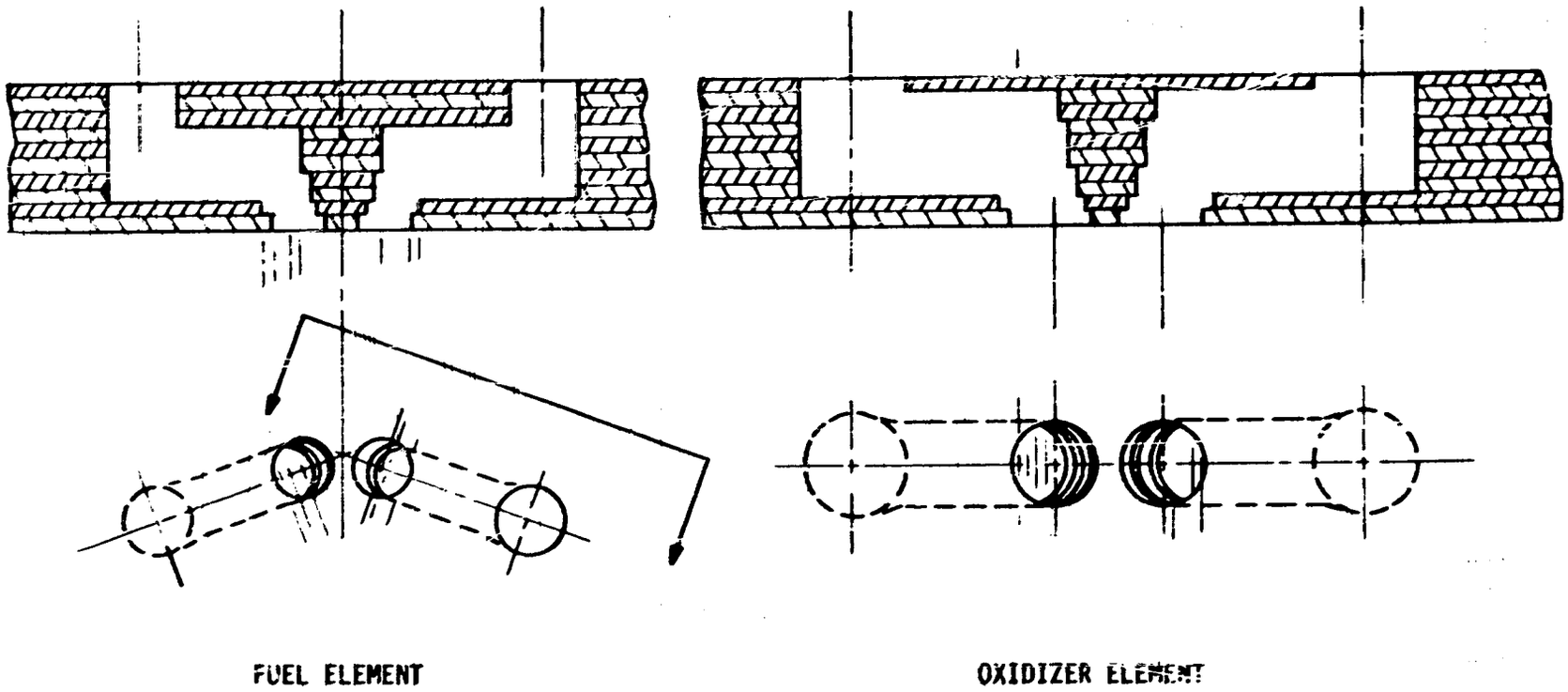

Figure 5. Schematic of Transverse Like-on-Like Injector Element (TLOL)

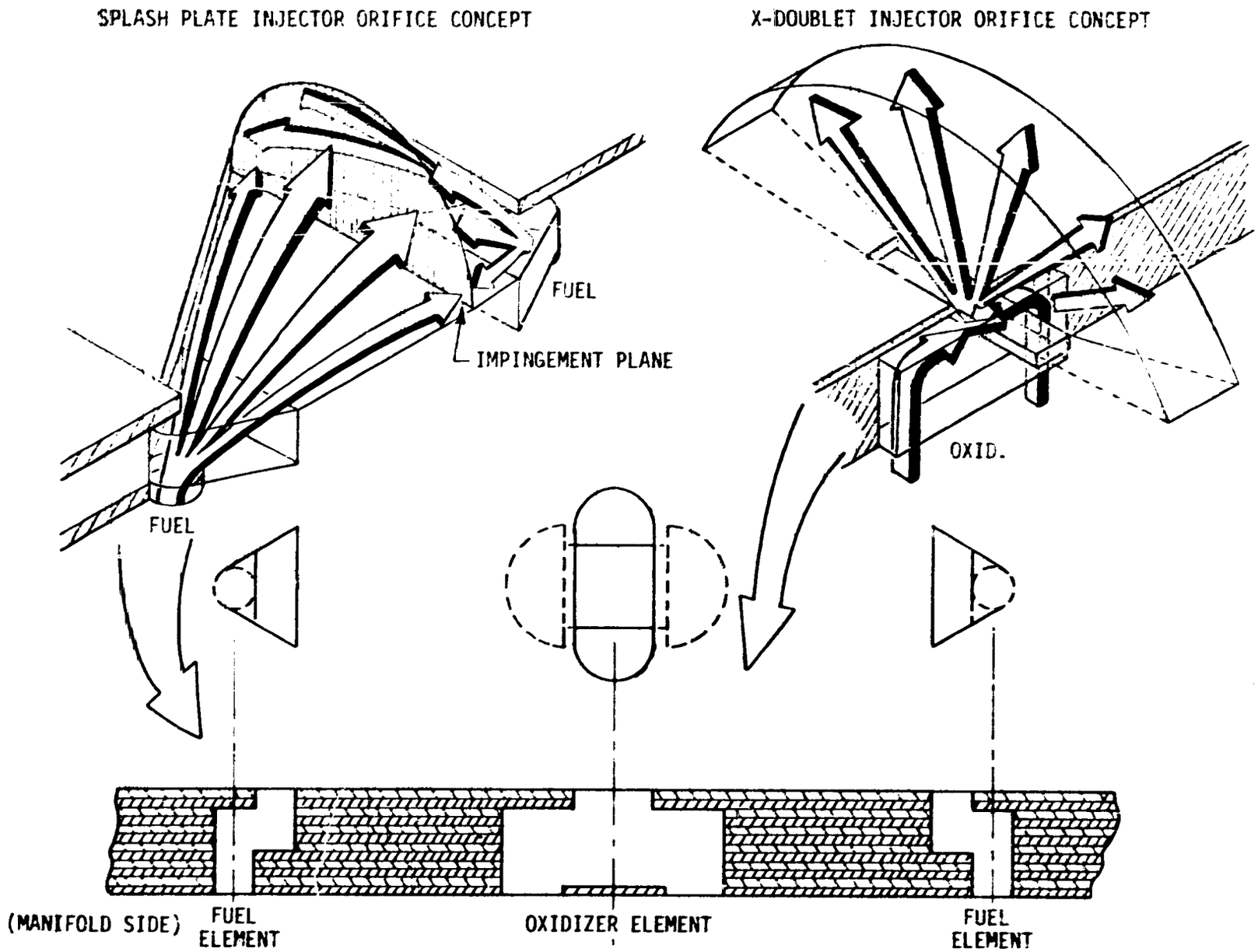

Figure 6. Schematic of Pre-Atomized Triplet Injector Element (PAT)

P_c = 13790 kPa (2000 psia)

O/F = 2.80

$\dot{W}_{ox}$ = 17.64 kg/sec (38.9 lb/sec)

$\dot{W}_f$ = 6.30 kg/sec (13.9 lb/sec)

ΔP_{ox} = 2413 kPa (350 psi)

ΔP_f = 2413 kPa (350 psi)

D_{ox} = 0.180 cm (0.071 in.)

D_f = 0.094 cm (0.037 in.)

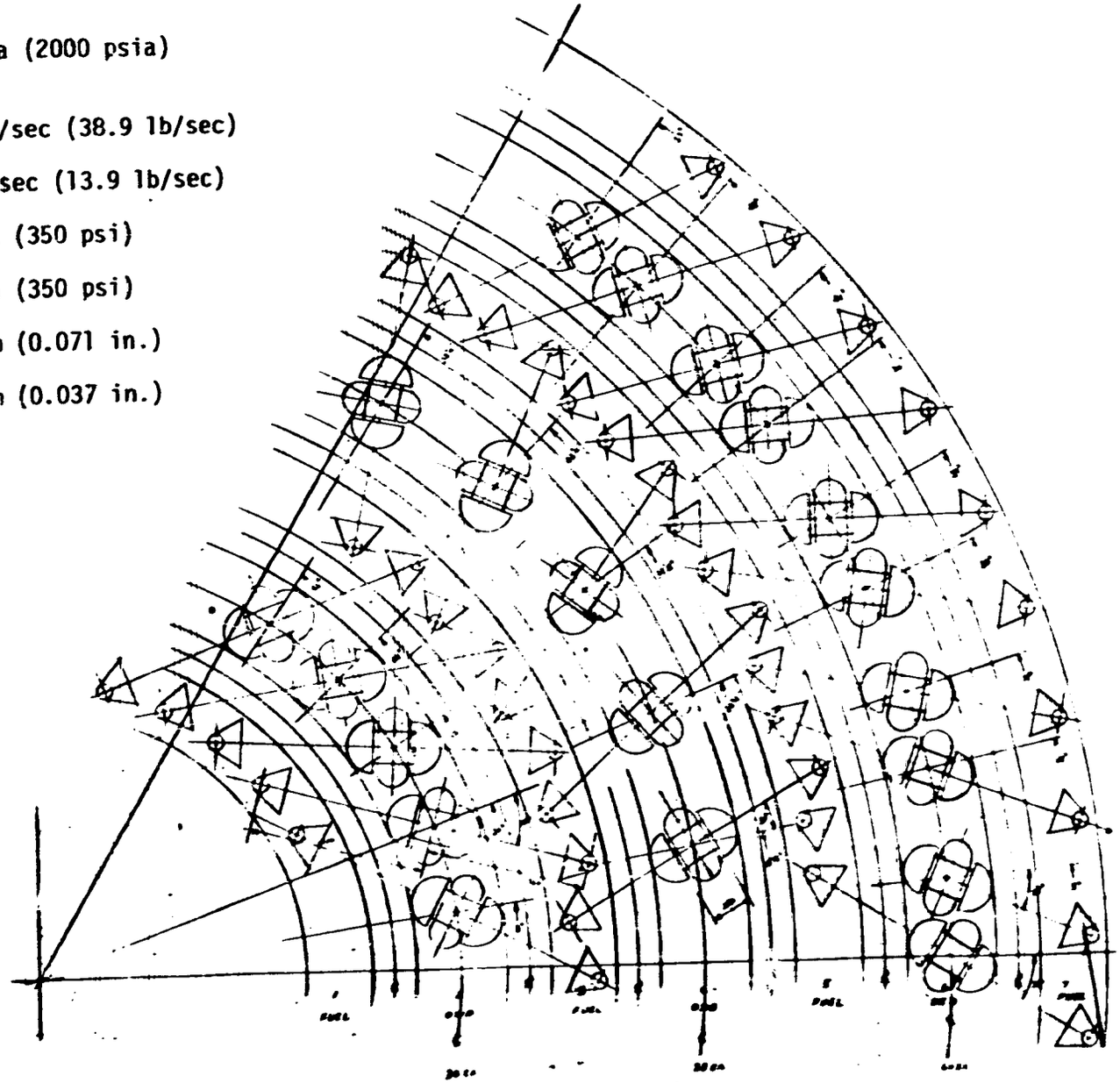

Figure 7. Pre-Atomized Triplet Injector Pattern Layout

c. Resonator

The resonator surrounds the forward portion of the injector body and forms the acoustic cavities. Two resonator designs were prepared: an uncooled copper heat sink and a water-cooled design. Details of the resonator are shown in Figure 8, while the calorimetric thrust chamber assembly which illustrates the installation of the resonator is given in Figure 9.

The uncooled unit was used for injector checkout testing and contained 12 acoustic cavities with the following dimensional characteristics:

Width - 1.016 cm (0.4 in.)

Depth - 2.54 cm (1.0 in.)

Partition Thickness - C.318 cm (0.125 in.)

For "tuning" purposes, the depths of these cavities were varied by using block inserts. Shallow cavities (0 to 0.51 cm [0 to 0.2 in.]) were used to provide 2-T stability, and deep cavities (1.78 to 2.03 cm [.7 in. to .8 in.]) were used to provide 1-T stability.

The uncooled resonator was instrumented with four high-frequency transducers, four chamber gas-side thermocouples, four resonator gas-side thermocouples, and two resonator gas temperature probes.

2. Igniter Design

The LOX/RP-1 igniter is shown in Figure 10. The igniter consists of an oxygen-cooled spark electrode, an injector for atomizing and vaporizing the LOX and RP-1, and an RP-1-cooled combustion chamber. During testing, the igniter was provided with separate propellant valves to permit its being operated independently of the main propellant valves.

Ignition takes place through the following sequence: (1) a flame kernel is produced within the spark gap by the spark discharge; (2) the flame kernel spreads and ignites the oxidizer-rich core flow within the igniter chamber; (3) the igniter core flow mixes and reacts with the RP-1 coolant flow to produce a fuel-rich torch exhaust; and (4) the fuel-rich torch flow reacts with the main injector oxidizer lead flow to ignite the engine.

The igniter operates with a high mixture ratio core (O/F = 10) injected about the central spark plug. The fuel-cooled chamber provides the necessary combustion length such that complete combustion can be obtained.

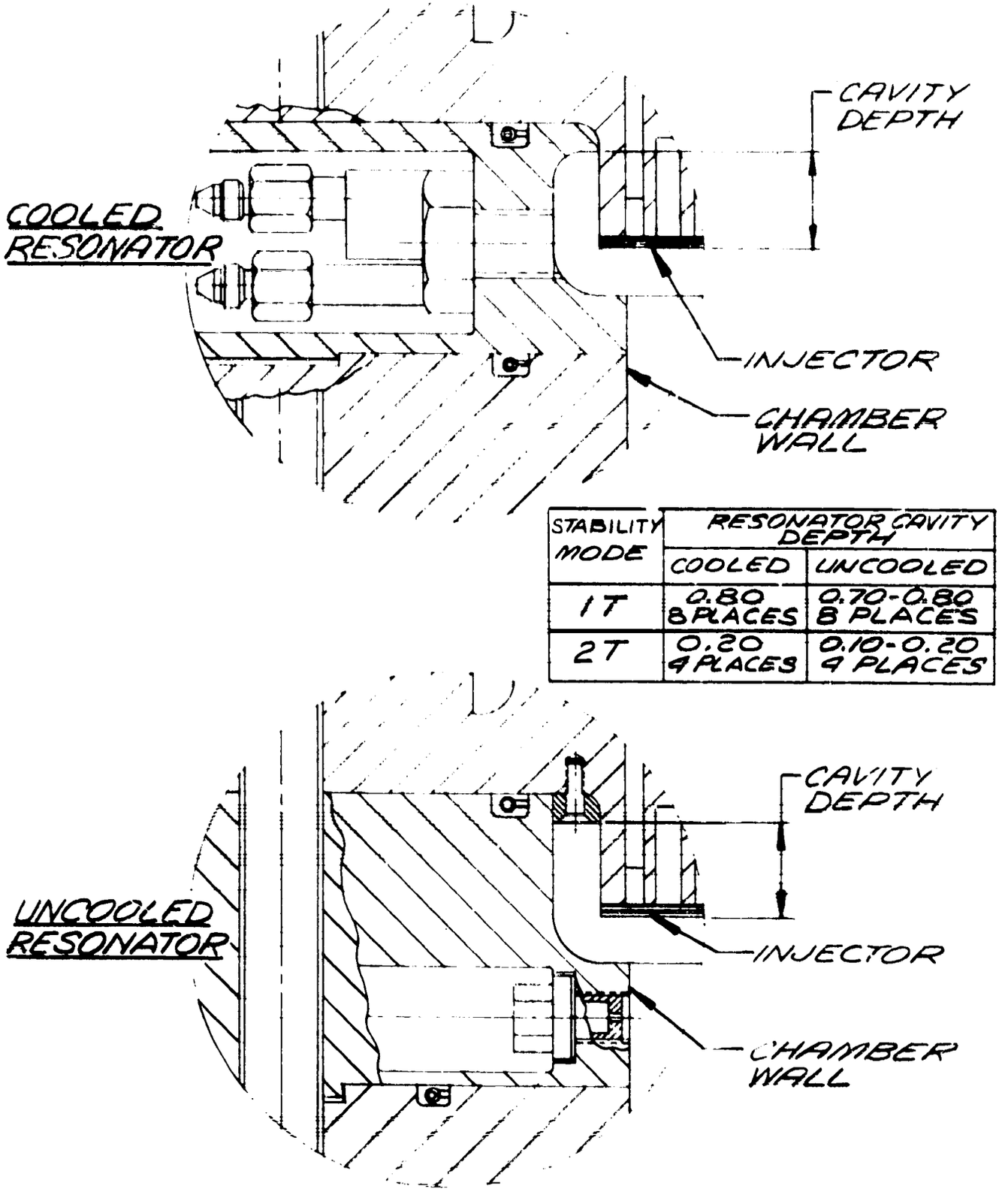

STABILITY MODE	RESONATOR CAVITY DEPTH	
	COOLED	UNCOOLED
1T	0.80 8 PLACES	0.70-0.80 8 PLACES
2T	0.20 4 PLACES	0.10-0.20 4 PLACES

Figure 8. Resonator Configuration

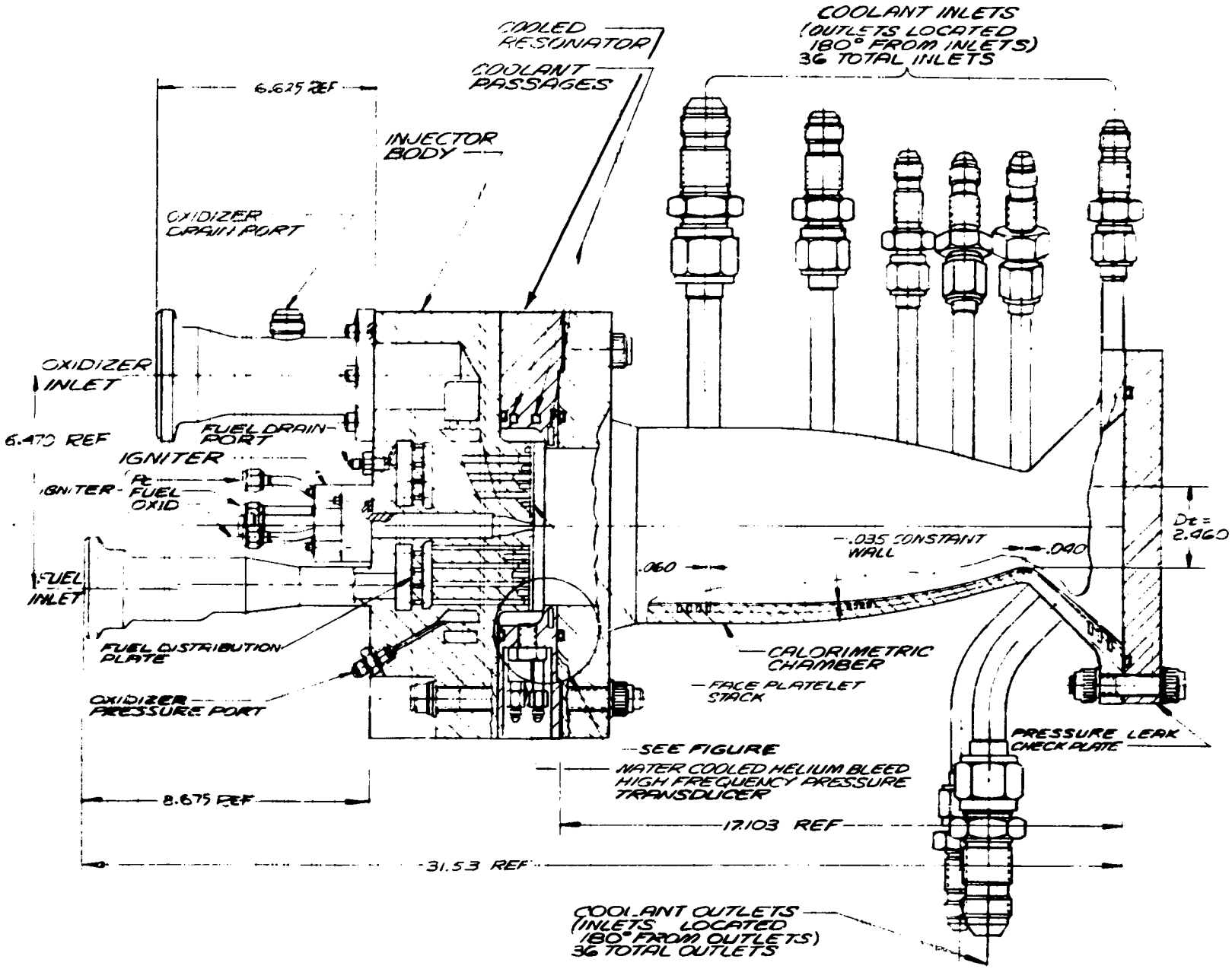

Figure 9. Calorimetric Thrust Chamber Assembly

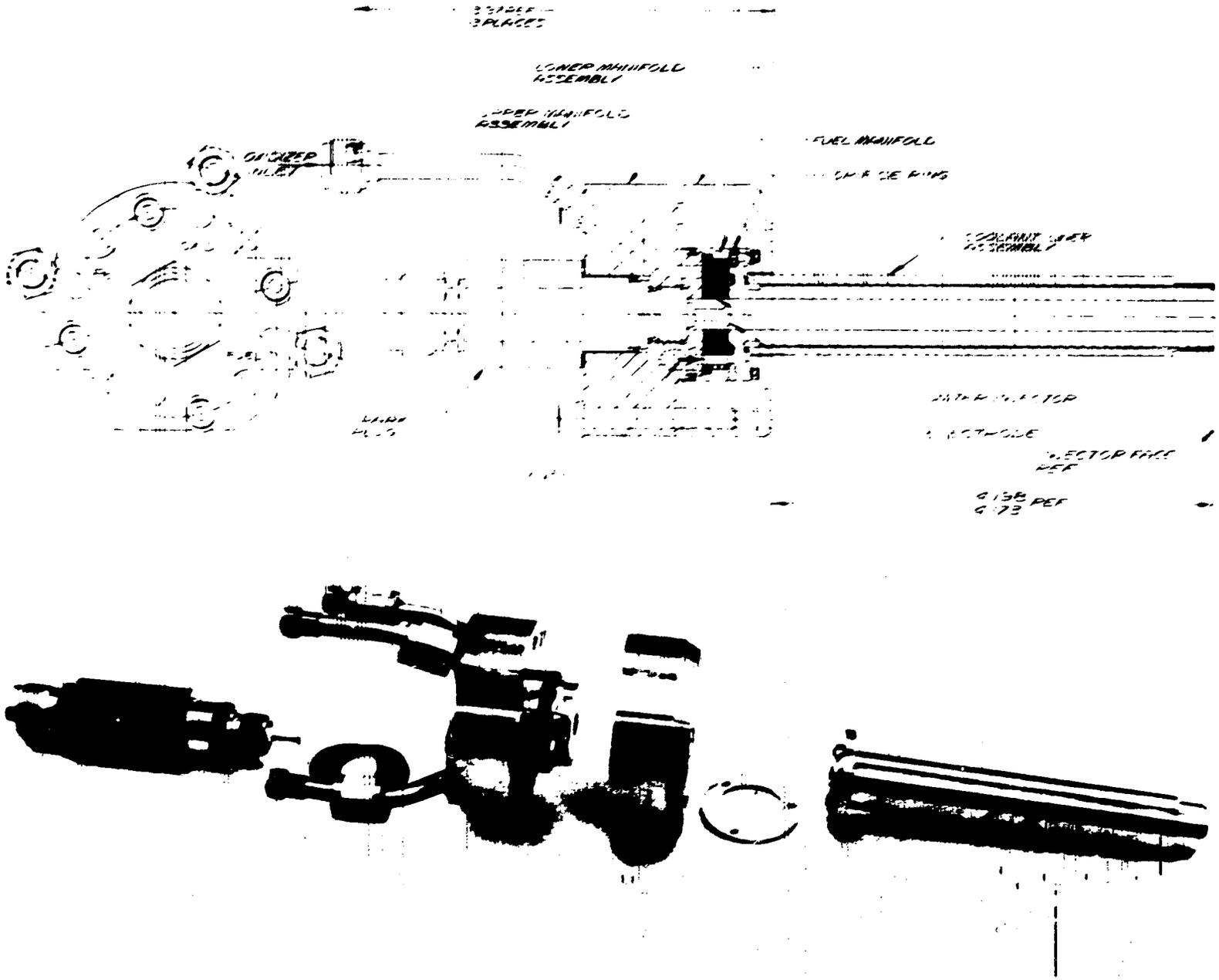

Figure 10. LOX-RP-1 Igniter, Exploded View

Upstream of the igniter throat, the fuel used to cool the chamber is injected into the high mixture ratio core, thereby film-cooling the throat and reacting with the core flow to provide a torch mixture ratio of 2.65 at the center of the injector face. Provisions were made in the design to vary the injector core mixture ratios by using a fuel orifice ring to split the fuel between the injector and chamber. Four igniters were fabricated.

3. Thrust Chamber Design

Three different chamber types were used in this program. An uncooled chamber with a graphite throat was employed for injector checkout and initial stability testing. The performance tests were conducted by using NASA-supplied water-cooled chambers, while the heat transfer tests were run with the water-cooled calorimeter chambers built under this contract. The calorimeter chambers were not used for the performance testing as the high divergence angle on the nozzle exit made data interpretation difficult.

a. Uncooled Workhorse Chamber

The uncooled chamber was used to perform the initial checkout testing on each injector. The chamber, consisting of a steel cylindrical section with a graphite liner, was designed to withstand firing durations of less than 2 seconds.

The chamber was fabricated in two sections to permit variations in chamber length. This hardware is shown in Figure 11.

b. NASA Water-Cooled Chamber

Existing NASA water-cooled chambers were utilized for performance testing of the injectors. These axially slotted chambers consisted of a copper liner with an EFNi jacket and were available in 2 lengths: 27.9 cm (11 in.) and 37.5 cm (15 in.), respectively. Each chamber contained 100 cooling slots which were 0.152 cm (.060 in.) wide at the injector and 0.102 cm (.040 in.) wide at the throat. The channel wall thickness was constant at 0.889 cm (.035 in.). The throat diameter was 9.60 cm (3.60 in.). The chambers, shown in Figure 12, were originally designed for LOX cooling; however, it was determined that the chambers could be water-cooled for this program.

c. Calorimetric Thrust Chamber

The design and fabrication of the calorimetric chambers was a major effort during the contract. Each of the two chambers consisted of an OFHC copper liner with machined circumferential channels (see Figure 13). Seventy channels were externally fitted with 34 inlets and outlets to measure

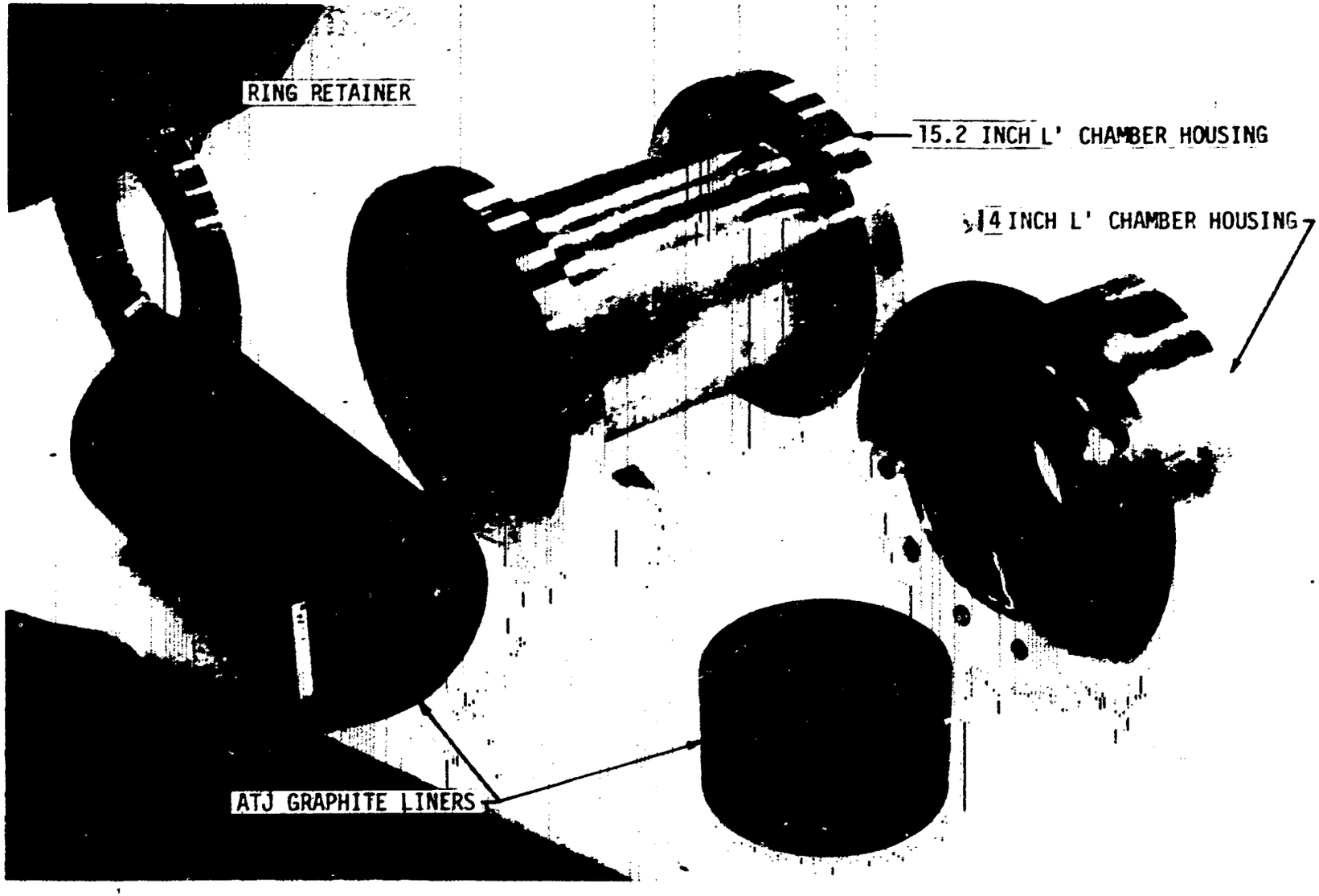

Figure 11. Workhorse Chambers, Graphite-Lined

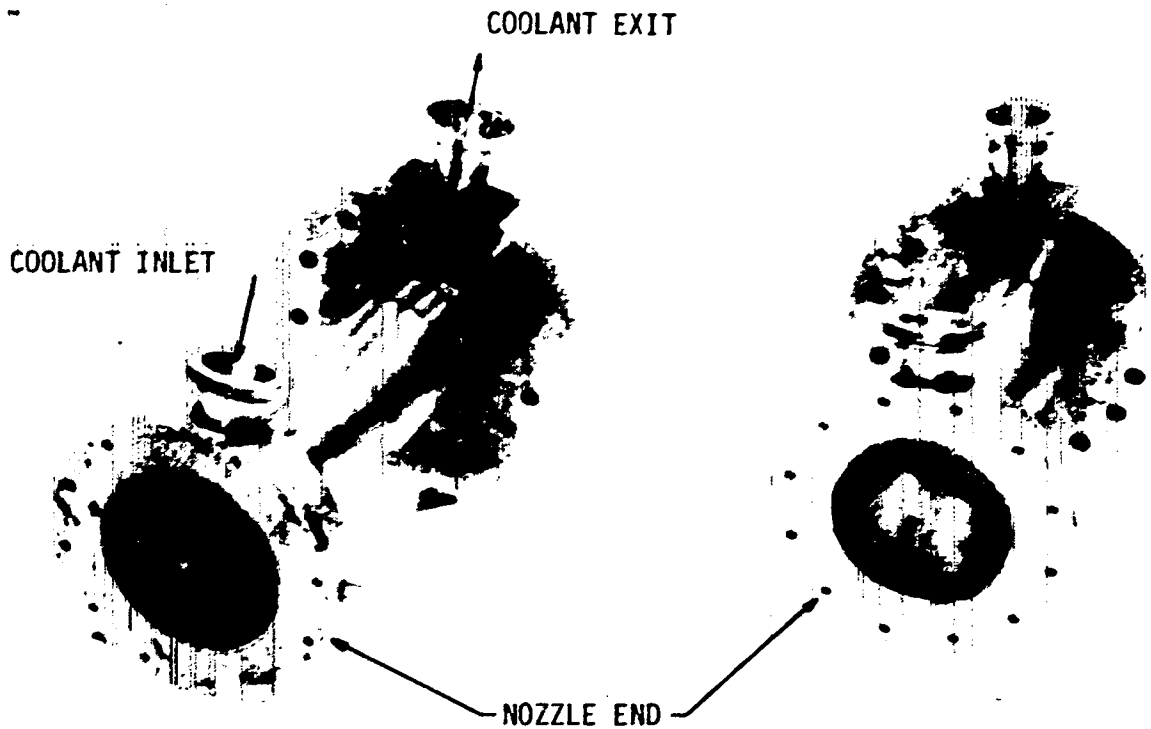

Figure 12. Water-Cooled Chambers, NASA-Supplied

Figure 13. Calorimetric Chamber Liner

the axial heat flux profile over the entire chamber length. The chambers were fabricated in two lengths of L' = 27.9 and 34.0 cm (11 and 13.4 in.) (injector face to throat), respectively. The latter chamber length was selected on the basis of performance and stability analyses which had indicated that both injectors might be sensitive to longitudinal instabilities at chamber lengths greater than 34.0 cm (13.4 in.). The throat diameter was 6.25 cm (2.46 in.). Closeout of the individual water channels was achieved by using electroformed nickel deposited on the outer surface of the copper liner. Pairs of channels were manifolded with inlet and outlet tubes. Each tube had provisions for installing a metering orifice, pressure transducer, and a thermocouple. This arrangement provided individual circuit flow control and a precise measure of individual circuit heat flux (via mass flowrate and temperature rise). The nozzle contour was selected to be representative of a truncated flight configuration engine. As a result, the heat flux measurements downstream of the throat were typical of a flight engine, although the high divergence angle (40° half angle) made accurate performance data more difficult. A photograph of the completed assembly is shown in Figure 14.

B. TEST FACILITY

A special test facility was constructed to run the tests for this program. This facility, shown in Figure 15, was equipped with dual-piston pressure intensifiers capable of delivering 41,369 kPa (6000 psia) propellants to the test stand. The fuel circuit intensifier had deliverable capacity of 0.303 m^3 (80 gallons) or 242 kg (534 lbs) of RP-1, while the oxidizer circuit had a 0.568 m^3 (150 gallon) or 653 kg (1440 lbs) of LOX capacity. The oxidizer intensifier and lines were LN_2-jacketed while the fuel intensifier and lines were equipped with Calrod heaters. The heaters made it possible to condition the fuel to temperatures between ambient (near 283°K [50°F] and 394°K [250°F]). Figure 16 is a closeup photograph of the NASA water-cooled chamber installed on the test stand with the aft leak check plate attached.

A key feature of this test stand was the propellant flow control system. A pair of rapid-response flow control valves (30 ms from fully closed to fully open) were used as thrust chamber valves. These valves were controlled by a HP 2100 MX computer which monitored test parameters, terminating the test if parameters were out of limits. The computer could be programmed to provide a ramped start as well as operation at a number of predetermined mixture ratios and pressures during the course of a single firing (see Figure 17). This multiple operating point capability was used extensively during the cooled chamber testing and proved to be very valuable.

During a firing, "real-time" processed data were available in the control room through a medium speed printer. As the engine was firing, the

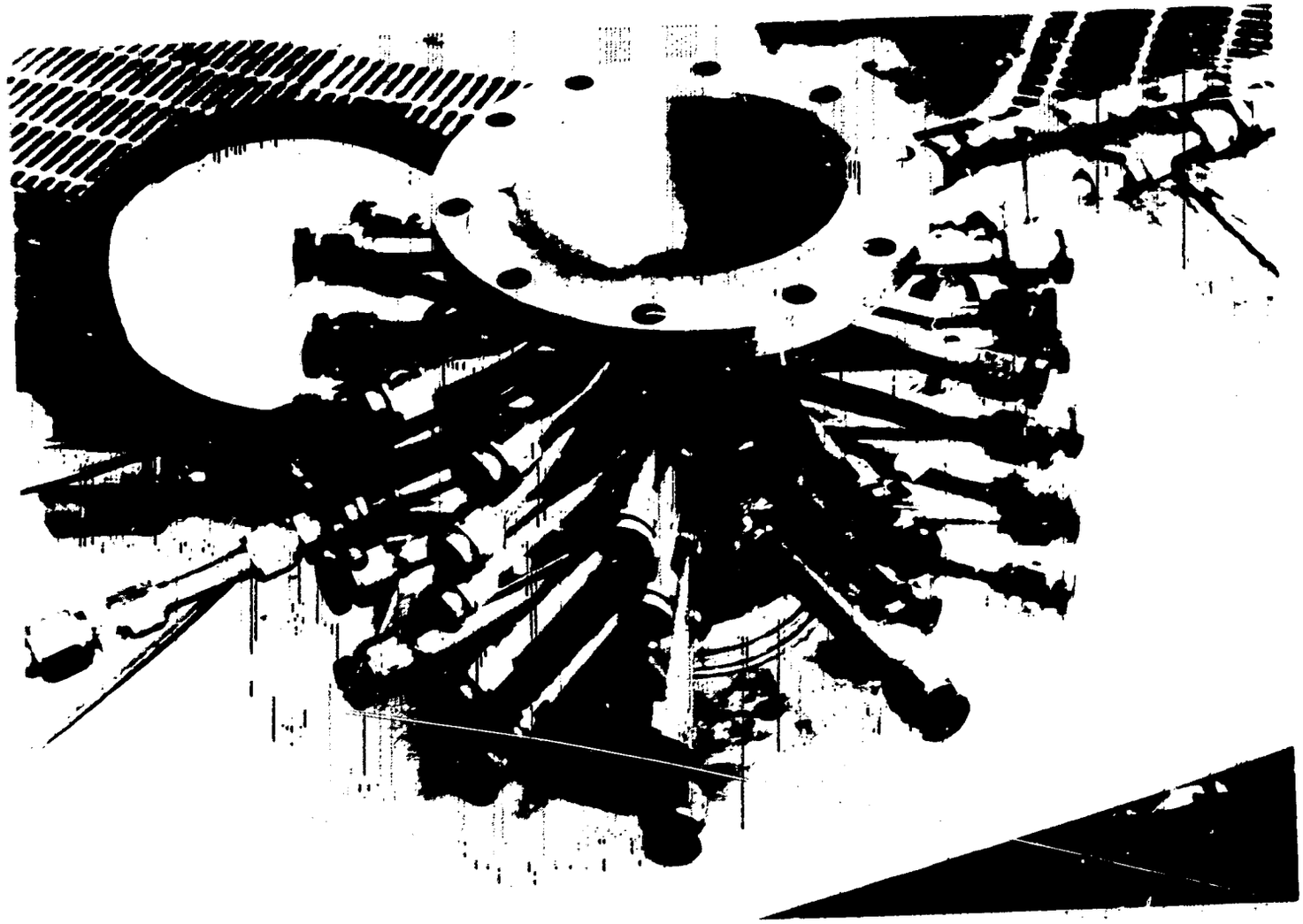

Figure 14. Flow Calibration of Completed Calorimetric Chamber

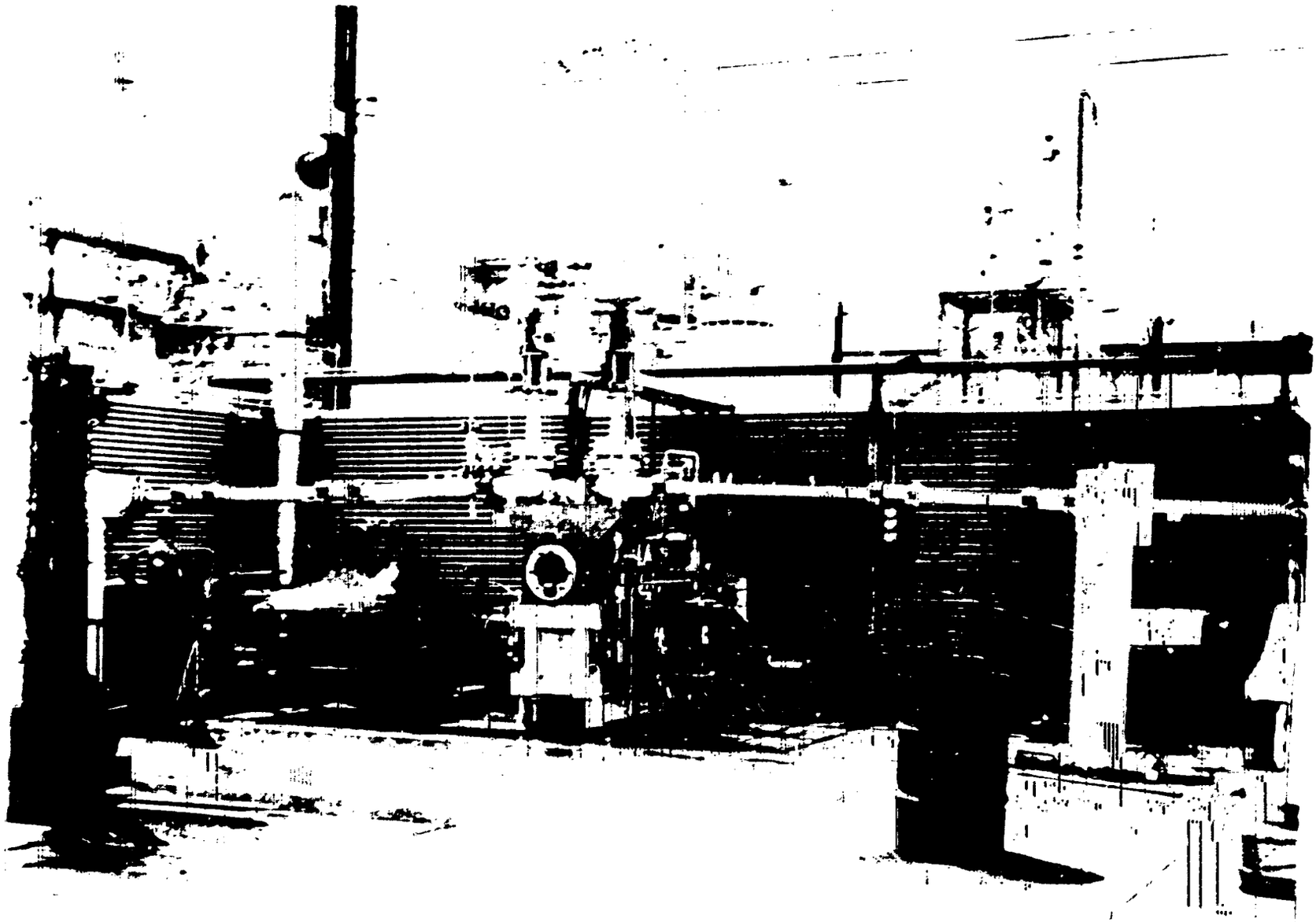

Figure 15. High-Pressure LOX/Hydrocarbon Test Facility

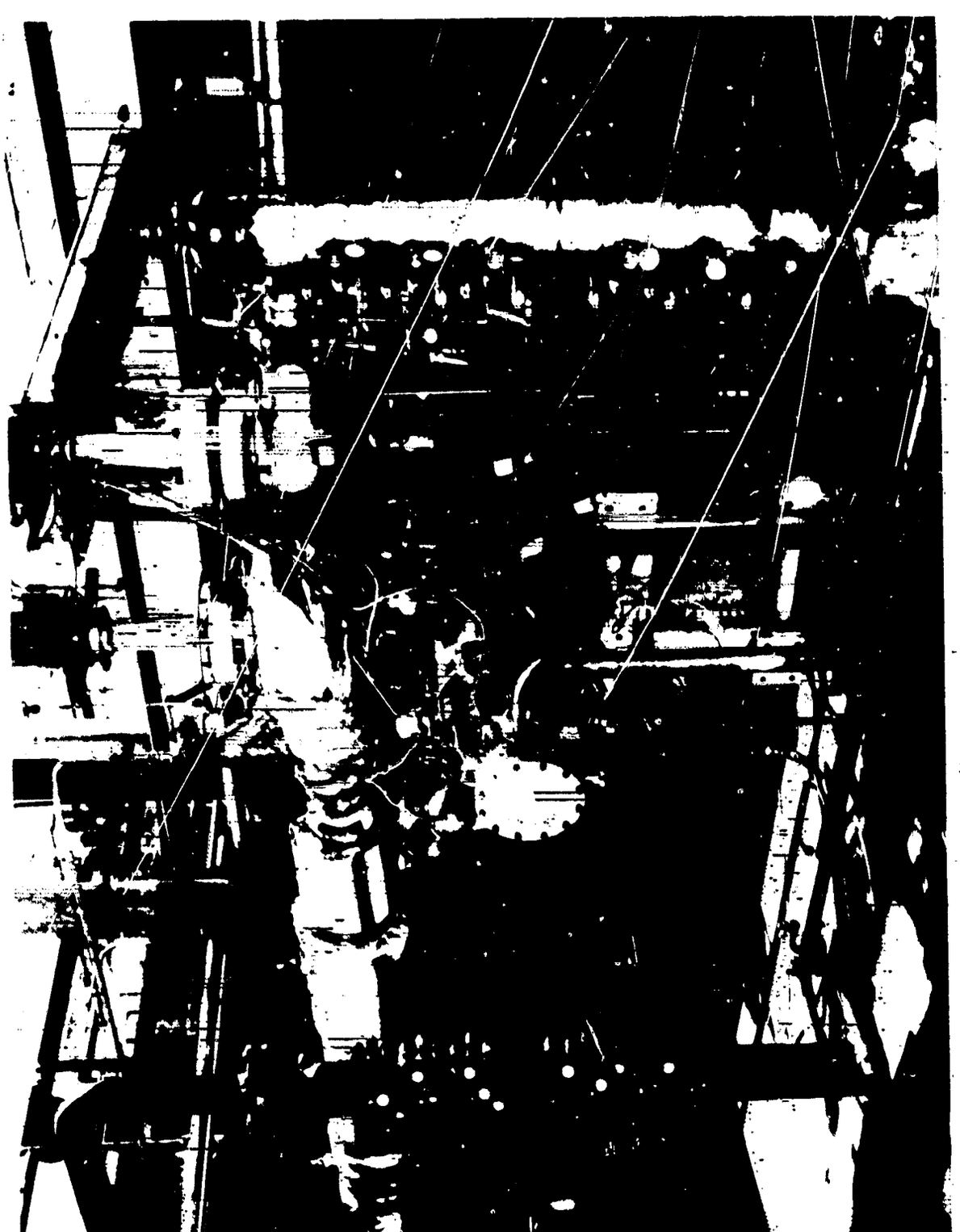

Figure 16. High-Density Fuel Test Installation, Test Stand J-1A

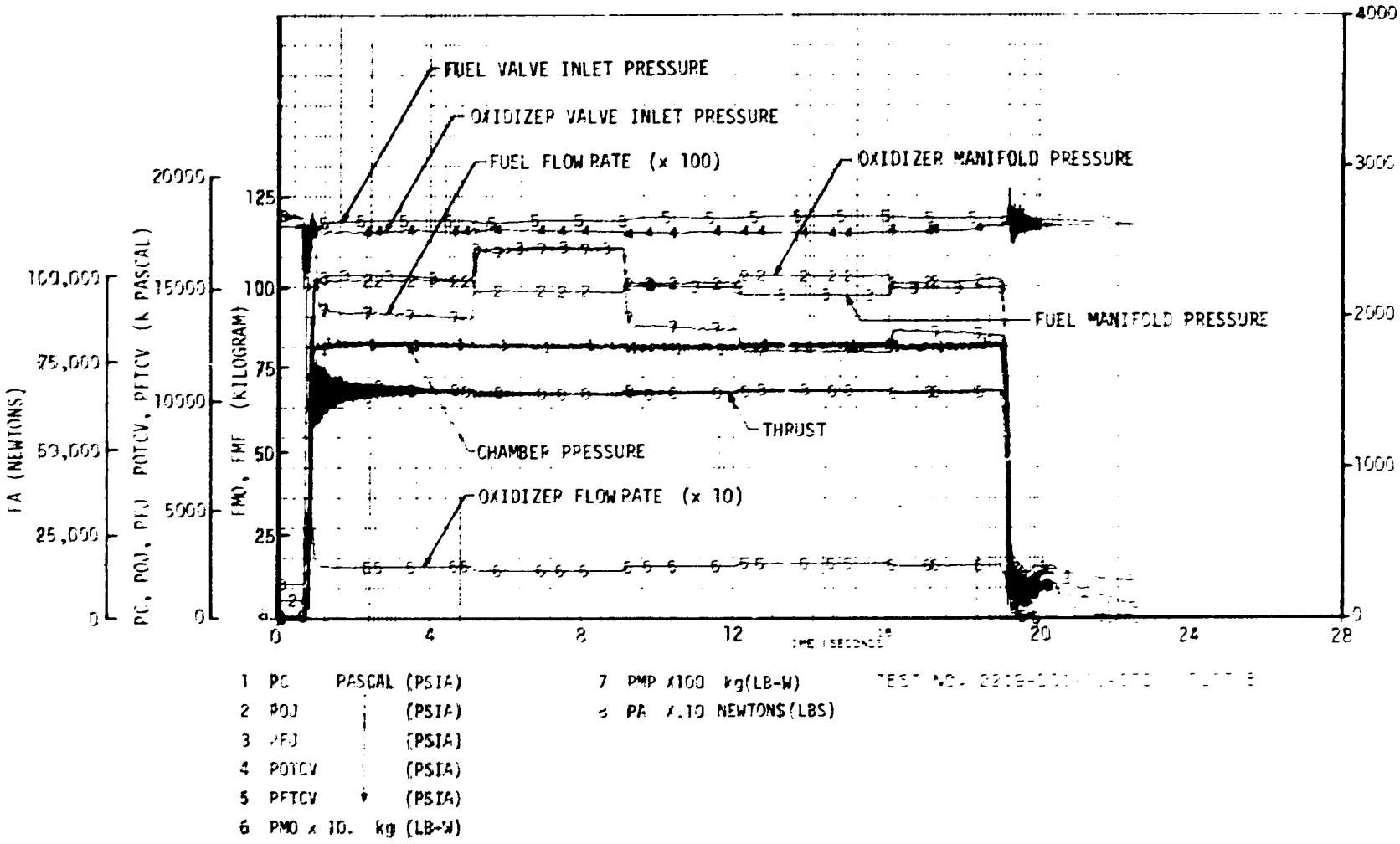

Figure 17. Typical Multi-Data-Point Test Record (Test 072)

test data were input to an analog-to-digital converter which, in turn, supplied data to the remote digital computer at a rate of 10,000 samples per second. The data were processed immediately and fed back to the control room printer where they were displayed as the test was being conducted.

No significant problems were encountered with the test stand in the course of conducting the test program. The hardware was flushed following each firing to remove residual hydrocarbons. However, no attempt was made to remove soot from the chamber walls; consequently, any soot deposition process was cumulative.

C. HOT-FIRE TESTING

The hot-fire test program was conducted in three phases: (1) igniter-only testing; (2) injector checkout and performance tests; and (3) calorimetric chamber tests.

1. Igniter-Only Testing

In January 1979, a series of igniter-only tests were performed. The objective of the igniter test program was to verify that the spark-activated torch igniter design had the reliability necessary to allow its use in full injector testing. In addition, this test program was to provide the critical operating parameters necessary to achieve satisfactory and reliable ignition. Sixty-nine igniter tests were conducted.

Figure 18 shows the igniter test assembly used to perform the igniter-only testing. A summary of the 69 tests conducted is contained in Table II. As a result of these tests, certain conclusions as to acceptable igniter operating conditions were reached. These conclusions are listed in Table III, along with the technical issues that were addressed by the various tests.

Early in the test program, it was thought that the non-ignitions might have been the result of fuel freezing in the igniter body due to pre-chilling of the igniter by the helium purge in the oxygen circuit. To eliminate this possibility, a heater was added to the helium purge. This not only kept the igniter body warm but also softened the oxygen flow transient by vaporizing the first oxygen through the injector. Later in the program, after the electrical and sequencing problems had been resolved, it was found that fuel freezing was not a problem and that reliable ignition could be achieved without the helium heater. The gaseous oxygen starts which resulted from the use of the heater were found to be smoother (i.e., exhibiting fewer and less severe pressure spikes) than the starts with liquid oxygen. A heater was not used in the engine test program.

Figure 18. LOX/RP-1 Igniter Test Assembly

TABLE II. - IGNITER TEST SUMMARY

	ACCOMPLISHMENTS	PLANNED
Total Number of Tests	69	65
Total Number of Ignitions	54 (36 Consecutive)	--
Duartion (sec)	0.18 → 1.02	0.25 → 1.0
Overall Mixture Ratio (O/F)	1.2 → 5.1	2.0 → 5.0
Core Mixture Ratio (O/F)	5.3 → 23.7	7.5 → 25.0
Spark Rate (Sparks/sec)	150 → 500	TBD → 500
Spark Energy (Inj)	10 → 50	TBD → 50
Sequencing (Ox Lead, msec)	-50 → +90	0 → TBD
No. of Tests W/O Flush*	45	None
No. of Igniters Tested	1	3
LOX Inlet Pressure (kPa)	8136 → 10135 (1180 → 1470 psia)	-
LOX Inlet Temperature (°K)	114 → 159 (205 → 287°R)	-
RP-1 Inlet Pressure (kPa)	3054 → 6329 (443 → 918 psia)	-
RP-1 Inlet Temperature (°K)	276 → 284 (496 → 511°R)	-
Igniter Chamber Pressure (kPa)	2344 → 2827 (340 → 410 psia)	3447 (500 psia)

*When igniter testing began the igniter oxidizer circuit was flushed with Freon 113 prior to each firing to remove any residual hydrocarbons from the preceding test. This procedure was discontinued after Test No. 22 and replaced with a single flush at the beginning of each test day. There was no observed difference between tests with a flush and tests without a flush.

TABLE III. - IGNITER TEST RESULTS

TECHNICAL ISSUE	PERTINENT TESTS	CONCLUSION
Shutdown Sequence	101-103	Post Shutdown Pc spike eliminated with high pressure purges
Erratic Spark	103-146	Cracks in the spark plug ceramic produced short circuits. Problem was alleviated by reducing the spark plug gap.
Torch Temperature	107	Not measured but melted steel in 0.7 sec.
Start Sequence	113-125	Fuel lead worked best. Fuel lead provides a low cold flow pressure which reduces the spark sequence. Fuel lead also gives transient O/F sweep (better ignitability) and less thermal shock of the ceramic.
Igniter cooling	139-145	Barrel - 1.0 sec. demonstrated. Throat - Analysis only
RP-1 Freezing	102-147	No evidence of freezing
LOX Flow Transient	103-154	LN_2 Jacket required on LOX line for fast controlled start, warm injector - OK
Prefire LOX Circuit Flush	101-169	Not required after first firing of day
Igniter O/F	All	Insensitive over 1.2-5.1 range
Spark Energy	161-167	Insensitive over 10-50 MJ range
Spark Rate	161-167	Insensitive over 150-500 MJ range
Ignition Reliability	134-169	Excellent with reliable spark and fuel lead

2. Injector Checkout and Performance Tests

The injector checkout and performance test series was designed to fulfill several objectives. It was to provide test facility flow and sequencing procedures and instrumentation checkout for subsequent testing. The program also was to be used to characterize the operation of the injectors in terms of performance and combustion stability and allow for tuning of the acoustic cavities in the case of a combustion stability problem. The results of this test series were to form the basis for the selection of the injector, resonator, and chamber configuration for use in the calorimeter testing.

The test hardware available for use in this test series consisted of the following:

Injectors	PAT-1200, PAT-2000 TLOL-1200, TLOL-2000
Chambers	36 cm (14 in.) Heat Sink 27.9 cm (11 in.) Water-Cooled 37.5 cm (15 in.) Water-Cooled
Acoustic Cavities	Variable Tune Heat Sink (2) Fixed Tune Water-Cooled (2)

Testing was initially delayed by leaks in the test assembly at the interface between the injector and propellant lines and that between the chamber and acoustic resonator. These leaks were eliminated by replacing glass-filled Teflon seals with more compliant virgin Teflon seals and by modifying the hardware to limit flange distortion. The test program than proceeded with an evaluation of three of the four injectors. (The PAT-1200 was not tested due to funding limitations.) Testing was initiated with brief tests of less than 2 seconds duration with uncooled hardware and ambient temperature fuel and then concluded with multiple data point tests of up to 30 seconds duration with cooled hardware and fuel conditioned up to 394°K (250°F). A summary of the significant long-duration performance tests is given in Table IV. Detailed listings of the significant performance and stability tests are given in Tables V and VI.

At the conclusion of the checkout and performance testing the PAT-2000 injector was selected for use in the calorimeter chamber testing. A major factor in the decision was the very stable combustion of this pattern.

3. Calorimeter Chamber Testing

The calorimeter chamber testing was conducted with the PAT-2000 injector, the 34 cm (13.4 in.) length (injector face to throat)

TABLE IV. - SIGNIFICANT PERFORMANCE TESTS

INJECTOR	TEST NO.	DUR (SEC)	L' (CM)	L' (IN)	T_f (°K)	T_f (°F)	O/F RANGE	REMARKS
PAT-2000	056	9	27.9	(11)	283	(49)	2.3-3.0	
	070	16	37.5	(15)	293	(68)	2.2-3.4	Hi Pc-Shutdown
	071	19	37.5	(15)	394	(250)	2.4-4.1	
	072	19	27.9	(11)	389	(240)	2.0-3.2	
TLOL-1200	073	16	27.9	(11)	378	(220)	2.5-3.0	Combustion Instability @ 16-sec
	074	30	37.5	(15)	311	(100)	2.2-2.8	
	075	16	27.9	(11)	297	(75)	2.7-2.9	Combustion Instability @ 16-sec

TABLE V. - PERFOPMANCE TEST DATA SUMMARY

(SI UNITS)

Injector-Design Pc Type (kPa)	Test No.	L* (cm)	T_{FJ} (°K)	Sum. Period (sec)	Pc kPa	O/F	F_v (N)	(ε =5.8) Isp (sec)	C* (m/sec)	%ERE	$\%\eta_{c^*}$	Remarks
PAT-2000	-056A	27.9	281	1.5-3.0	11,859	2.363	65,229	2795.9	1711	94.1	94.0	
	-056B	"	282	3.5-5.0	11,935	2.641	65,851	2795.9	1706	94.2	94.4	
	-056C	"	283	5.5-7.0	11,969	2.865	66,243	2792.9	1699	94.7	95.0	
	-056D	"	283	7.5-9.0	11,997	3.023	66,323	2778.2	1692	94.8	95.4	
	-070A	37.5	295	1.5-5.0	12,941	2.841	72,702	2842.0	1737	96.7	96.8	
	-070B	"	293	5.5-9.0	12,907	2.255	71,937	2825.3	1741	95.8	95.6	
	-070C	"	293	9.5-12.0	13,066	2.948	73,476	2836.1	1732	96.9	97.0	
	-070D	"	293	12.3-13.0	13,114	3.187	73,889	2817.5	1717	96.6	97.4	
	-070E	"	293	13.6-15.57	13,135	3.433	74,116	2796.9	1701	97.1	97.8	Test terminated due to high Pc shutdown.
	-071A	37.5	344	1.5-5.0	12,155	3.187	68,423	2838.0	1732	97.3	98.2	
	-071B	"	387	5.5-9.0	12,073	2.465	67,515	2862.6	1758	96.6	96.6	
	-071C	"	393	9.5-12.0	11,976	3.547	67,560	2807 7	1706	97.9	98.6	
	-071D	"	394	12.5-16.0	11,962	4.144	67,613	2733.1	1661	99.2	99.0	
	-071E	"	395	16.5-19.0	11,969	3.648	67,551	2791.0	1698	98.1	98.7	
	-072A	27.9	344	1.5-5.0	12,231	2.572	69,214	2815.5	1718	95.1	94.7	C* appears 0.4% to 0.7% low relative to ERE.
	-072B		384	5.5-9.0	12,121	2.016	68,240	2784.1	1708	95.8	94.9	
	-072C		388	9.5-12.0	12,080	2.807	68,609	2818.4	1714	95.8	95.4	
	-072D		389	12.5-16.0	12,135	3.210	69,152	2795.9	1694	96.0	96.3	
	-072E		390	16.5-19.0	12,100	2.894	68,761	2813.5	1709	96.0	95.5	
PLOC-1200	-073A	27.9	313	1.2-2.0	7,095	2.710	40,199	2842.0	INV	96.2	INV	C* data is invalid
	-073B		345	2.5-10.0	7,018	2.485	40,052	2865.5	INV	96.6	INV	
	-073C		377	10.5-14.0	7,102	3.055	40,457	2839.0	INV	97.5	INV	
	-073D		380	14.0-16.38	7,060	2.563	40,070	2855.7	INV	96.3	INV	Combustion instability encountered @ 16 sec.
	-074A	37.5	304	2.0-10.0	7,308	2.603	41,021	2877.3	1759	97.0	97.6	
	-074B		311	10.5-13.0	7,371	2.831	41,524	2862.6	1744	97.3	97.7	
	-074C		312	13.5-16.0	7,350	2.763	41,377	2867.5	1748	97.2	97.7	
	-074D		312	16.5-19.0	7,322	2.658	41,213	2873.3	1752	97.0	97.4	
	-074E	"	312	19.5-22.0	7,302	2.455	40,995	2877.3	1759	97.1	97.1	
	-074F		312	22.5-25.0	7,253	2.286	40,612	2971.4	1759	97.2	97.0	
	-074G		313	25.5-30.0	7,322	2.680	41,226	2877.3	1753	97.2	97.6	
	-075A	27.9	293	2.0-10.0	7,315	2.698	41,417	2835.1	INV	95.9	INV	C* data is invalid
	-075B		297	10.5-13.0	7,364	2.895	41,804	2822.4	INV	96.2	INV	
	-075C		297	13.5-16.0	7,364	2.831	41,738	2832.2	INV	96.3	INV	Combustion Instability encountered @ 16 sec

TABLE 7. - PERFORMANCE TEST DATA SUMMARY (cont.)

(ENGLISH UNITS)

Injector-Test Type	Nom. Test Pc (psia)	Test No.	L^* (in.)	T_{EI} (°F)	Sum Period (sec)	Pc (psia)	O/F	F_v (lbF)	(ε=5.8) Isp (sec)	C* (fps)	%ERE	η_{C^*}	Remarks
PAT-2300		-056A	11	46.3	1.5-3.0	1720	2.363	14,664	285.1	5613	94.1	94.0	
		-056B		48.0	3.5-5.0	1731	2.641	14,804	285.1	5597	94.2	94.4	
		-056C		49.0	5.5-7.0	1736	2.865	14,892	284.8	5575	94.7	95.0	
		-056D		49.9	7.5-9.0	1740	3.023	14,910	283.3	5551	94.8	95.4	
		-070A	15	70.3	1.5-5.0	1877	2.841	16,344	289.8	5700	96.7	96.8	
		-070B		67.0	5.5-9.0	1872	2.255	16,172	288.1	5712	95.8	95.6	
		-070C		67.5	9.5-12.0	1895	2.948	16,518	289.2	5681	96.9	97.0	
		-070D		67.7	12.3-13.0	1902	3.187	16,611	287.3	5634	96.6	97.4	
		-070E		67.7	13.6-15.57	1905	3.433	16,662	285.2	5582	97.1	97.8	← Test terminated due to high Pc shutdown.
		-071A	15	159.2	1.5-5.0	1763	3.187	15,382	289.4	5681	97.3	98.2	
		-071B		236.5	5.5-9.0	1751	2.465	15,178	291.9	5767	96.6	96.6	
		-071C		246.8	9.5-12.0	1737	3.547	15,188	285.8	5597	97.9	98.6	
		-071D		249.4	12.5-16.0	1735	4.144	15,200	278.7	5450	99.2	99.0	
		-071E		251.3	16.5-19.0	1736	3.468	15,186	284.6	5572	98.1	98.7	
		-072A	11	159.3	1.5-5.0	1774	2.572	15,560	287.1	5636	95.1	94.7	C* appears 0.4% to 0.7% low relative to ERE
		-072B		230.5	5.5-9.0	1758	2.016	15,341	283.9	5605	95.8	94.9	
		-072C		237.9	9.5-12.0	1752	2.807	15,424	287.4	5622	95.8	95.4	
		-072D		240.2	12.5-16.0	1760	3.210	15,546	285.1	5559	96.0	96.3	
		-072E		241.5	16.5-19.0	1755	2.894	15,458	286.9	5608	96.0	95.5	
TLOL-1200		-073A	11	102.6	1.2-2.0	1029	2.710	9,037	289.8	Inv.	96.2	Inv.	C* data is invalid
		-073B		160.6	2.5-10.0	1027	2.485	9,004	292.2	Inv.	96.6	Inv.	
		-073C		219.0	10.5-14.0	1030	3.055	9,095	289.5	Inv.	97.5	Inv.	
		-073D		223.9	14.0-16.38	1024	2.563	9,008	291.2	Inv.	96.3	Inv.	Combustion Instability encountered @ 16-sec
		-074A	15	86.6	2.0-10.0	1060	2.063	9,222	293.4	5570	97.0	97.6	
		-074B		99.6	10.5-13.0	1069	2.831	9,335	291.9	5721	97.3	97.7	
		-074C		100.8	13.5-16.0	1066	2.763	9,302	292.4	5736	97.2	97.7	
		-074D		101.5	16.5-19.0	1062	2.658	9,265	293.0	5749	97.0	97.4	
		-074E		101.7	19.5-22.0	1059	2.455	9,216	293.4	5771	97.1	97.1	
		-074F		102.0	22.5-25.0	1052	2.286	9,130	292.8	5772	97.2	97.0	
		-074G		102.8	25.5-30.0	1062	2.680	9,268	293.4	5751	97.2	97.6	
		-075A	11	67.6	2.0-10.0	1061	2.698	9,311	289.1	Inv.	95.9	Inv.	C* data is Invalid
		-075B		74.7	10.5-13.0	1068	2.895	9,398	287.8	Inv.	96.2	Inv.	C* data is Invalid
		-075C		75.4	13.5-16.0	1067	2.831	9,383	288.8	Inv.	96.3	Inv.	Combustion Instab. encountered @ 16-sec

TABLE VI. - STABILITY TEST DATA SUMMARY

Test	Injector	Chamber & Length*	Firing Duration (sec)	Chamber Pressure (kPa)	Chamber Pressure (psia)	Mixture Ratio	Fuel Temperature (°K)	Fuel Temperature (°F)	Acoustic Resonator Depth (Number)	Results
045	TLOL 1200	HT.SK.-15	0.9	7998	1160	2.7	300	80	0.0(6) +0.7(6)(Uncooled)	1-T @ 0.4 sec
046	TLOL 1200	NASA-15	0.9	7515	1090	2.8	303	85	0.2(6)(Uncooled) +0.8(6)	Stable
047	TLOL 1200	NASA-15	1.4	7515	1090	2.8	303	85	0.2(6) +0.8(6)(Uncooled)	Stable
050	TLOL 2000	HT.SK.-15	0.3	12824	1860	2.5	297	75	0.2(6) +0.8(6)(Uncooled)	1-T immediately
051B	TLOL 2000	NASA-11	0.7	12203	1770	2.5	292	65	0.2(4) +0.8(8)(Uncooled)	1-T immediately
053	PAT 2000	NASA-11	0.6	12066	1750	2.8	289	60	0.2(4) +0.8(8)(Uncooled)	Stable
056	PAT 2000	NASA-11	8.4	11997	1740	2.4,2.6, 2.9,3.0	283	50	0.2(4) +0.8(8) Cooled	Stable
057	TLOL 2000	NASA 15	4.1	12548	1820	2.4	289	60		1-T immediately, delayed CSM shutdown
059	TLOL 2000	NASA 15	0.3	12411	1800	2.8	289	60		1-T immediately, severe face erosion
070	PAT 2000	NASA 15	14.9	13376	1940	2.8,2.3, 3.0,3.2, 3.4	294	70		Stable
071	PAT 2000	NASA-15	18.4	12342	1790	3.2,2.5, 3.5,4.1, 3.6	394	250		Stable
072	PAT 2000	NASA-11	18.4	12411	1800	2.6,2.0, 2.8,3.2, 2.9	378	220		Stable
073	TLOL 1200	NASA-11	15.7	7239	1050	2.7,2.5 3.1,2.6	378	220		1-T 2 seconds into O/F = 2.6, CSM shutdown
074	TLOL 1200	NASA-15	29.3	7308	1060	2.6,2.8,2.7, 2.5,2.3,2.7	311	100		Stable
075	TLOL 1200	NASA-11	16.0	7515	1090	2.7,2.9,2.8	294	70		1-T while changing from O/F = 2.8 to lower O/F, CSM shutdown

TABLE VI. - STABILITY TEST DATA SUMMARY (cont.)

Test	Injector	Chamber & Length*	Firing Duration (sec)	Chamber Pressure (kPa)	(psia)	Mixture Ratio	Fuel Temperature (°K)	(°F)	Acoustic Resonator Depth (Number)	Results
		Calorimeter Chamber Testing								
084	PAT 2000	CAL. 15	11.5	13652	1980	2.5,1.9	367	200	0.2(4) +0.8(8) Cooled	Stable
085	PAT 2000	CAL. 15	19.3	13652	1980	2.6,2.7,2.8	372	210		Stable

*

Chamber Configuration	Chamber Length (cm)	(in)	Nominal Throat Dia (cm)	(in)
HT.SK.-15	40.1	15.8	6.25	2.46
CAL.-15	34.0	13.4	6.25	2.46
NASA-11	29.0	11.4	6.60	2.60
NASA-15	39.1	15.4	6.60	2.60

water-cooled calorimeter chamber, and the water-cooled resonator. The test series consisted of two multiple data point tests, both at the 13790 kPa (2000 psia) chamber pressure condition. A list of the test durations and conditions for the calorimeter tests is given in Table VII.

Both tests were run with hot 367°K (200°F) fuel to 1) maximize performance and 2) because it was more representative of operation with a regeneratively cooled chamber. The decision to use the 34 cm (13.4 in.) chamber instead of the 27.9 cm (11 in.) calorimeter chamber was also to maximize performance.

The calorimeter chamber test installation is shown in Figure 19. The large number of flexible high-pressure coolant hoses attached to the chamber were thought to make accurate thrust measurements difficult during the calorimeter testing. The test data indicated this not to be the case as both the stand bias and data reproducibility appeared to be consistent. However, the performance data obtained during the calorimeter chamber testing were not believed to be as good as that of the earlier performance test series due to the greater analytical uncertainty resulting from the high divergence angle (40° half angle) of the truncated calorimeter nozzle exit.

D. INJECTOR PERFORMANCE

As noted previously, the performance assessment of the injectors was based on data obtained during the performance test series. Performance data from the calorimeter test series were not reviewed in depth. A detailed list of all the performance data points is given in Table V.

The experimental Energy Release Efficiencies (ERE) for the PAT-2000 and TLOL-1200 injectors are given as a function of chamber length and fuel temperature in Figures 20 and 21. These nominal performance efficiencies are for an O/F = 2.8. They were obtained with a 5.8:1 nozzle expansion ratio and were adjusted to an O/F = 2.8 by interpolating plots of ERE versus mixture ratio. Note that the heated fuel curve for the TLOL-1200 injector is shown as a dashed line. A complete data matrix (hot and cold fuel, long and short chambers) was not obtained with this injector. The slope of the performance curve for heated fuel was estimated on the basis of the ambient data and the vaporization and mixing analyses described later. No valid performance data were obtained with the TLOL-2000 injector due to the consistent instability of that unit.

A comparison of the performance for the PAT-2000 and TLOL-1200 is given in Figure 22.

TABLE VII. - CALORIMETER CHAMBER TEST SUMMARY

Test	Time Interval (sec)	Chamber Pressure (kPa)	(psia)	Mixture Ratio	Fuel Temperature (°K)	(°F)
084	2 → 8	13686	1985	2.49	349	169
084	8.5 → 12	13555	1966	1.90	367	200
085	2.5 → 5	13714	1989	2.63	357	182
085	5 → 10	13672	1983	2.74	371	207
085	10 → 15	13652	1980	2.78	373	212
085	15 → 20	13645	1979	2.80	374	214

Figure 19. Calorimeter Chamber Test Setup

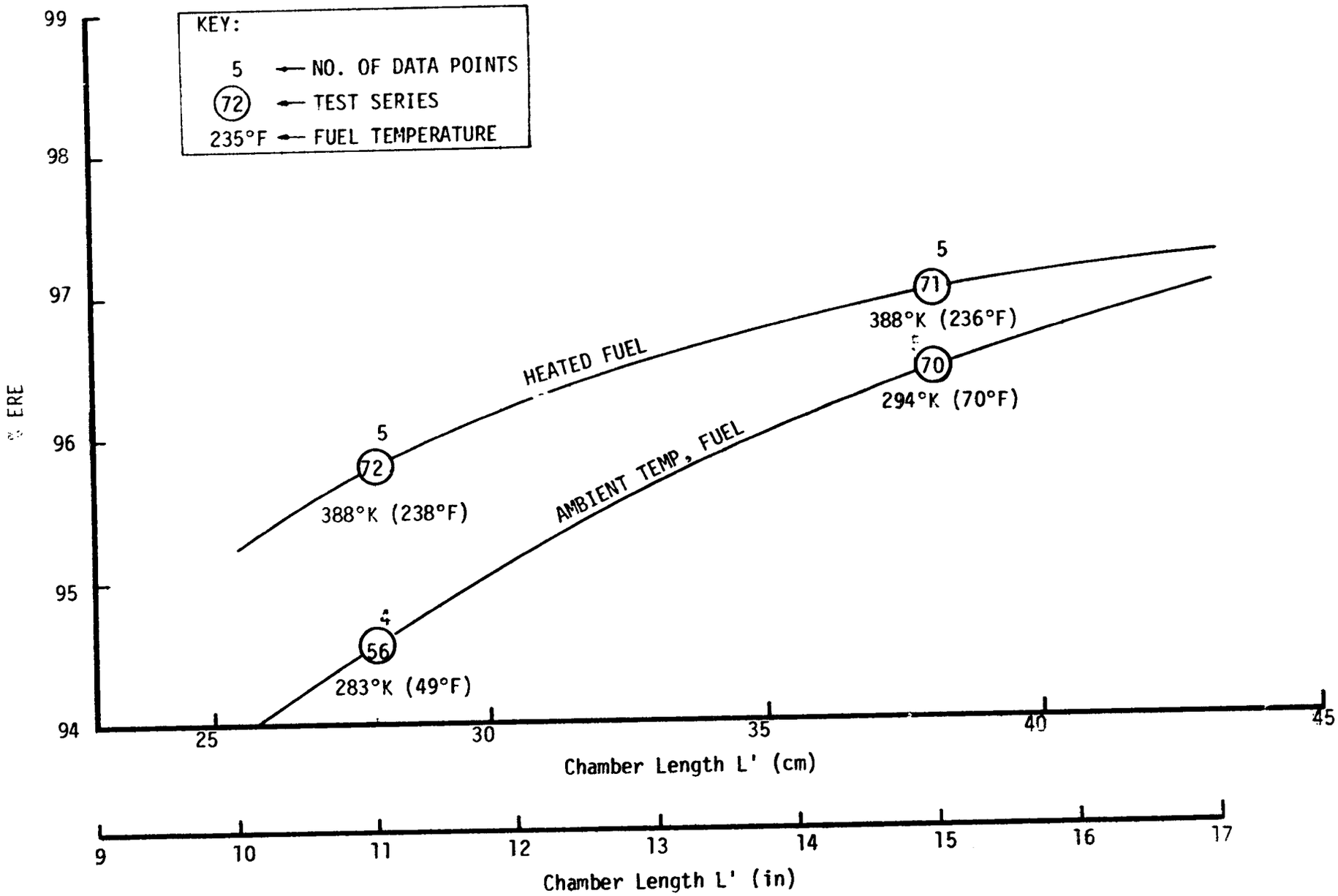

Figure 20. PAT-2000 Injector Performance

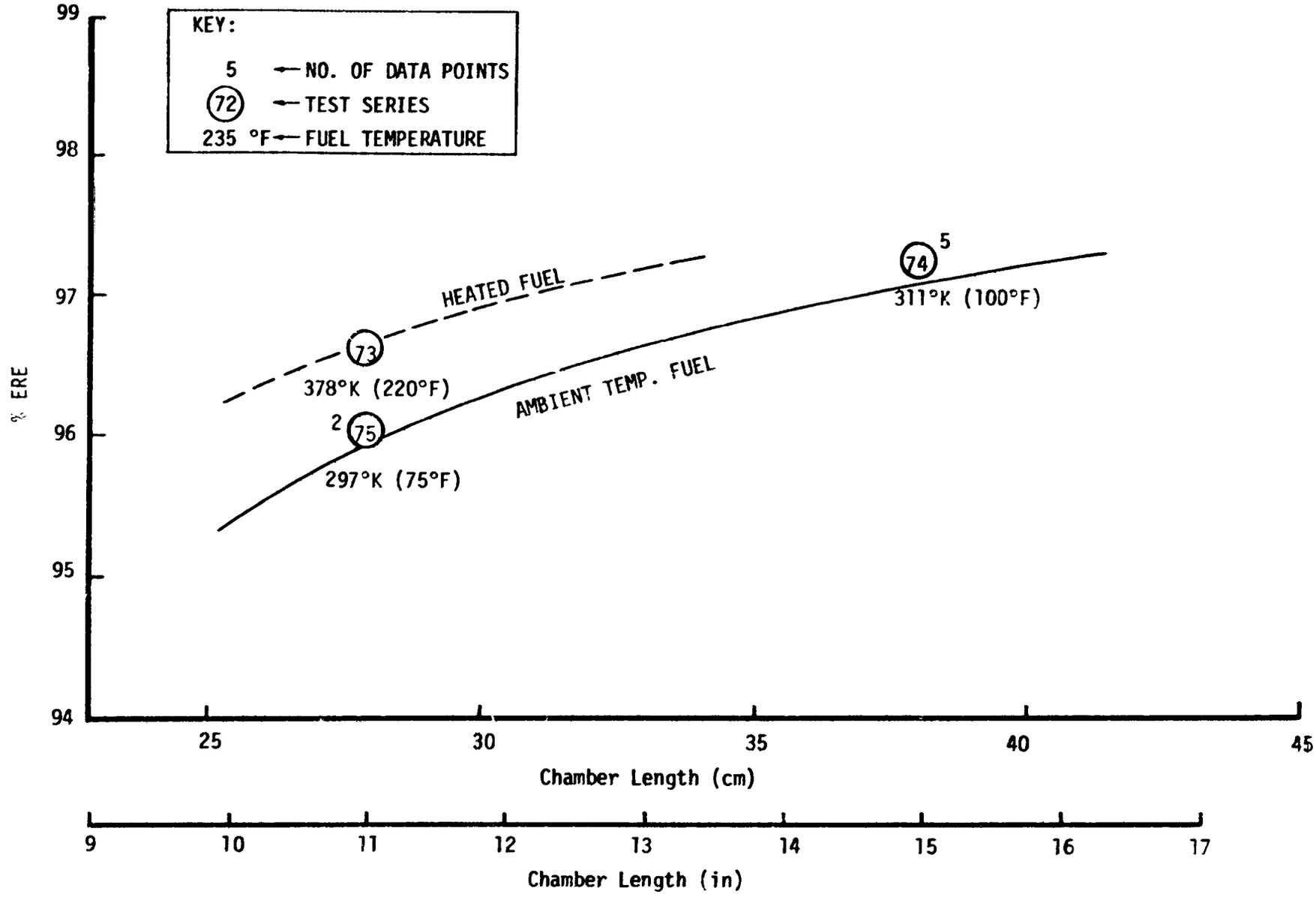

Figure 21. TLOL-1200 Injector Performance

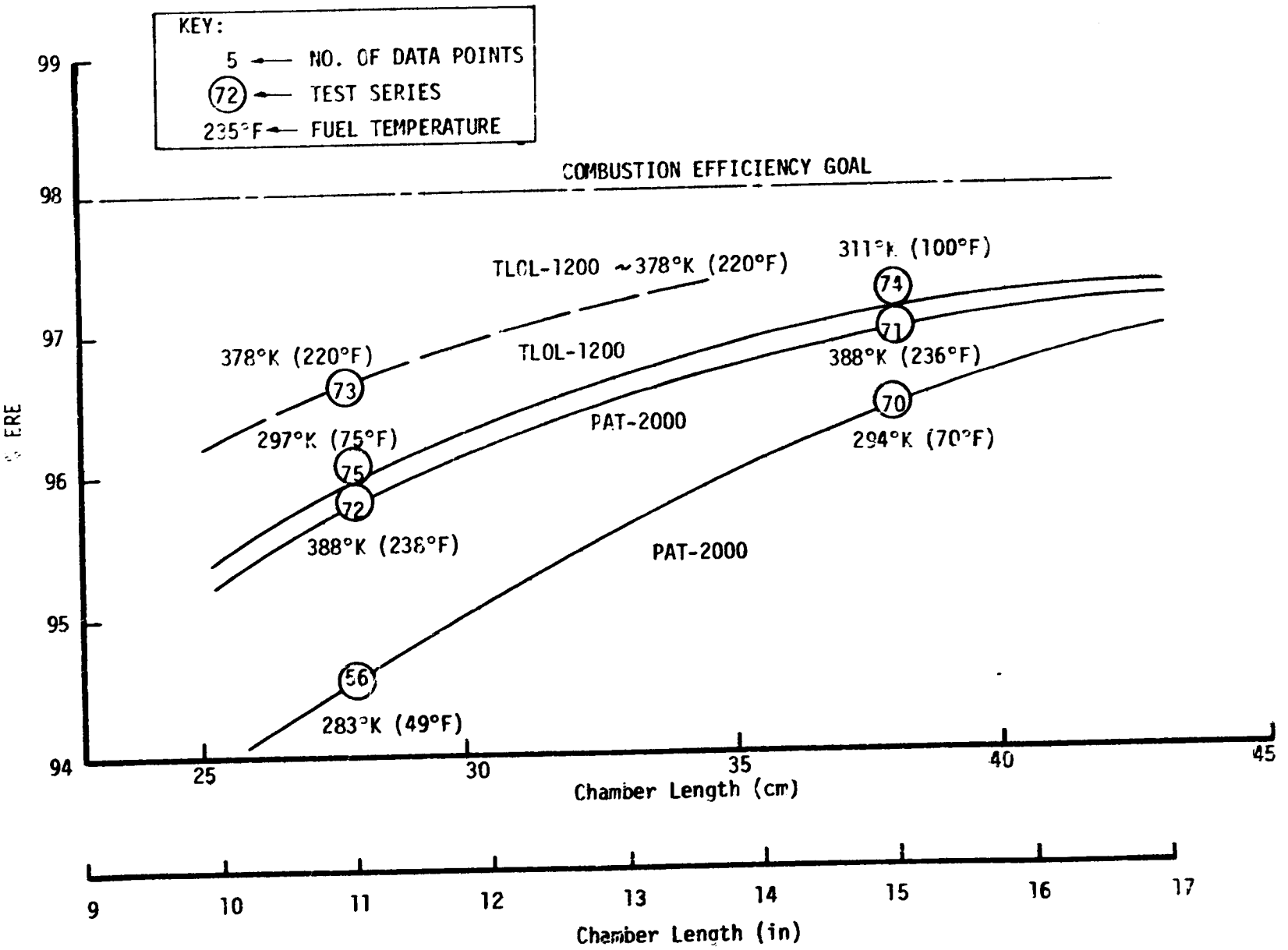

Figure 22. Injector Performance Comparison

The experimental combustion efficiencies, while substantially higher than those of earlier production LOX/RP-1 injectors such as the F-1 (93.8%C*) and Atlas booster (95.5%C*) were below the program goal of 98%. The data were evaluated and compared with analytical predictions to identify the source of the performance losses. The results of these analyses are given in subsequent sections.

1. Identification of Performance Losses

It is possible to separate observed performance losses into those resulting from non-uniform mixing and incomplete fuel vaporization if performance data over a wide mixture ratio range are available. Separation of the losses is done by first plotting the experimental ERE and C* efficiency versus mixture ratio. Similar plots are then made of analytically predicted ERE and %C* where the predicted values have been obtained by varying the mixing efficiency and fuel vaporization efficiency as independent parameters. (The oxidizer vaporization efficiency is held constant at 100%. This is a reasonable assumption when working with LOX/RP-1 because the LOX is predicted to be completely vaporized within 16 cm [6.3 in.]). The experimental vaporization and mixing efficiencies are then found by comparing the experimental and analytical ERE (and %C*) versus MR plots to determine which combination of fuel vaporization and mixing efficiencies best matches the experimental data in both magnitude and mixture ratio sensitivity. This has been done for a number of tests on this program, with typical results presented in Figures 23 and 24. Figure 23 shows the variation in both %C* and %ERE as a function of test mixture ratio for Run 71 with the PAT-2000 injector. Based on the slope and magnitudes of the C* and ERE efficiencies, it is apparent that the PAT-2000 injector performance in the long chamber and with hot fuel [394°K (250°F)] is bounded by a combination of either 99% maximum fuel vaporization efficiency with 75% E_m mixing efficiency or by a minimum 98% fuel vaporization with an E_m of 77%. These mixing and fuel vaporization parameters represent the highest ERE performance achieved by the PAT-2000 injector shown on Figure 20.

Similar calculations were performed for Run 56 with the short chamber and cold fuel. This test represented the lowest performance point shown on Figure 20 and thus provided lower bounds for both E_m and fuel vaporization efficiency. Both the ERE and %C* correlation from this test showed that the PAT-2000 yielded 73% E_m with 92% fuel vaporization efficiency under these conditions. The experimental influence of both fuel temperature and chamber length upon the fuel vaporization efficiency is discussed further in subsection IV,D,3.

The mixing efficinecy, E_m, was remarkably insensitive to the wide (283-394°K [50°-250°F]) fuel temperature range and the 28-38 cm (11 to 15 in.) chamber length variation. Since the 73% E_m from Run 56 was the

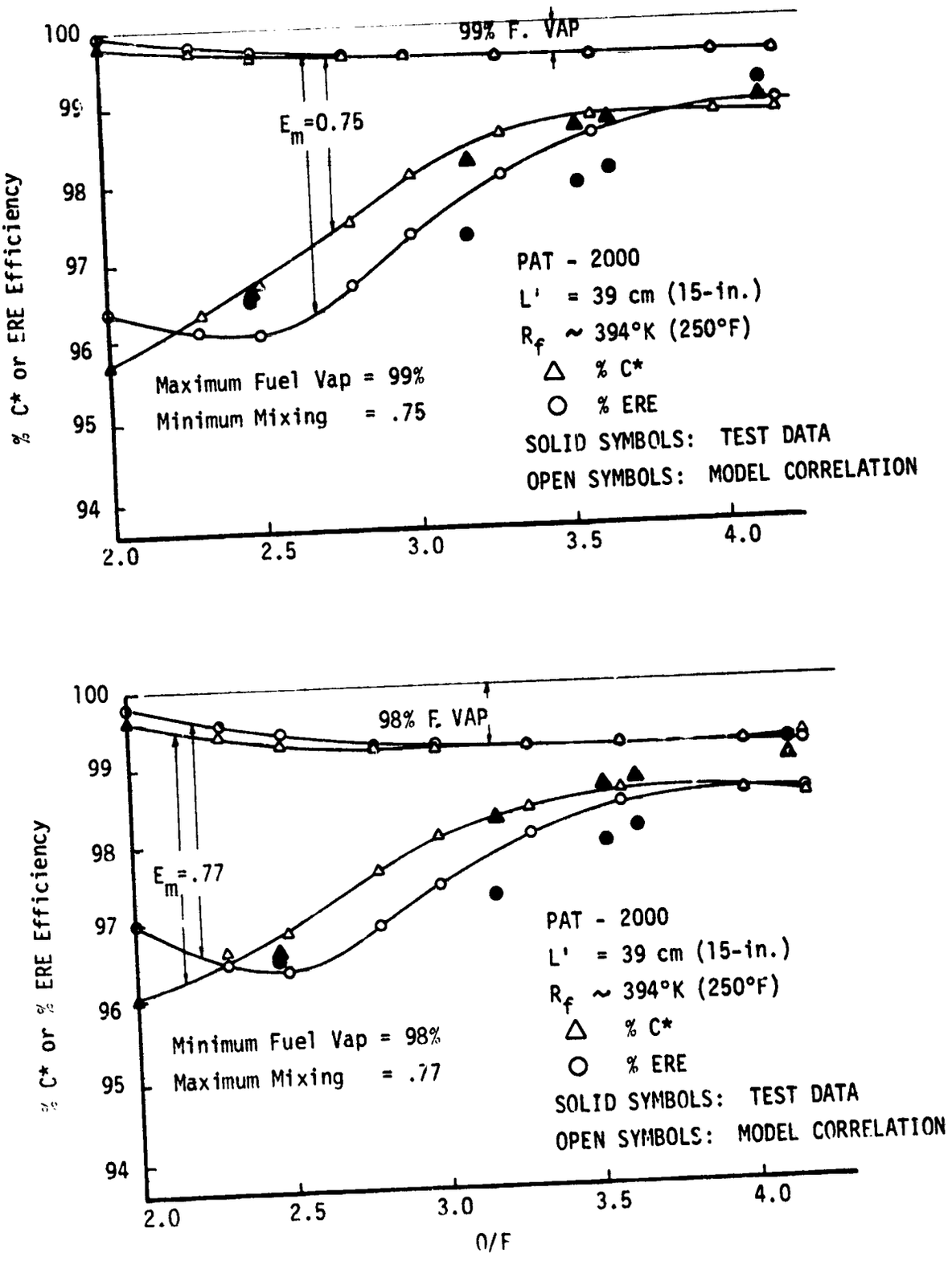

Figure 23. PAT-2000 Fuel Vaporization and Mixing Loss Performance Limits Bounded in the Long Chamber with Heated Fuel

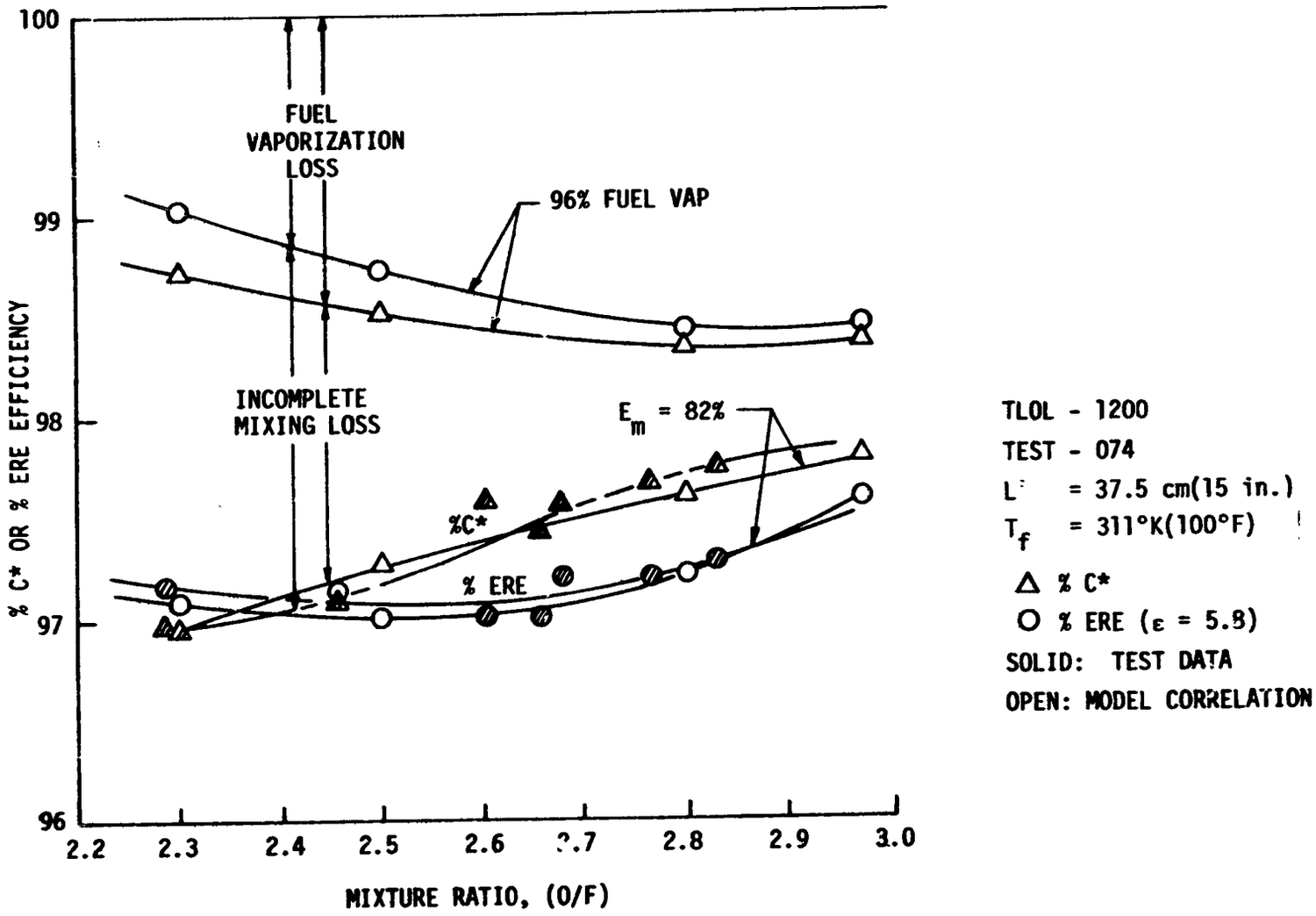

Figure 24. TLOL-1200 Performance Loss Identification

first chronologically computed value and since subsequent changes were very minor, it was assumed to be constant for the PAT-2000 injector for all subsequent analyses. Insufficient data were available from wide mixture ratio excursion tests to establish the influence of fuel temperature and chamber length upon E_m.

Figure 24 shows the test C* and ERE efficiencies from Test No. 74 with the TLOL-1200 injector. This test encompassed the widest range of test mixture ratios on the TLOL-1200 injector. With 311°K (100°F) fuel and 37.5 cm (15 in.) chamber length, the inferred fuel vaporization efficiency is approximately 96% and its corresponding E_m = 82%. This combination closely approximates the magnitude and slope of both the %C* and %ERE with the TLOL-1200 injector on Test 74.

2. Constant E_m Performance Correlations

Based on the empirical observation that E_m changed little with changes in test chamber length or with fuel heating, a simple parametric analysis was conducted to correlate the measured performance data by assuming that the E_m of a given injector remains constant for all tests.

The %C* relationships between test and analytical correlations as a function of engine test mixture ratio and % fuel vaporized for 3 tests with the PAT-2000 injector is shown in Figure 25. It is apparent that the C* efficiency of Test 71 with 394°K (250°F fuel) is nearly asymptotic to the mixing performance loss corresponding to 73% E_m with 100% OX and fuel vaporization efficiency. Lines of predicted C* efficiency for fuel vaporization efficiencies of 99%, 97%, and 92% closely approximate the measured C* efficiency of Tests 71, 70, and 56, respectively. As discussed in the previous subsection, the C* data in the 28 cm (11 in.) chamber with heated fuel (Test 72) has been omitted from the plot because of the suspected invalidity of the C* data which would subject the results to misinterpretation.

Figure 26 shows the corresponding ERE correlation for the PAT-2000 injector, assuming a constant 73% E_m for all four tests and varying fuel vaporization efficiencies of 100%, 99%, 96%, and 92% which appear to bound the test data. Since the experimental ERE slope closely approximates the analytically predicted trend, it appears reasonable to estimate the fuel vaporization efficiencies from these correlations. The only two data points which appear to be slightly inconsistent are those from Tests 70 and 71 at low mixture ratio. They appear to have benefited from some minor improvement in E_m. This may have been due to either the longer chamber length or to the improved fuel volatility resulting from fuel heating. In any case, the maximum reasonable performance attainable from improved fuel vaporization seems to have been achieved. Further performance efficiency improvements can only be achieved by improving the injector E_m (mixing efficiency).

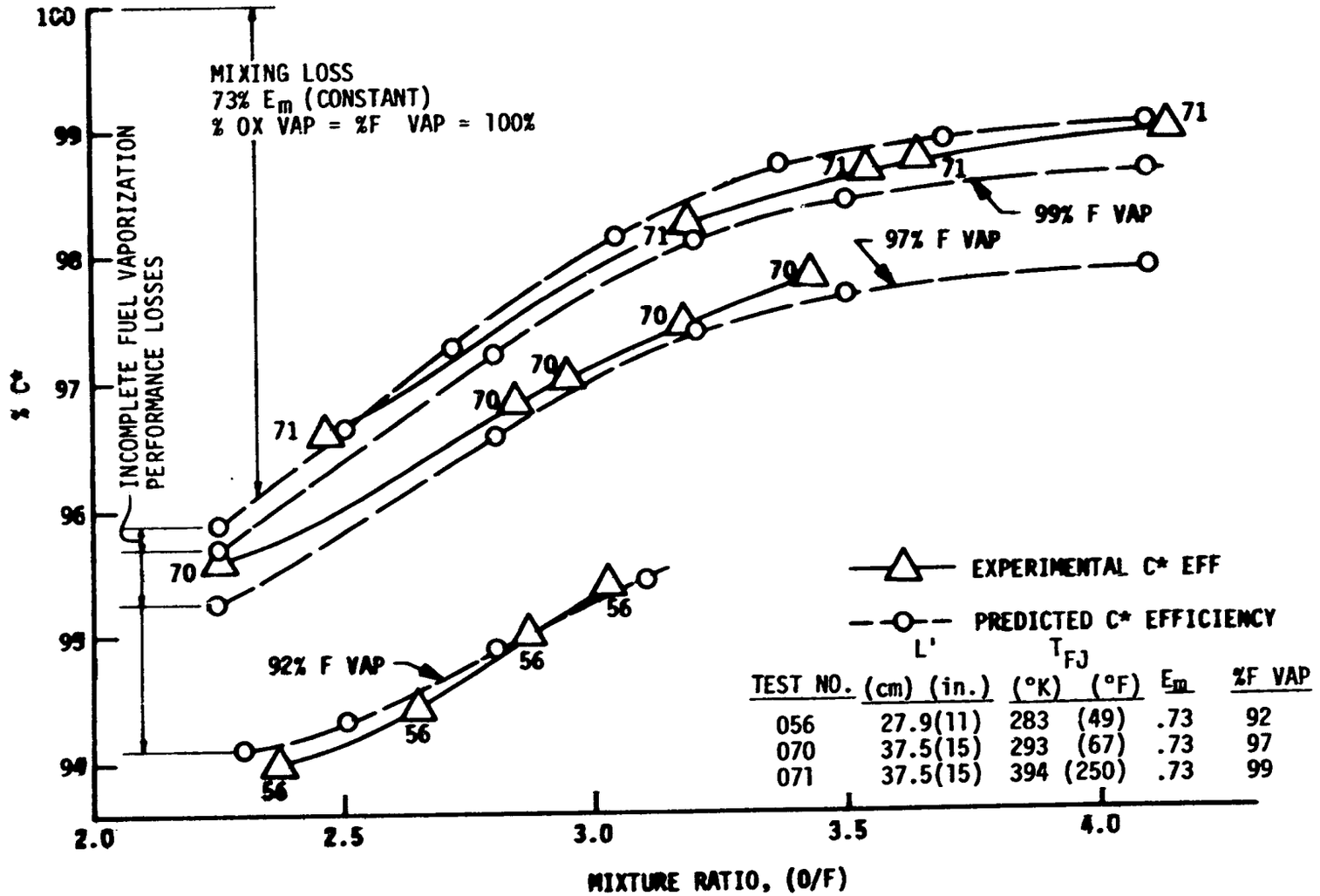

TEST NO.	L' (cm)	L' (in.)	T_{FJ} (°K)	T_{FJ} (°F)	E_m	%F VAP
056	27.9	(11)	283	(49)	.73	92
070	37.5	(15)	293	(67)	.73	97
071	37.5	(15)	394	(250)	.73	99

Figure 25. C* Correlation For Constant E_m, PAT-2000 Injector

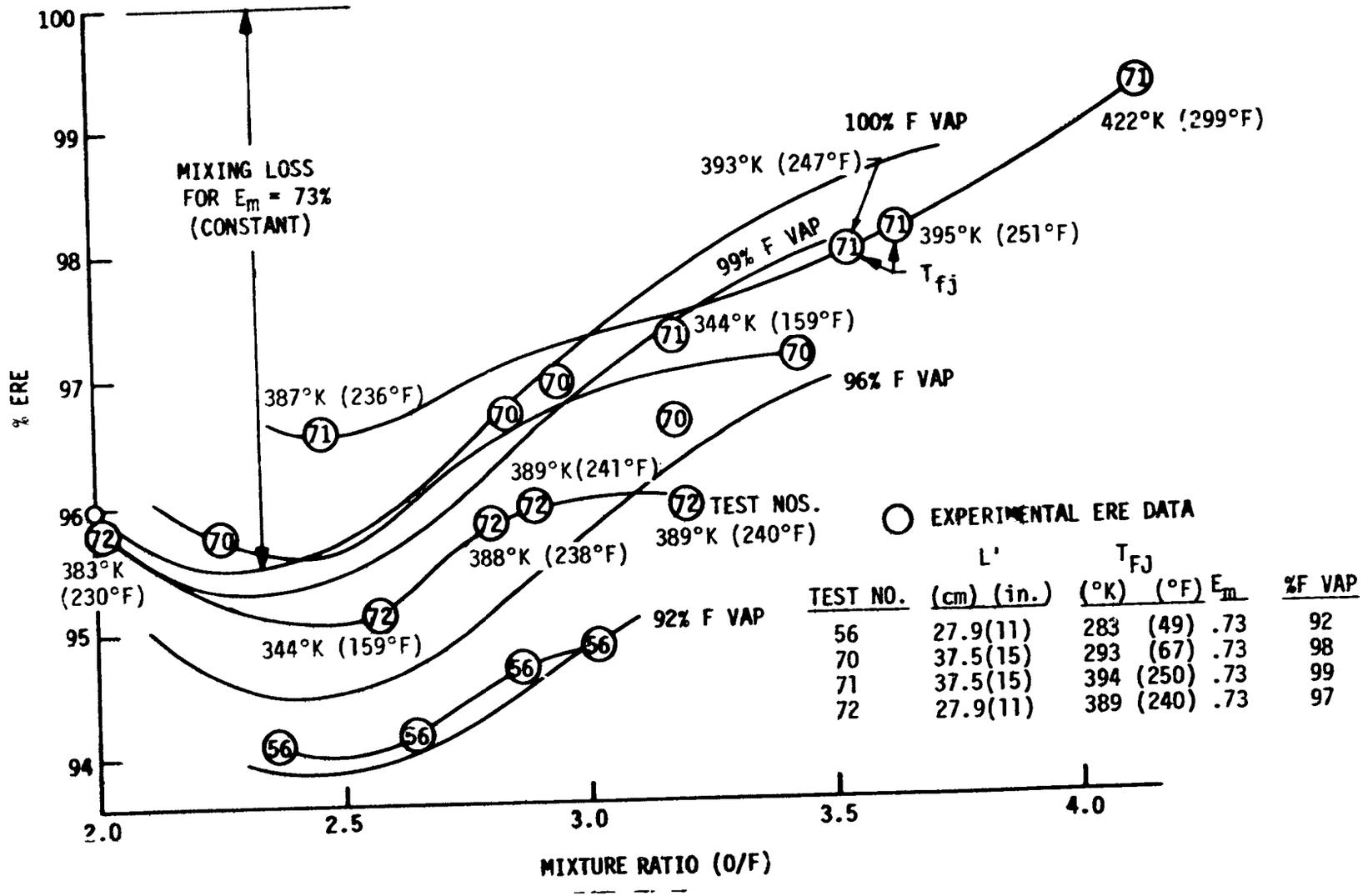

TEST NO.	L' (cm)	L' (in.)	T_{FJ} (°K)	T_{FJ} (°F)	E_m	%F VAP
56	27.9	(11)	283	(49)	.73	92
70	37.5	(15)	293	(67)	.73	98
71	37.5	(15)	394	(250)	.73	99
72	27.9	(11)	389	(240)	.73	97

Figure 26. ERE Correlation For Constant E_m, PAT-2000 Injector

Figure 27 shows the comparable ERE versus mixture ratio correlation for the TLOL-1200 injector with an assumed E_m of 82%. Test 74 in the long chamber and with 311°K (100°F) fuel is matched best with a 96% fuel vaporization efficiency. Test 75 in the short chamber with ambient fuel only has data available within a narrow mixture ratio range prior to encountering combustion instability, but it has a 93.5% inferred fuel vaporization efficiency during its stable operation. The results from Test 73 in the short chamber with heated fuel are difficult to interpret because the fuel temperature varied widely from approximately 311°K to 378°K (100°F to 220°F) during the test mixture ratio range (see Table V). Thus an empirical slope has combined in it not only mixture ratio variations but simultaneous fuel temperature variations as well. Nevertheless, it appears safe to assume that Test 73 in the short chamber would have produced ~94.2% fuel vaporization efficiency at 311°K (100°F) and 95% fuel vaporization efficiency with 378°K (220°F) heated RP-1.

3. Correlation with Analytical Models

Figure 28 shows the inferred fuel vaporization efficiencies of the PAT-2000 and TLOL-1200 injectors as a function of chamber length and fuel temperature. These fuel vaporization efficiencies were previously determined from Figures 23 and 24 and have estimated tolerances of approximately ± 1% due to some uncertainties as to how much of the performance loss is attributable to incomplete fuel vaporization and how much to non-uniform mixing. In all cases, the Priem vaporization model was used to extrapolate the generalized length corresponding to the fuel vaporization efficiency inferred in the short chamber to predict the L_{gen} and fuel vaporization in the longer chamber at comparable fuel temperature.

By comparing the model predictions with the test data, it appears that the fuel vaporization improvement versus chamber length for the TLOL-1200 injector is predicted reasonably well by the model. On the other hand, the PAT-2000 fuel vaporization efficiency outperforms the model prediction. From this it was concluded that the PAT fuel drop size distribution, σ_g, is less than the 2.3 value normally attributed to the doublet injector elements. This conclusion can be analytically supported in another manner. The TLOL-1200 vaporization improvement with length is closely approximated by the Priem vaporization model (which assumes $\sigma_g = 2.3$). Both the TLOL and PAT patterns have comparable overall fuel vaporization efficiencies near the nozzle throat plane in the short combustion chamber. However, the TLOL has been much more sensitive to high-frequency combustion instability for the same resonator configurations tested. Both of these events can be explained if the σ_{PAT} is assumed to be lower (i.e., more uniform) than $\sigma_{TLOL} = \sigma_{EDM\text{-}LOL} = 2.3$. It was demonstrated on the OMS Subscale Program that of all the elements tested, the V-Doublet element had the lowest high-frequency combustion gain.

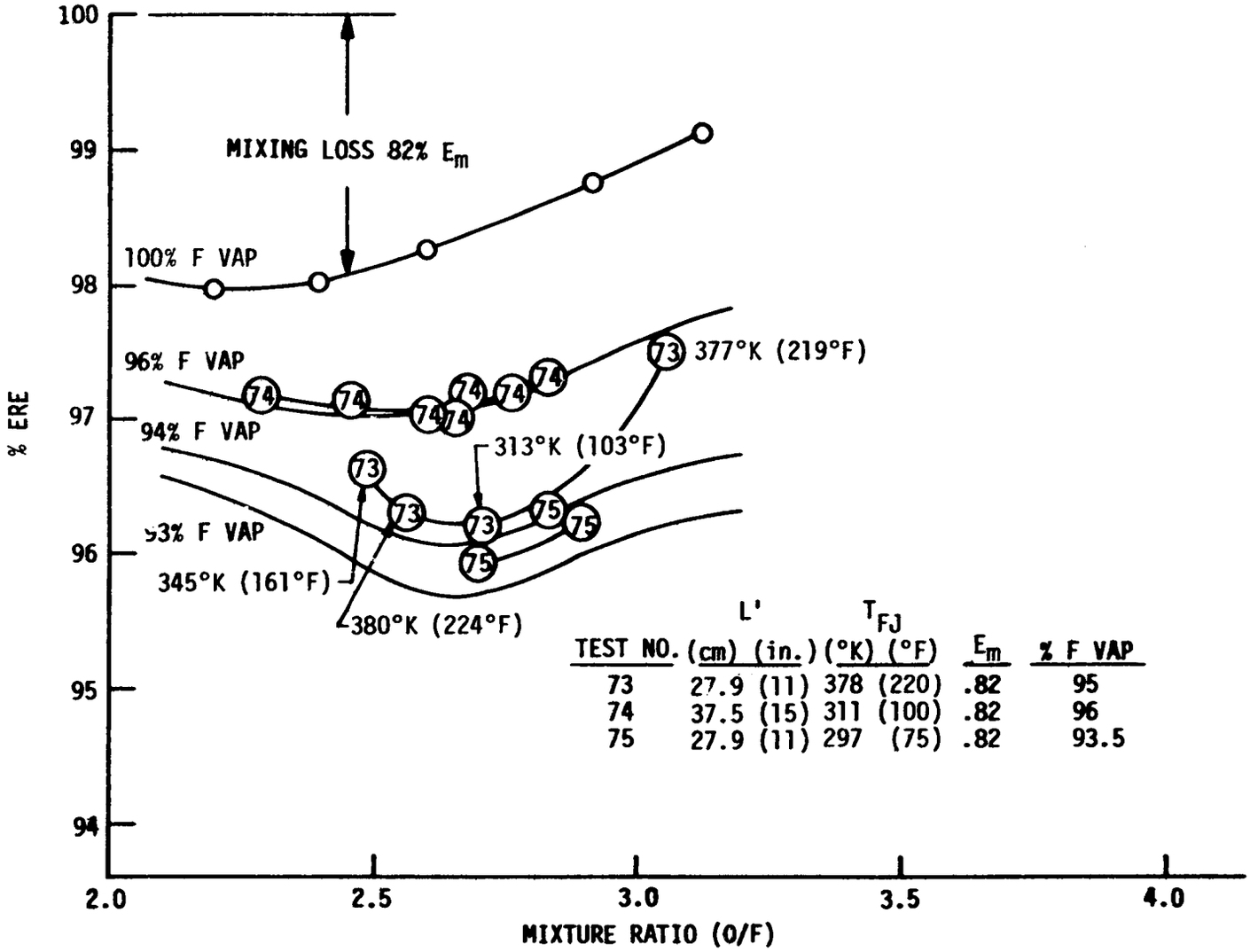

TEST NO.	L' (cm)	L' (in.)	T_{FJ} (°K)	T_{FJ} (°F)	E_m	% F VAP
73	27.9	(11)	378	(220)	.82	95
74	37.5	(15)	311	(100)	.82	96
75	27.9	(11)	297	(75)	.82	93.5

Figure 27. ERE Correlation For Constant E_m, TLOL-1200 Injector

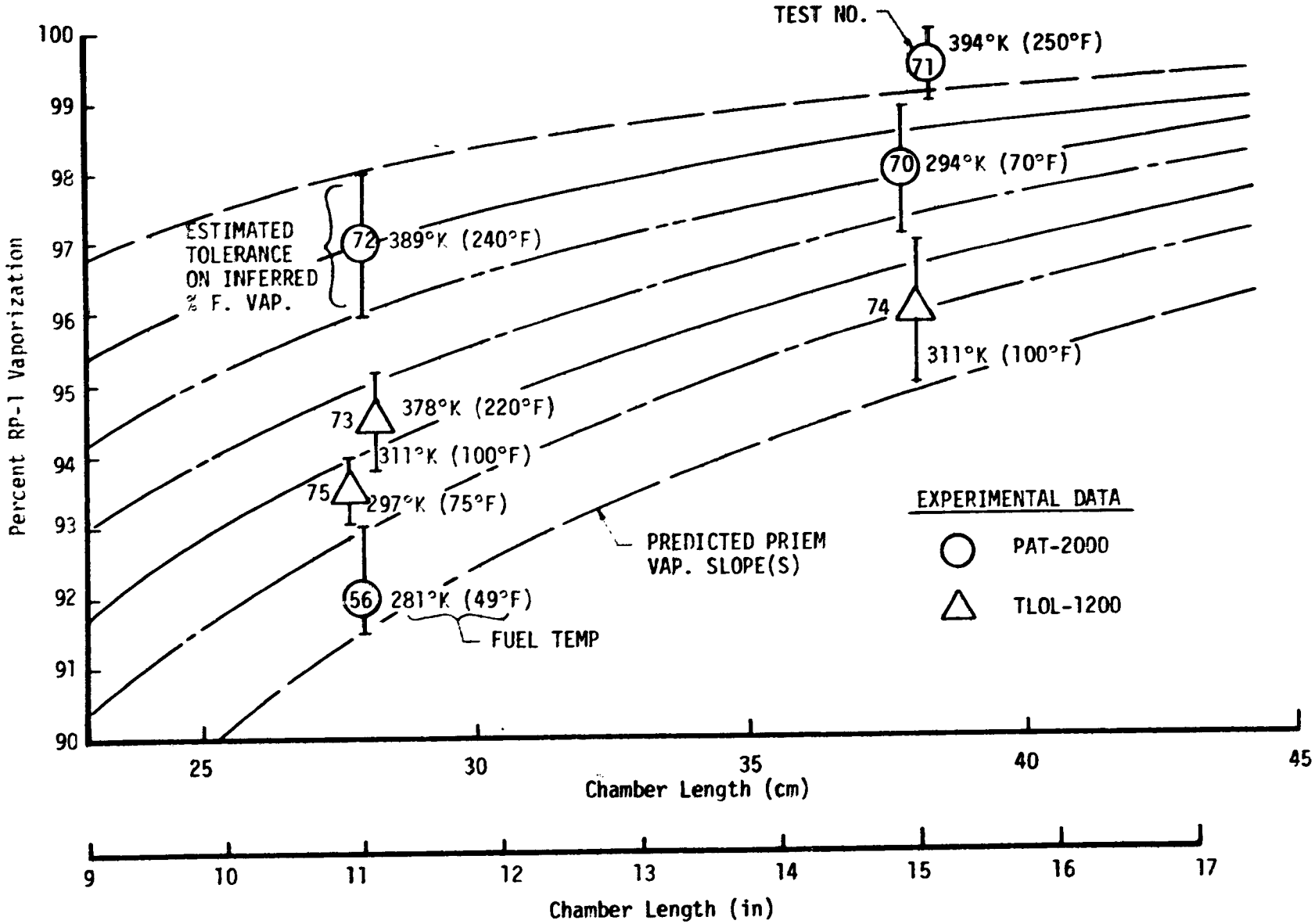

Figure 28. Inferred Fuel Vaporization Sensitivity Compared with Priem Vaporization Model Prediction

On the same program uni-element cold-flow shadowgraphs demonstrated the V-Doublet to have the most uniform spray distribution. The conclusion that uniform droplet size enhances stability can also be derived theoretically from the Priem velocity sensitive droplet vaporization model. It appears that the PAT may have uniform fuel atomization distributions similar to those of the V-Doublet. If this were verified by uni-element cold-flow shadowgraphs, the PAT element would be an attractive candidate for full-scale 2224K to 4448KN (500K to 1M lbF) LO_2/HDF booster engine applications.

As shown in Figure 29, both injectors yielded less performance improvement with fuel heating than was initially anticipated. It was assumed that testing with heated fuel would substantially reduce the fuel viscosity and result in significant atomization and fuel vaporization improvement. It had also been anticipated that fuel heating would more nearly equalize the fuel and oxidizer vaporization rates, thus enhancing the mixing efficiency. However, it has already been experimentally shown that the mixing was not strongly affected by increasing the fuel temperature.

Two mathematical models for predicting the influence of fuel heating upon atomization are presently in use at ALRC. The Priem empirical drop size correlation has been modified so that $r_m \alpha (V_f^{-0.2} [\sigma\mu/\rho]^{0.25}$. A slightly different atomization sensitivity versus fuel temperature is predicted by using the ALRC analytical spray fan and atomization prediction model. This assumes a viscous boundary layer solution for which $r_m \alpha [R_{ef}]^{-0.2}$. For a fixed injector geometry in which only the fuel is heated, $\rho_f V_f$ = constant; therefore, $r_m \alpha [\mu_f]^{.20}$.

Figure 29 presents a comparative view of the influence of hot fuel as predicted by the two analytical models. In terms of the two different atomization models, the PAT-2000 data can be seen to lie between that of the modified Priem emprirical and the ALRC analytical atomization model and can be correlated by either. The TLOL-1200 temperature dependence is predicted more accurately by the ALRC analytical model. Overall, the ALRC analytical atomization model appears to provide better correlation than the Priem empirical model. However, the Priem model formulation has adequately correlated liquid rocket injector performance efficiencies over the last 14 years. It would not seem good judgment to discard the empirical Priem correlation in favor of the purely analytical model on the basis of the data from this program alone without first exploring other possible explanations more thoroughly.

4. Comparison of the PAT and TLOL Injectors

(1) The TLOL-1200 injector has higher mixing efficiency than the PAT-2000; this results in 1% higher ERE for the TLOL-1200.

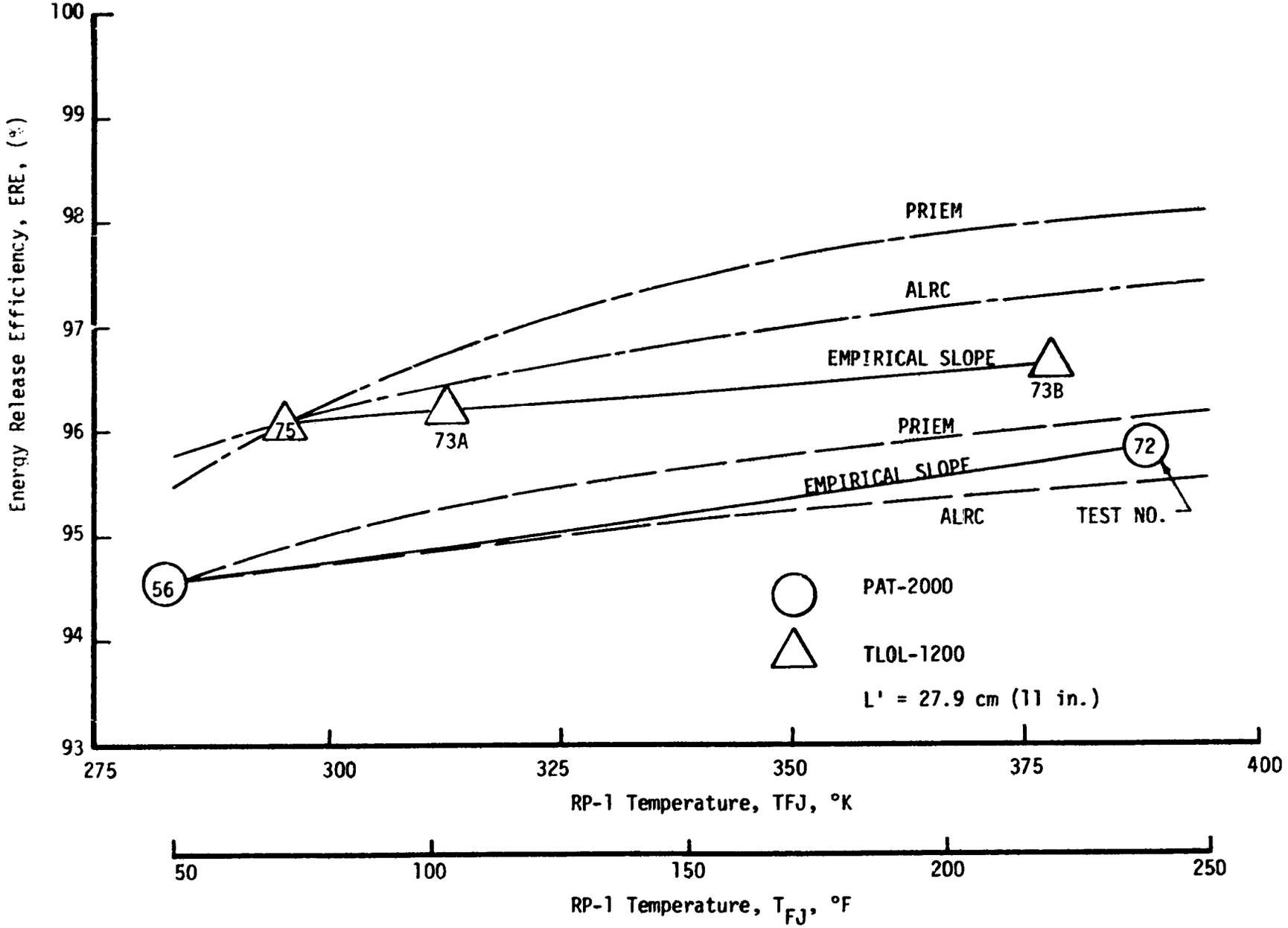

Figure 29. Comparison of Analytical and Experimental ERE Improvements Resulting From Fuel Heating

IV, D, Injector Performance (cont.)

(2) The mass median fuel drop size of the PAT and TLOL injectors is comparable. This is evident from the fact that both injectors have nearly equal fuel vaporization efficiencies.

(3) The PAT injector appears to have a more uniform distribution of fuel drop size about the mass median. This is supported by both its greater sensitivity of performance to chamber length and its reduced high-frequency combustion gain characteristics.

(4) The TLOL injector pattern is characterized by hot oxidizer streaks between the fuel fans. This is evident by the face erosion characteristics on the TLOL-2000 as well as the chamber wall heat marks on the NASA chambers.

(5) From the standpoint of fuel vaporization rate, high-frequency combustion stability, injector face thermal compatibility, and chamber wall compatibility, the PAT injector appears superior to the TLOL element. However, the mixing efficiency of the PAT must be improved to make its performance comparable to that of the TLOL.

E. CHAMBER HEAT TRANSFER

Chamber heat transfer data was obtained during both the performance test series and the calorimeter test series. In the performance series, a total of seven long-duration tests were conducted with the two NASA-supplied water-cooled axially slotted chambers. Total heat load measurements were made during these tests by measuring the total coolant flowrate and the coolant temperature rise. Data were obtained with both the PAT-2000 and the TLOL-1200 injectors at 27.9 cm (11 in.) and 37.5 cm (15 in.) chamber lengths over a range of mixture ratios. Local heat fluxes could not be measured with this hardware.

Calorimeter testing employed the 34.04 cm (13.4 in.) L' calorimeter chamber and the PAT-2000 injector. This chamber had 34 separately measured circumferential cooling circuits which allowed both local heat flux and total heat flux measurements to be made.

The results of the heat transfer testing and data analyses will be presented in this section.

1. Performance Test Series Heat Transfer Results

a. Instrumentation and Data Reduction

Figure 30 is a schematic diagram showing the thermal instrumentation used with the NASA water-cooled chambers. As this figure shows, the cooling water for the chamber and water-cooled resonator were supplied from a common source. The total coolant flowrate (FMWC), the coolant water inlet pressure (PWCI), and the coolant inlet temperature (TWCI) were all measured. Downstream of the measurement point, the coolant water flow was divided with part of the flow being bled-off to supply the resonator. The portion of the flow going to the resonator was measured with a turbine-type flowmeter (FMRES). Both the resonator cooling circuit and the chamber cooling circuit were supplied with discharge orifices which maintained the pressures in the cooling channels at the proper levels. The chamber cooling water temperature (TWCO) was measured downstream of the discharge orifice but upstream of the point where the resonator coolant flow and chamber coolant flow were mixed in the 15.2 cm (6 in.) diameter discharge manifold. The pressure in the discharge manifold was measured and was found to be generally within a few psi of being atmospheric. Data recording with the above instrumentation began 0.5 seconds before each firing and continued for 5 seconds after the firing.

The chamber heat load was calculated by multiplying the coolant flowrate by the coolant temperature rise, i.e.,

$$Q = \dot{W}_c \times \Delta T_c$$

The chamber coolant flowrate, $\dot{W}_c$, was obtained by subtracting the resonator coolant flow from the total coolant flow:

$$\dot{W}_c = FMWC - FMRES$$

The coolant bulk temperature rise, ΔT_c, could be obtained two different ways. The first consists of simply taking the difference between the coolant outlet and inlet temperatures, TWCO-TWCI. However, there are two potential sources of error with this approach. First, there is a substantial pressure drop in the coolant circuit which produces frictional heating of the coolant water. Unless compensated for in some manner, this can introduce an appreciable error in the results. A second source of error could be the existence of a bias between the inlet and outlet thermocouples. To avoid these possible errors, the coolant bulk temperature rise was obtained by comparing the steady-state coolant outlet temperature during firing with the steady-state non-firing value, i.e.,

$$TWCO_\tau - TWCO(FS-2) + 5$$

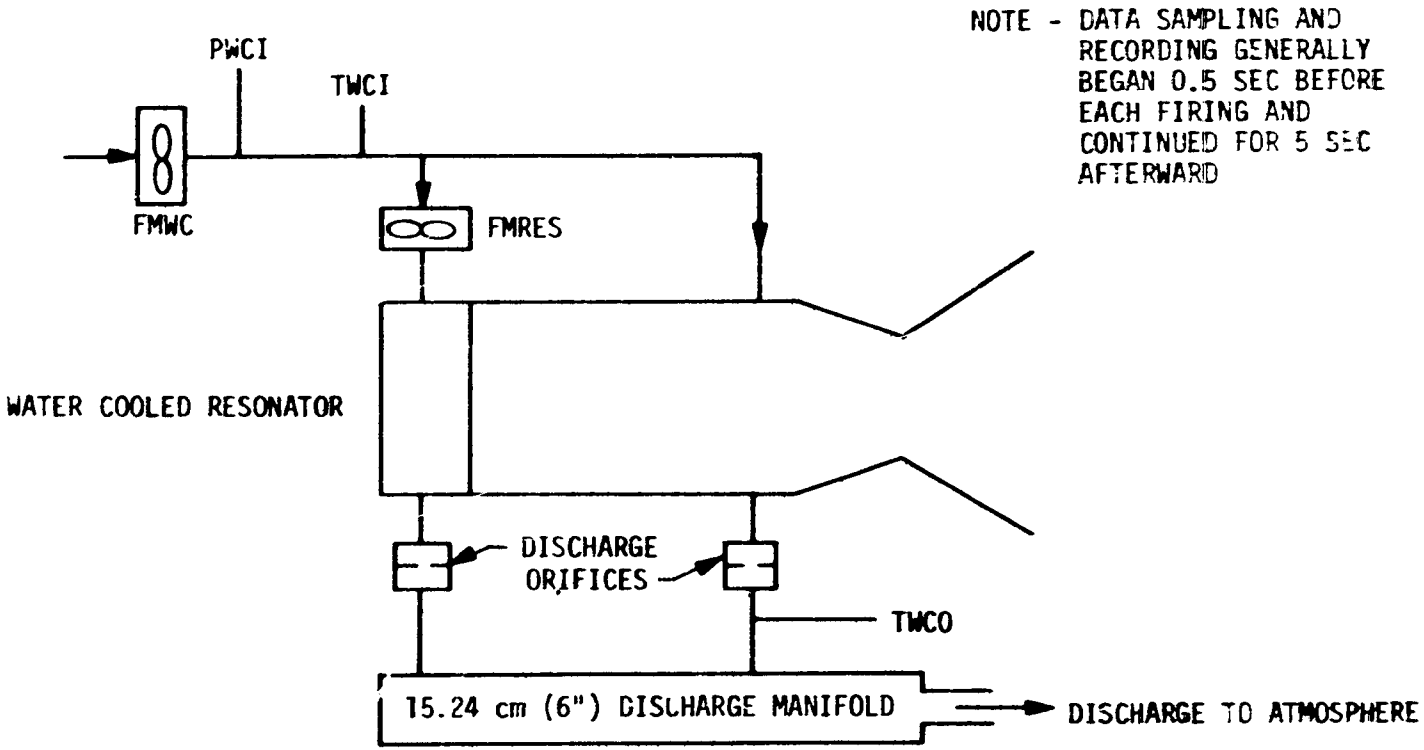

DATA REDUCTION PROCEDURE

CHAMBER COOLANT FLOWRATE = FMWC - FMRES

BULK TEMPERATURE RISE = $TWCO_{T} - TWCO_{(FS-2)\div5} + (TWCI_{(FS-2)+5} - TWCI_{T})$

CHAMBER HEAT FLUX = (CHAMBER COOLANT FLOWRATE) x (BULK TEMPERATURE RISE)

Figure 30. Instrumentation Schematic - NASA Water-Cooled Chambers

The steady-state non-firing temperature, $TWCO_{(FS-2)+5}$, was taken 5 seconds after the firing. Waiting for 5 seconds after the firing before taking the non-firing temperature provided a sufficient time period for monitoring the temperature to assure that non-firing steady state had been established.

When obtaining the coolant bulk temperature rise by comparing coolant exit temperatures at 2 different points in time, it is necessary to recognize that the coolant inlet temperature could also be changing with time. Normally, the coolant inlet temperature changed less than 0.5 or 1°K (1 or 2°F) during the course of a firing. However, this change was also accounted for in the data reduction. The resulting relationship used to determine the coolant temperature change was

$$\Delta T_c = TWCO_T - TWCO_{(FS-2)+5} + TWCI_{(FS-2)+5} - TWCI_T$$

b. Performance Series Heat Transfer Results

Performance tests with the NASA chambers were conducted at two chamber pressure levels: nominally at 7287 kPa (1050 psia) and at 12411 kPa (1800 psia). To allow injector-to-injector comparisons to be made and to put all the test data on a common basis, the data were adjusted to a pressure of 12252 kPa (1777 psia) using the relationship

$$Q \propto P_c^{0.8}$$

The 12252 kPa (1777 psia) value was selected because geometry differences (primarily throat diameters) between the NASA chambers and the calorimeter chamber made them thermally equivalent when the NASA chambers were at 12252 kPa (1777 psia) and the calorimeter chamber was at 13790 kPa (2000 psia). Use of these correlating pressures allowed for comparisons between the NASA chamber and the calorimeter chamber results to be made.

The results of the performance tests are given in Figure 31. This figure shows the total heat load (BTU's/sec) as a function of mixture ratio for both the PAT-2000 and TLOL-1200 injectors in 27.9 cm (11 in.) and 37.5 cm (15 in.) L' chambers. Results are given for operation with both ambient and hot fuel.

The data of Figure 31 are significant for several reasons. Somewhat surprisingly, the data clearly indicate that the chamber heat load is essentially independent of fuel temperature. Data points obtained with hot fuel and those obtained with ambient fuel all fall on the same heat load versus mixture ratio line. Initially it was assumed that hot fuel would produce early fuel vaporization and more rapid and intense combustion, thereby increasing the severity of the thermal environment in

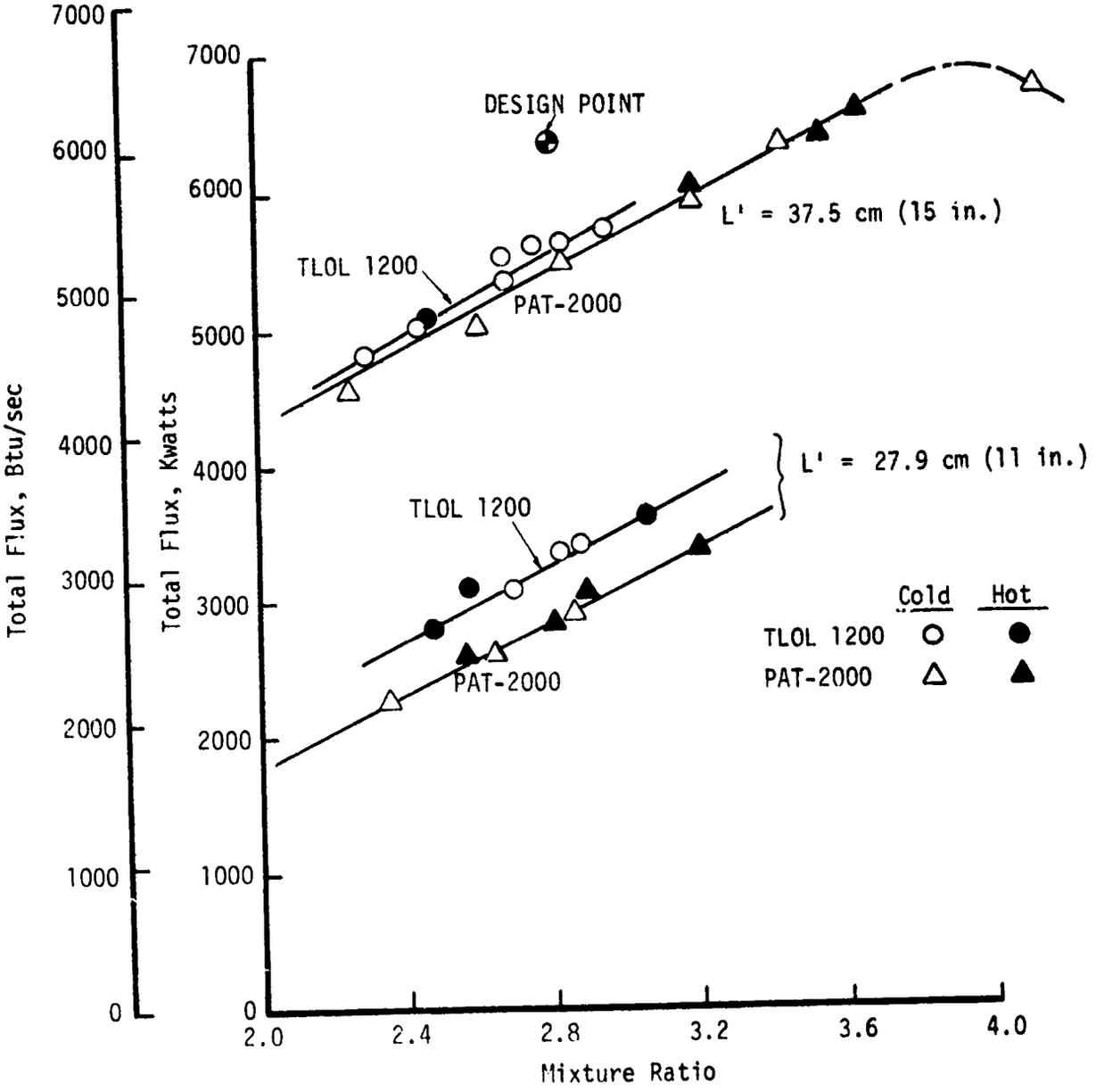

Figure 31. Tota Heat Load - NASA Water-Cooled Chambers

the chamber. However, the thermal data indicate that any changes in combustion which may have occurred as a result of the hot fuel had little effect on the chamber wall.

The data also show surprisingly little scatter. This not only indicates that the data are internally consistent, but also implies that the relationship $Q \propto Pc^{0.8}$ is valid inasmuch as it was used to bring all the data to a common reference condition. The agreement between the 6895 kPa (1000 psia) and 12411 kPa (1800 psia) results also would seem to indicate that either there is little or no soot affecting the thermal results or that, provided there is soot, the soot layer resistance is proportional to $Pc^{-0.8}$.

The PAT-2000 injector gives a somewhat lower heat load than the TLOL-1200 at the 27.9 cm (11 in.) length and nearly the same heat load at 37.5 cm (15 in.). This is generally consistent with the performance results which showed the TLOL-1200 to be slightly higher-performing than the PAT-2000.

The total heat load is very sensitive to the engine mixture ratio, with a linear relationship existing between heat load and mixture ratio over a mixture ratio range of 2.0 to 3.65. Only at the highest mixture ratio point tested (MR = 4.2) does the relationship become nonlinear. It is apparent that the heat load can be reduced very dramatically simply by decreasing the mixture ratio. The same effect can probably also be achieved by locally decreasing the mixture ratio at the wall, i.e., through the use of fuel film cooling.

An aspect of the data which has not been adequately explained is the very large difference in heat load between the 27.9 cm (11 in.) and 37.5 cm (15 in.) chambers. In the case of the PAT-2000, the additional 10.2 cm (4 in.) of cylindrical section increases the heat load by 2530 kwatts (2400 BTU's/sec). This more than doubles the heat load at the lower mixture ratios. It was predicted analytically that the added surface area would increase the total heat input by about 1054 kwatts (1000 BTU's/sec). This prediction was based on the assumption that the added chamber length would not impact the nozzle heat flux. The data indicate that this assumption is not valid and that the added 10.2 cm (4 in.) of cylindrical section produces an increase in the nozzle flux.

Figure 31 also shows a point labeled "DESIGN POINT." Prior to testing the NASA water-cooled chambers, a brief thermal analysis was conducted to evaluate the suitability of these chambers for use on the program. The total heat load predicted for the 37.5 cm (15 in.) chamber length is shown as the "design point." The measured heat load was about 15% lower than analytically predicted. The analytically predicted value was based on

the assumption of a clean (i.e., soot-free) wall. Thus, based on the total heat load data, it would be possible to hypothesize the existence of a low thermal resistance soot layer.

2. Calorimetric Chamber Heat Transfer Results

All of the calorimetric chamber testing was conducted with the 34.04 cm (13.4 in.) L' water-cooled calorimeter chamber with the PAT-2000 injector and heated fuel. As noted previoulsy, this chamber had 34 separately measured circumferential cooling circuits consisting of 2 or 3 channels per circuit. The engine had a separate water-cooled acoustic resonator.

a. Instrumentation and Data Reduction

A schematic diagram of the calorimeter chamber test configuration showing the heat transfer instrumentation is given in Figure 32. The total water coolant inlet flowrate (FMWC), pressure (PWCI), and temperature (TWCI) were measured. The inlet manifold supplied 35 separate coolant lines, 34 of which fed chamber cooling circuits and one of which supplied the water-cooled resonator. Five of the lines to the chamber and the line supplying the resonator contained turbine type flowmeters (FMWC-XX, FMRES). Each of the 34 cooling circuits contained a thermocouple in its discharge line (TWC-XX). Each cooling circuit also had a calibrated discharge orifice which operated in a cavitating mode at the chamber operating conditions. Fifteen of the chamber cooling circuits contained pressure transducers immediately upstream of the cavitating orifice (PWCC-XX). All of the cooling circuits discharged into the 6-inch diameter discharge manifold which normally operated at about atmospheric pressure. The mixed mean discharge temperature was measured (TWCD).

This experimental setup provided for redundancy in a number of key measurements. Each chamber cooling circuit had been separately flowed, with a Kw (flow coefficient) established for the circuit. This flow coefficient could be combined with the flow coefficient for the calibrated discharge orifice to obtain a flow coefficient ($\bar{K}w$) for the assembled circuit. Since all the discharge orifices flowed in a cavitating mode, the flow for each circuit could be calculated by using the inlet manifold pressure (PWCI) and the circuit flow coefficient ($\bar{K}w$). This provided a separate coolant flowrate for each of the 34 circuits. In addition, the flow in the 15 circuits which had transducers in their discharge lines (PWCC-XX) was calculated by using the discharge line pressure (PWC-XX) and the discharge orifice flow coefficient. As a result, 15 coolant circuits had redundant flow measurements. Furthermore, 5 of these 15 circuits had inlet flowmeters which provided another independent flowrate measurement and gave five circuits with double redundancy on flowrates. A final check on flowrates could be obtained

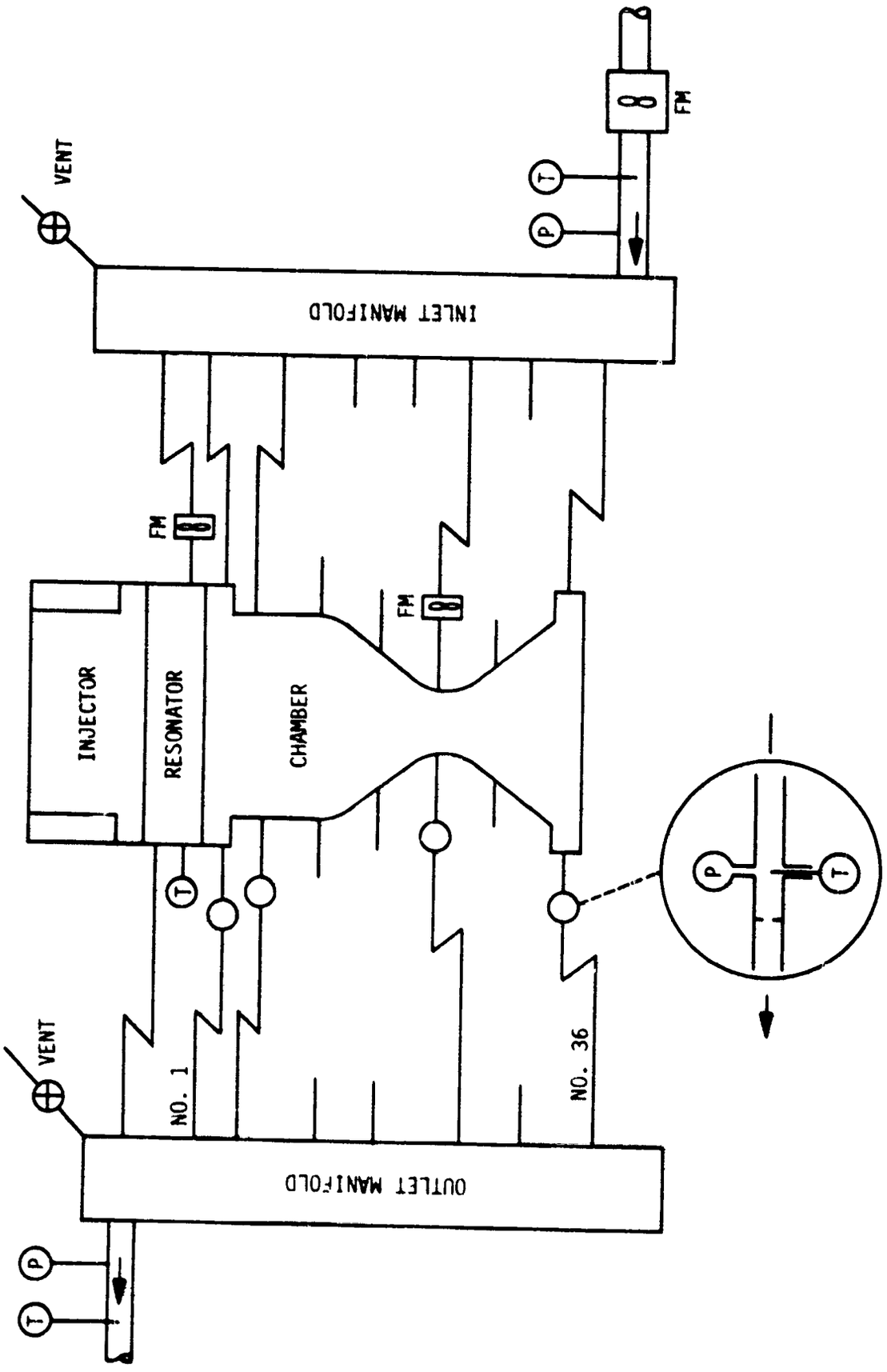

Figure 32. Calorimeter Chamber Flow and Instrumentation Schematic

by comparing the sum of the individual circuit flows with the total flow as measured by the inlet line turbine flowmeter (FMWC).

Though to a lesser extent, there also was redundancy in the heat flow measurements. The sum of the heat flows for the individual circuits could be compared with the total heat flow as determined by the total flowrate and mixed mean discharge temperature.

The data reduction followed the procedure outlined in the previous section for the NASA water-cooled chambers. Coolant temperature rises were determined on the basis of changes in discharge temperatures. It should be noted that in calculating the local heat fluxes, the heated area used for each circuit was simply the exposed hot-gas surface area. No corrections were made to account for axial conduction. Additionally, in determining the total heat load to the chamber, it was necessary to correct for the heat load to the water-cooled resonator since the mixed mean discharge coolant included the resonator coolant. To make this correction, the resonator heat flow was estimated by taking the projected surface area of the resonator and multiplying it by the heat flux in the first chamber circuit (located immediately adjacent to the resonator). The resonator thermal load calculated in this way was found to constitute only about 2% of the total measured heat input to the chamber.

b. Data Consistency

With the redundant measurements, it was possible to check the internal consistency of the data obtained during the calorimeter tests. This was done by (1) comparing the individual circuit flows as measured by the three different methods described in the previous subsection, (2) comparing the sum of the individual circuit coolant flows with the total measured flow, and (3) comparing the individual circuit heat loads with the total measured heat load.

Table VIII is a comparison of the water flow data from Test 085 for the 15 circuits on which redundant measurements were made. The three columns are 1) the flowrate found using the inlet manifold pressure and the effective Kw for the channels and orifice ($\dot{W}[\overline{K}]$); 2) the flowrate based on the pressure drop across the orifice (W [ORIFICE]); and 3) the flowrate from the flowmeter (W [FLOWMETER]). In general, the readings are in good agreement. The flowrates obtained using the orifice pressure drop are on the average 3% higher than those obtained using the inlet pressure, whereas the flowmeter values are 3% higher than the orifice values. In subsequent calculations, the flowrates used were the average of the measurements for each channel.

TABLE VIII. - INDIVIDUAL CIRCUIT FLOW DATA CONSISTENCY

TEST 085 (15 → 20 SEC)

CIRCUIT	W (R)		W (orfice)		W (Flow Meter)	
	kg/sec	(lbm/sec)	kg/sec	(lbm/sec)	kg/sec	(lbm/sec)
1	1.588	(3.55)	1.760	(3.88)	-	-
3	1.080	(2.38)	1.093	(2.41)	1.134	(2.50)
8	1.774	(3.91)	1.774	(3.91)	1.724	(3.80)
12	1.098	(2.42)	1.107	(2.44)	-	-
15	1.148	(2.53)	1.188	(2.62)	1.225	(2.70)
18	0.816	(1.80)	0.794	(1.75)	-	-
21	0.803	(1.77)	0.812	(1.79)	-	-
24	0.866	(1.91)	0.880	(1.94)	-	-
26	0.912	(2.01)	0.939	(2.07)	-	-
27	0.912	(2.01)	0.889	(1.96)	-	-
28	0.916	(2.02)	0.953	(2.10)	0.984	(2.17)
29	0.839	(1.85)	0.907	(2.00)	-	-
30	0.730	(1.61)	0.785	(1.73)	-	-
32	0.386	(.85)	0.467	(1.03)	0.463	(1.02)
36	0.544	(1.20)	0.576	(1.27)	-	-

Table IX is a comparison of total measured flowrates and the sum of the individual channel flowrates. Again, the data show good agreement, with the sum of the individual channel flows being consistently 3 to 4% lower than the total measured flow. Since the sum of the channel flows (Σ Circuits) is based primarily on the channel flowrates determined by using "R" (i.e., $\dot{W}[\bar{K}]$), the bias towards low flowrates shown in the individual channel measurements is also showing up here. In all likelihood, the $\dot{W}(\bar{K})$ values are low by about 3%, but the error is small. The source of the error is perhaps explainable in that the pressure drop of two hydraulic resistances closely coupled in series (chamber and orifice) is less than the sum of the two measured separately.

Table X presents a comparison of the total heat load determined on the basis of 1) a summary of the individual circuit heat loads and 2) the total flowrate and temperature rise. There is very close agreement between the two sets of values, but with Q (TOTAL FLOW) always being somewhat higher than Q (Σ Circuits). This is consistent with the bias seen in the coolant flow data where the summation of the individual flows was less than the measured total flow. The relatively large error (11%) in the Test 084, 8-5 ▸ 12.0 sec data period is probably partially due to the very small coolant temperature rise [~6°K (15°F)] in a number of the chamber circuits during that time.

Overall, the data were found to exhibit a high degree of consistency. No reason exists to question their validity.

c. Calorimeter Chamber Total Heat Load Data

The total heat load for the calorimeter chamber was determined on the basis of the measured total coolant flowrate and bulk temperature rise. In order to allow the results to be compared with results from the NASA chambers, 2 corrections were made. All of the calorimeter data were adjusted to a pressure of 13790 kPa (2000 psia) to account for the throat area difference between the NASA chambers and the calorimeter chambers. In addition, it was necessary to adjust the calorimeter data to account for the divergent nozzle geometry differences between the NASA and calorimeter chambers. The divergent nozzle of the NASA chambers expanded to an area ratio of 5.8 with a 15° half angle cone while the calorimeter chamber, which was designed to simulate a truncated high area ratio nozzle, expanded to an area ratio of 8.3 with a 40° half angle. It was determined analytically that the supersonic region thermal loads in the calorimeter chamber must be multipled by a factor of 1.93 in order to make them comparable to the NASA chamber values. This was done by taking the measured total heat load in the supersonic portion of the calorimeter chamber, obtaining a ΔQ by multiplying it by the factor of 0.93, and then adding this ΔQ to the total load as calculated

TABLE IX. - COMPARISON OF TOTAL COOLANT FLOWRATES

TOTAL FLOW

TEST	DATA PERIOD	FMWC - FMRES		Σ CIRCUITS	
		kg/sec	(lbm/sec)	kg/sec	(lbm/sec)
84	7.5 → 8.0	33.66	(74.2)	32.30	(71.2)
84	8.5 → 12	33.70	(74.3)	32.30	(71.2)
85	15 → 20	34.70	(76.5)	33.38	(73.6)

TABLE X. - TOTAL HEAT LOAD COMPARISON

TEST	DATA PERIOD	Q (TOTAL FLOW)		Q (Σ CIRCUITS)	
		k watt	(BTU/sec	k watt	(BTU/sec)
084	7.5 → 8.0	3515	(3334)	3502	(3321)
084	8.5 → 12.0	2767	(2624)	2790	(2362)
085	15 → 20	3989	(3783)	3895	(3694)

from the total flowrate and bulk temperature rise. The net effect of this adjustment to the data was to increase the total heat load for the calorimeter chambers by about 10% in each case.

Figure 33 shows the adjusted total heat load for the calorimeter chamber plotted as a function of mixture ratio. Also shown for comparison are the curves obtained with the same injector and the 27.9 cm (11 in.) and 37.5 cm (15 in.) NASA chambers. The calorimeter data, like the NASA chamber data, show very little scatter. The calorimeter chamber data are in excellent agreement with the NASA chamber data both in terms of magnitude and mixture ratio sensitivity. The data for the 34.04 cm (13.4 in.) calorimeter chamber lie almost midway between the 27.9 and 37.5 cm (11 and 15 in.) NASA chamber data. Using the NASA chamber data as a base, the total heat load to the calorimeter chamber could have been accurately predicted with a simple linear interpolation on chamber L'. The total heat load at the 2.8 mixture ratio point is about 5% below the predicted design point value based on the "clean wall" calorimeter chamber design analysis.

d. Local Heat Flux

The local heat flux data for the three different mixture ratio test points are given in Figures 34, 35, and 36. These figures show the heat flux as a function of axial position, with the chamber configuration and circuit number both identified on the abcissa. All the data shown are steady state. It should be noted that although the circuits were numbered to 36, the chamber had only 34 circuits. There were no circuits 4 and 5. Data were not obtained on every channel at each operating point due to thermocouple problems.

As the data of Figures 34, 35, and 36 show, the heat fluxes were in good agreement, exhibiting very little scatter. The slight discontinuity in flux between circuits 8 and 9 is the result of a change in channel geometry which produced axial heat conduction which was not accounted for in the data reduction.

Figure 37 is a composite plot of the data from Figures 34, 35, and 36. Figure 37 also shows the design heat flux for a mixture ratio of 2.8. This design heat flux assumes a "clean wall" and is based on "Cg" values obtained at NASA/LeRC with O_2/H_2. The experimental curves show the same strong dependence of heat flux on mixture ratio that was observed previously in the total heat load data. The variation in heat flux with axial location is significant. At the upstream end of the chamber, the heat fluxes are very low (approximately 1/3 of the design value) and independent of mixture ratio. This low heat flux condition only exists near the injector. Farther down the chamber, the measured heat flux increases to meet, and then

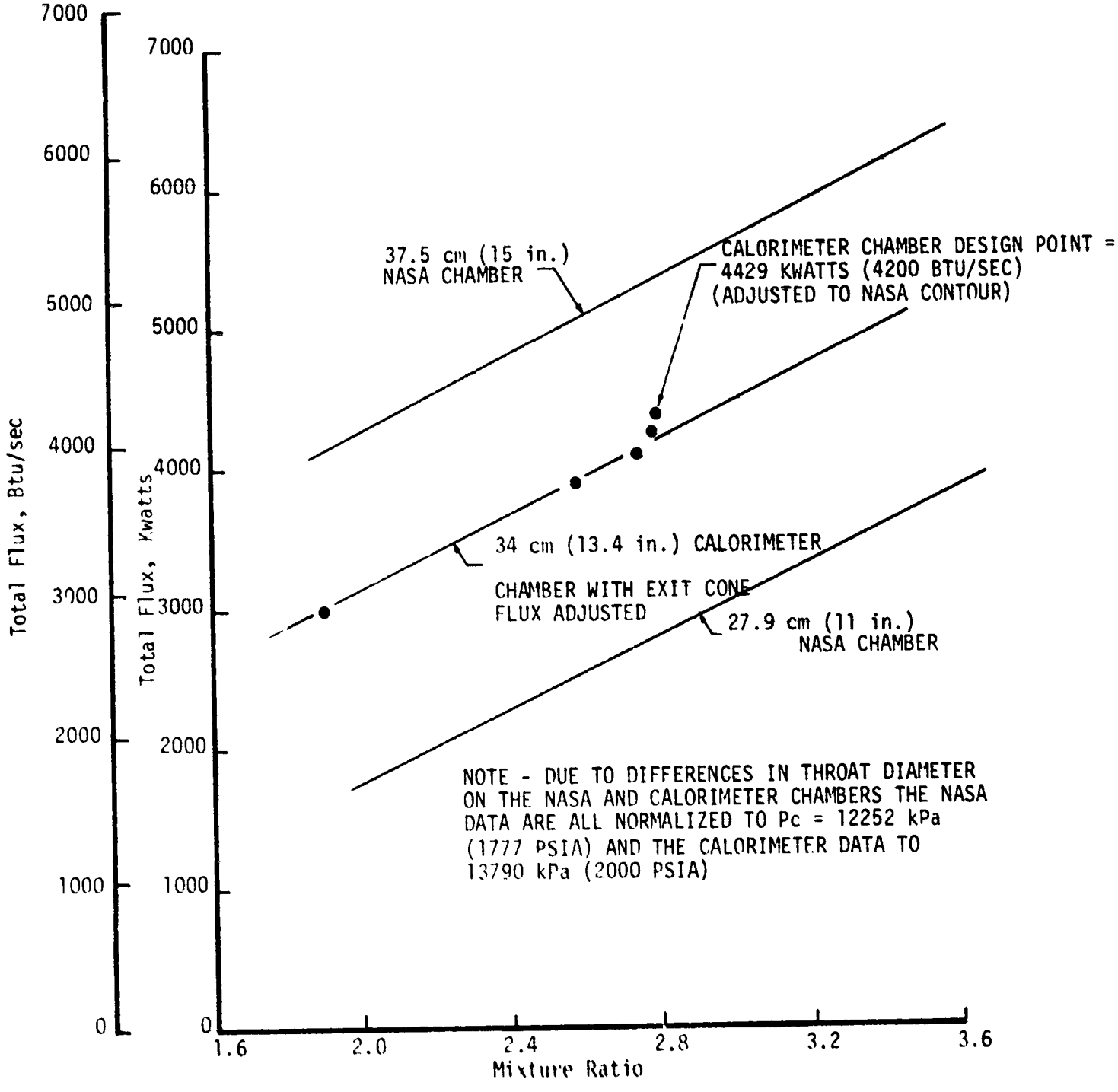

Figure 33. Comparison of Total Heat Load for NASA and Calorimeter Chambers

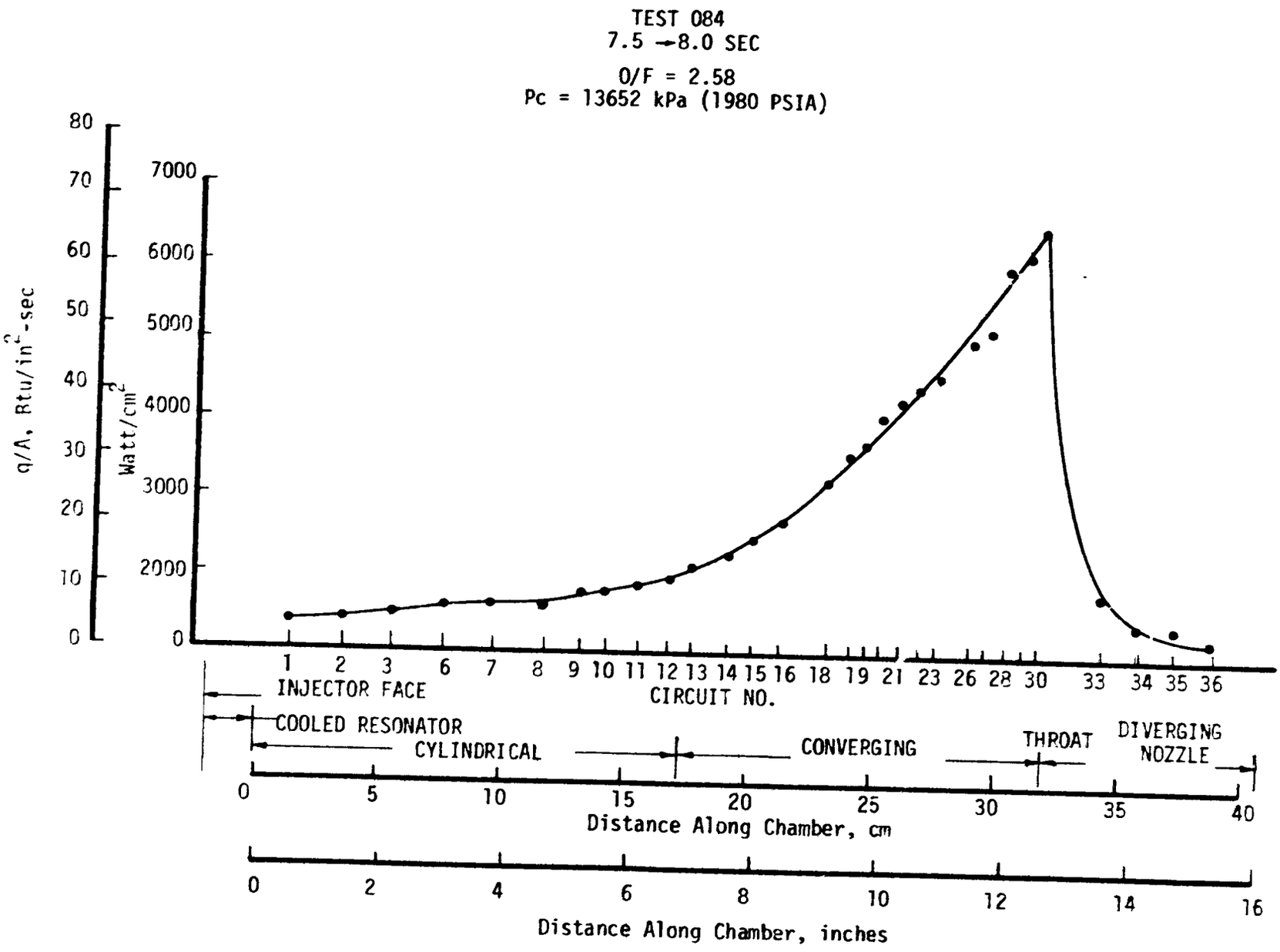

Figure 34. Test 084 Heat Flux, 7.5 to 8 Seconds

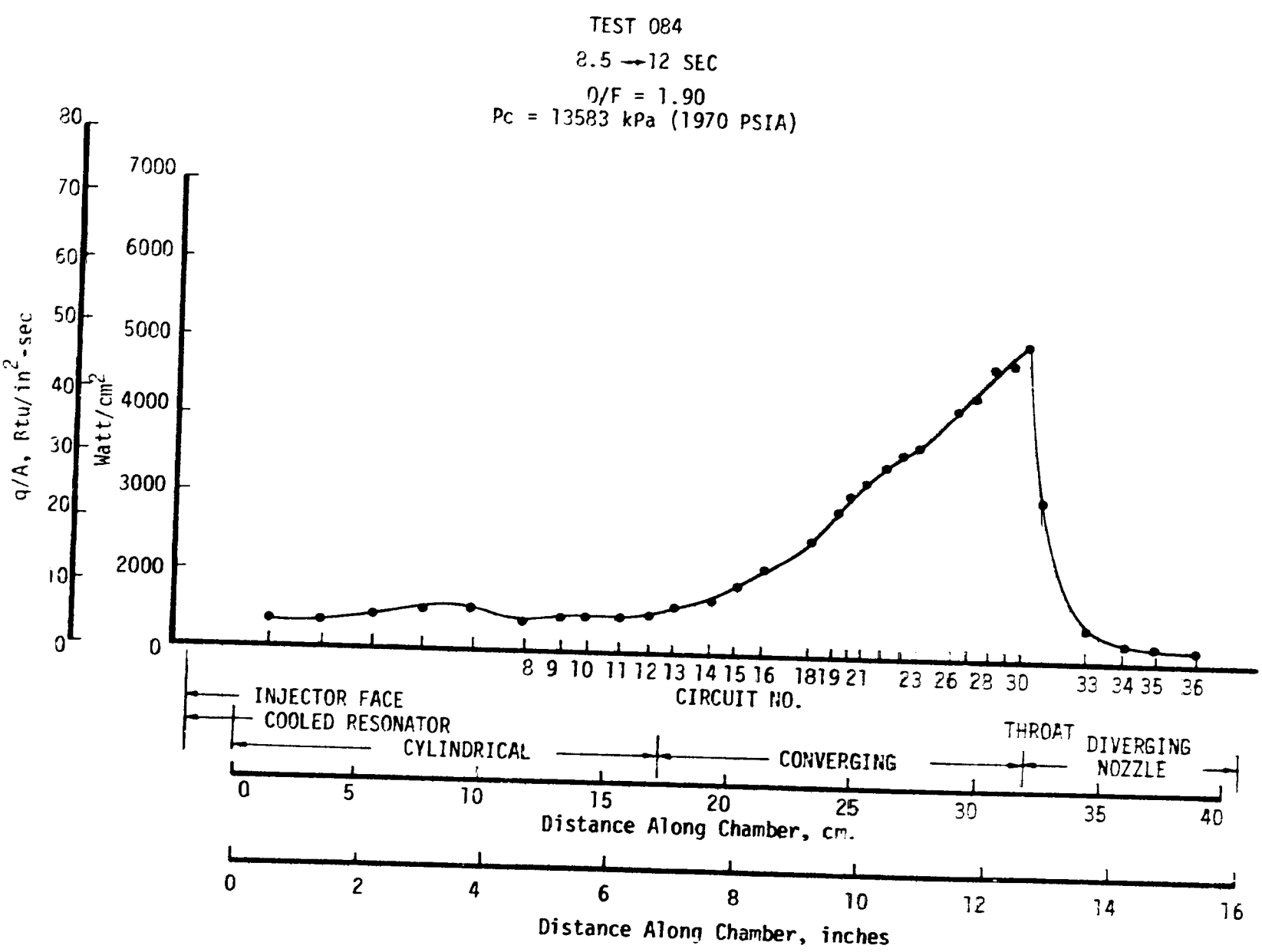

Figure 35. Test 084 Heat Flux, 8.5 to 12 Seconds

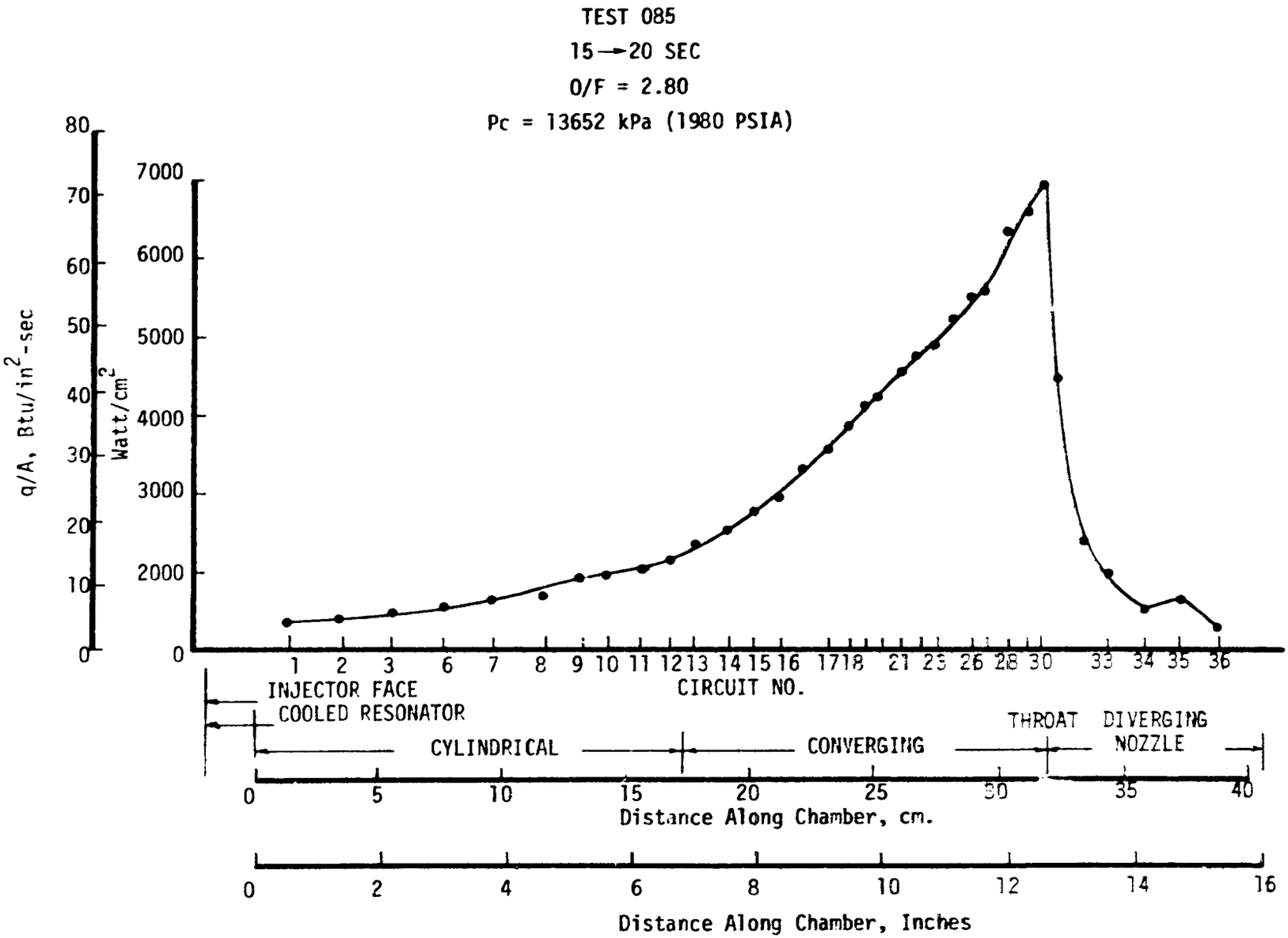

Figure 36. Test 085 Heat Flux, 15 to 20 Seconds

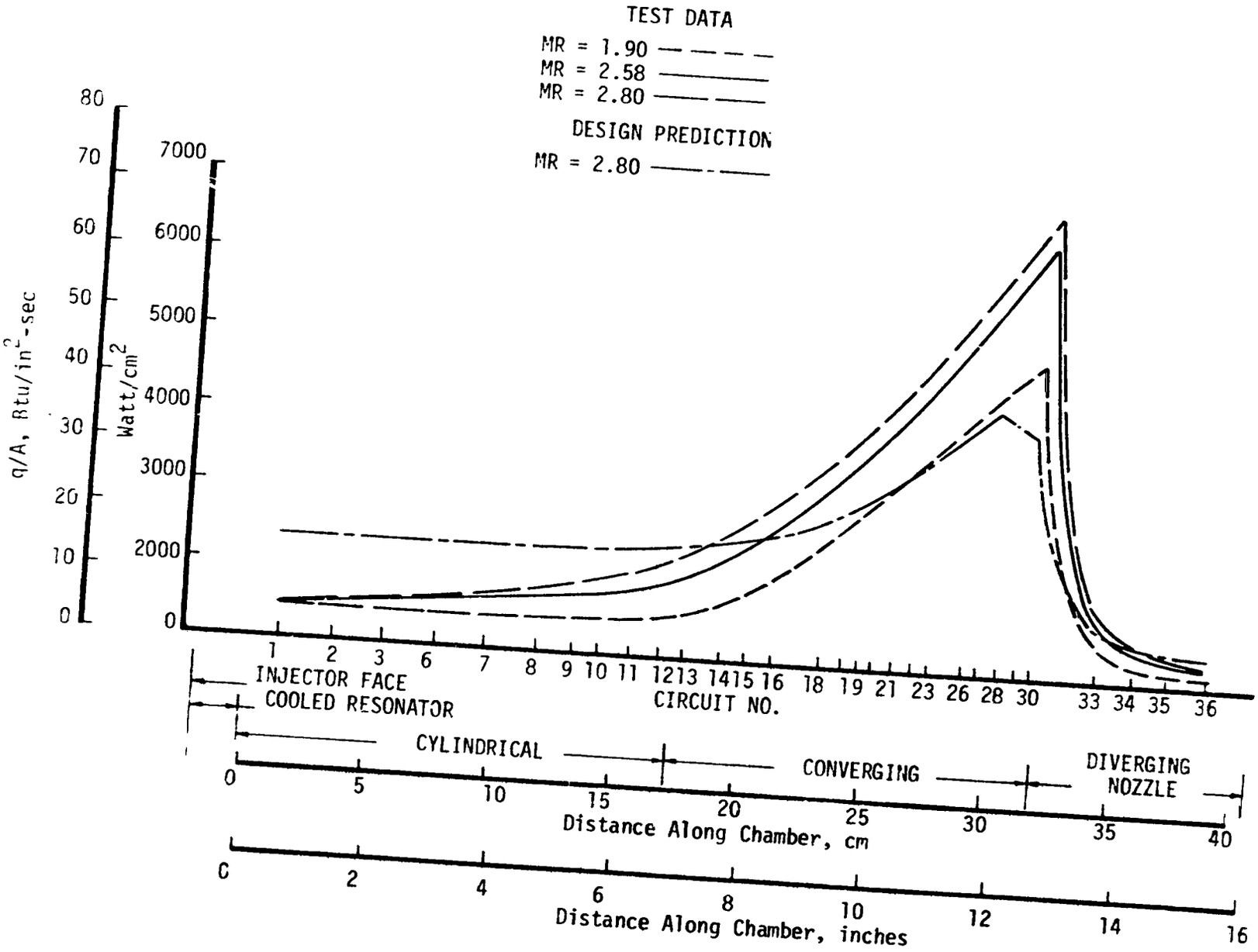

Figure 37. Effect of Engine Mixture Ratio on Heat Flux

exceed, the design values. At the throat, all three data lines are well in excess of the design curve, indicating a significant under-prediction of the throat heat flux. Downstream of the throat, the data lines drop off more rapidly than the design curve.

It was noted earlier that the predicted and measured total heat loads were in good agreement. Based on the above results, it is apparent that the accuracy of the design prediction of the total heat load was fortuitous. The over-prediction of the chamber heat loads was very nearly offset by the under-prediction of the throat heat loads, thus the two errors compensated for each other.

In assessing the differences between the predicted and actual heat flux profiles, both the over-prediction of the cylindrical section flux and the under-prediction of the throat flux must be addressed. One explanation for the low heat flux in the cylindrical section would be the existence of a soot layer which acts as a thermal barrier. The predicted flux curve was based on a clean wall, and the presence of any soot would normally be expected to decrease the heat flux. Correlations for soot layer effects such as those of Figure 43 indicate a maximum soot resistance where the combustion gas mass velocity is lowest, which, in this case, is in the cylindrical combustion chamber. Perhaps the most significant problem with the soot resistance explanation for the low chamber heat fluxes is the post-fire condition of the combustion chamber. Inspection of the chamber showed what appeared to be generally uniform soot deposits over the entire chamber and nozzle with the exception of the injector end of the chamber. The first 10.2 to 15.2 cm (4 to 6 in.) of the chamber had noticeably lighter soot deposits, with copper showing through the soot in some locations. Although it is possible that the soot pattern present in the chamber after a firing is largely the result of the shutdown transient, a more likely explanation of the low heat flux and minimal soot deposit is that propellant mixing is very limited near the injector such that the wall sees cold fuel vapors which undergo little cracking or thermal decomposition.

The much higher than predicted throat fluxes pose a more serious problem than the low chamber fluxes. Normally, the throat heat flux limits the maximum pressure capability and the cycle life of an engine. Throat heat fluxes approximately 70% above predicted present a significant problem for any high-pressure rocket engine. Several explanations for the high flux can be hypothesized. The most obvious explanation is that the design prediction was in error. In the design phase, the gas-side film coefficients were calculated using the following relationship:

$$h_g = 0.026\, C_g\, (Z)\, \rho_f\, U_e\, C_{pf}\, Re_f^{-0.2}\, p_{r_f}^{0.6}$$

$$= C_g\, (Z)\, DB_f\, \frac{1}{D^{1.8}} \left(W_T\, F_{2D}\, \frac{T_e}{T_f} \right)^{0.8}$$

IV, E, Heat Transfer Results (cont.)

with all properties evaluated at a film temperature (T_f) equal to the average of the recovery and wall temperatures. The C_g profile used is shown in Figure 38. It was developed from NASA data for a chamber with a much larger convergent angle (30°) than that tested herein (13°). These NASA data are included in Figure 38 at the corresponding Z/r_t in the convergent section and the same ratio on the nozzle. Also shown for comparison are recent OMS data ranges which show the same general trend.

The C_g profile derived from the test data for a mixture ratio of 2.8 is presented in Figure 39. This figure gives the area ratio and Cg as a function of axial location. Comparing the experimental C_g curve of Figure 39 with the design curve of Figure 38, it appears they are almost complementary, i.e., the design C_g is high where the experimental values are low, and vice versa. As noted before, the low injector end C_g's are probably injector-produced. Obviously, the design C_g curve, even though based on experimental data, does not describe what is occurring in the convergent section or throat. The use of a constant C9 correlation such as that of Bartz* would have come much closer to predicting the results.** However, this still would have resulted in an under-prediction of the throat flux. At this time, there is no generally accepted C_g profile which would predict the data of this program.

It is also possible that there was a soot layer in the throat which acted to increase rather than decrease the heat flux. This would happen when the wall roughness caused by carbon deposition reduces the resistance of the hot-gas boundary layer more than the presence of the carbon increases the wall resistance. This particular mechanism would be peculiar to high-pressure, low-thrust engines where the boundary layer laminar sublayer is very thin. Carbon deposits which appear hydraulically smooth in engines such as F-1 and Titan I could be rough in engines of the configuration tested in this program. NASA/LeRC data*** for slightly thicker sublayers indicate that a heat flux enhancement of 20-30% might occur in this way. However, the required 70% enhancement appears unreasonable with only this mechanism involved.

---

*Bartz, D.R., "A Simple Equation for Rapid Estimation of Rocket Nozzle Convective Heat Transfer Coefficients," Jet Propulsion, January 1957.

**Interestingly, the data used by Bartz to substantiate his correlation give a peak C_g of about 1.25 to 1.30 slightly upstream of the throat, much the same as the data from this program.

***Reshotko, M., et al., "Heat Transfer in a 60° Half-Angle of Convergence Nozzle with Various Degrees of Roughness," NASA TN D-5887, July 1970.

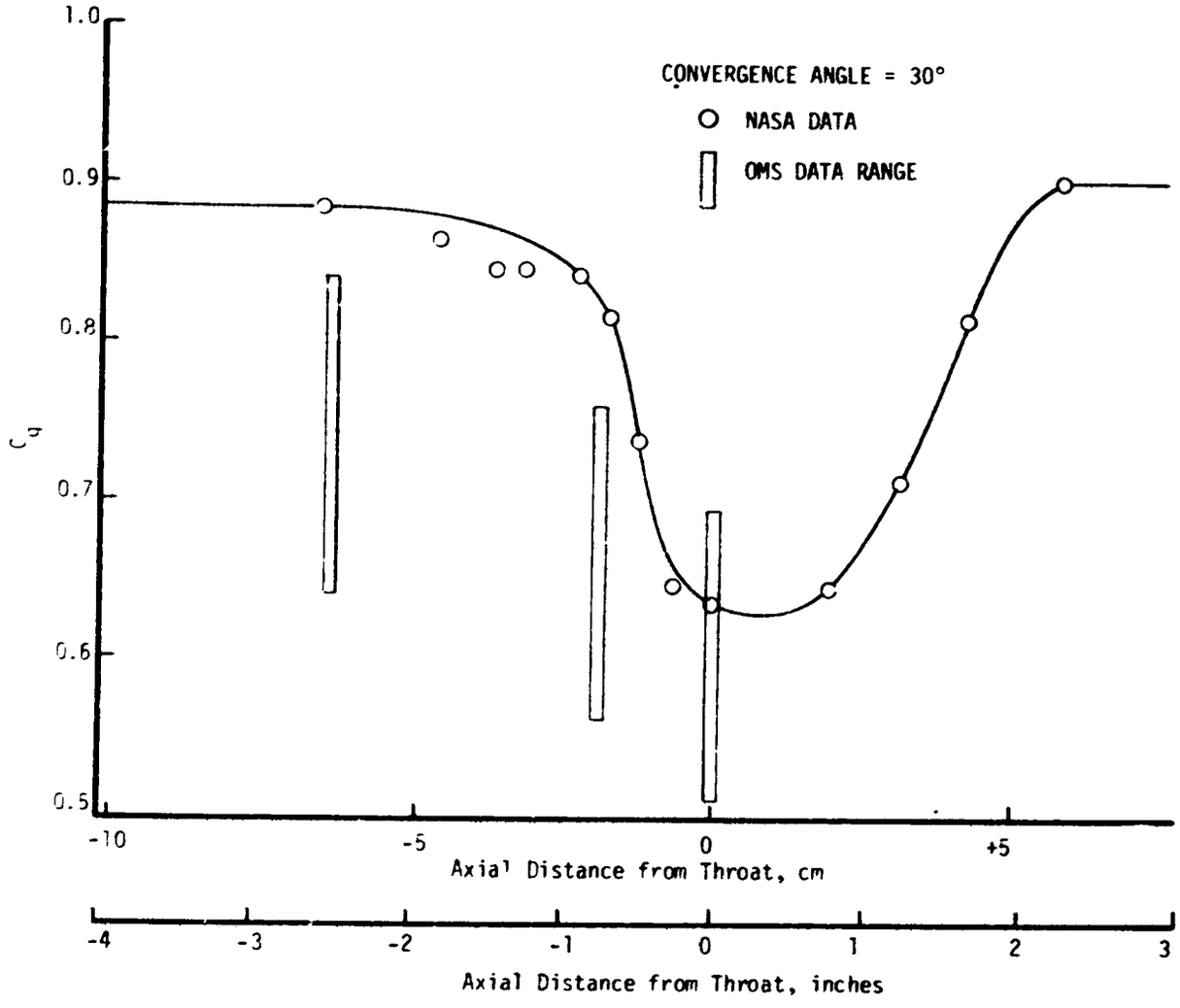

Figure 38. Design Gas-Side Heat Transfer Coefficient Correlation

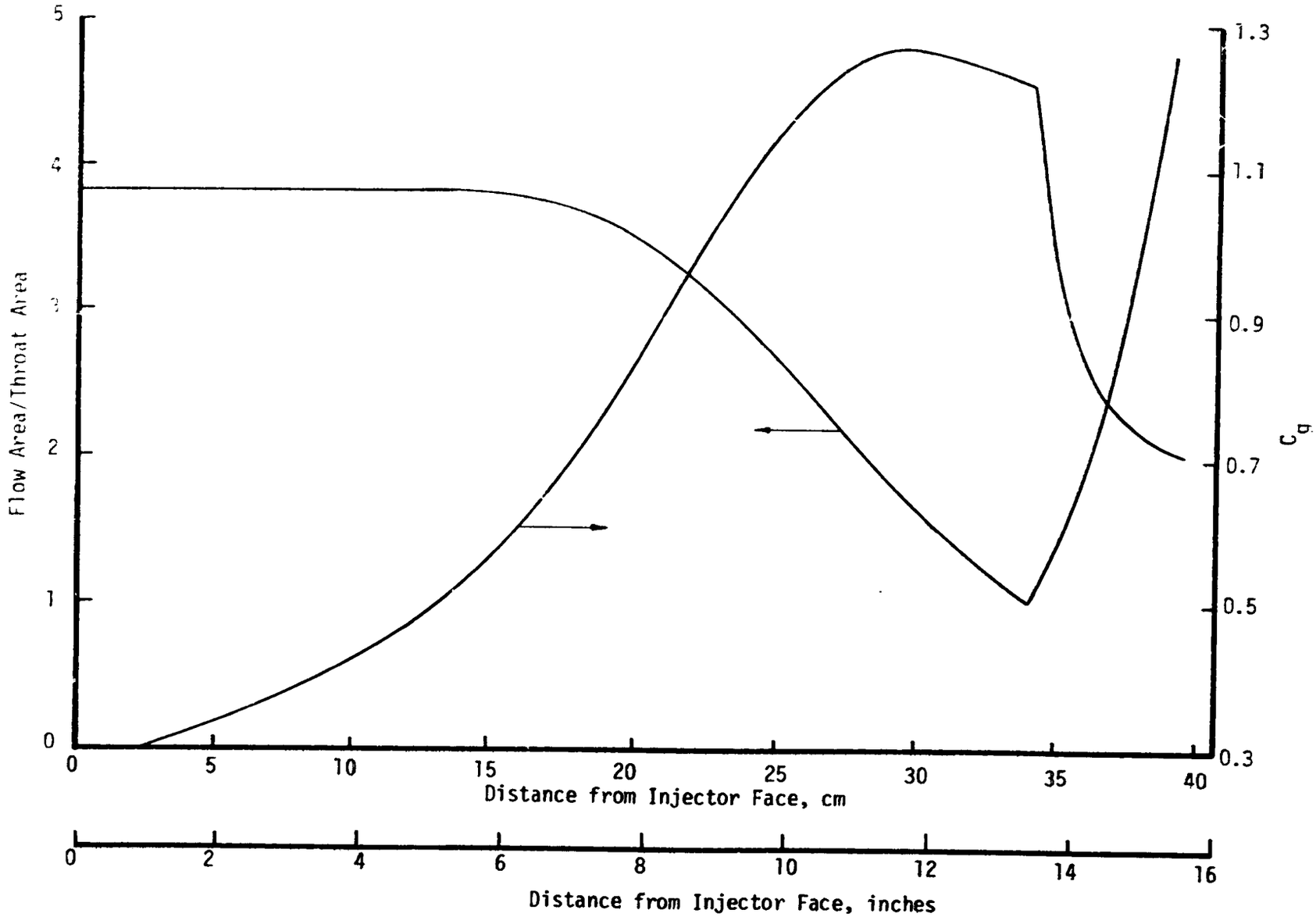

Figure 39. Experimental Gas-Side Heat Transfer Coefficient Correlation

Additional discussion of the heat transfer results and possible explanations for the differences between the predicted and measured values is given in Section IV,E,4.

3. Interrelationship Between Combustion Performance and Heat Transfer Analyses

The heat transfer data obtained with the NASA water-cooled chambers and the calorimeter chamber were evaluated to determine what insight they would provide into the combustion process and, conversely, what insight the performance modeling might provide into the heat transfer results. A key element in this analysis was the conclusion (based on the performance data) that the combustion process with the PAT and TLOL injectors is mixing-limited. This allowed the use of results obtained on Contract NAS 3-14379 with gas-gas propellants. Combustion with gas-gas propellants is inherently mixing-limited. The extensive cold-flow and hot-fire testing on Contract NAS 3-14379 showed that the gases within an incompletely mixed combustion chamber can be approximated by a pair of streamtubes, one fuel-rich and one oxidizer-rich. The mixture ratio of these streamtubes can be related to the overall test mixture ratio by the mixing efficiency, E_m, as follows:

$$O/F\ (\text{Fuel-Rich}) = E_m \times (O/F)_{\text{overall}}$$

$$O/F\ (\text{Oxid-Rich}) = (O/F)_{\text{overall}}/E_m$$

With the two-streamtube, mixing-limited model, the first question to be raised is which streamtube (fuel-rich or oxidizer-rich) is representative of the environment at the wall. While neither the PAT or TLOL patterns provided any film cooling, both were designed to yield a fuel-rich bias at the wall. The post-fire condition of the chambers showed the walls to be soot-free or lightly sooted near the injector and rather uniformly but not heavily sooted over the remainder of the chamber. By itself, this could be interpreted two ways: either the wall was oxidizer-rich near the injector and became fuel-rich several inches downstream, or else it was fuel-rich from the injector all the way to the exit but with temperatures so low near the injector that the fuel was not hot enough to form soot. Thus the chemical environment at the wall could not be established conclusively from visual inspection of the chamber.

The heat transfer data give a more positive indication of the wall environment. The total heat load data obtained with both the PAT and TLOL injectors with the NASA water-cooled chambers and those obtained with the PAT with the calorimeter chamber all indicate the average wall environment to be fuel-rich. A plot of this data is given in Figure 31. It shows the wall compatibility to be a strong function of mixture ratio, with the flux

increasing with increasing mixture ratio. This is typical of a fuel-rich wall environment. The calorimeter chamber data of Figure 37 provide further support to this conclusion. These data show that, at every axial station, the heat flux increases monotonically with O/F, indicative of a wall that is fuel-rich from the injector face through the nozzle exit plane. Based on these results, it is concluded that the fuel-rich streamtube is characteristic of the wall environment.

The two-streamtube model allows a more quantitative assessment of the heat transfer results. The performance anlaysis indicated an E_m = .73 for the PAT-2000 and an E_m = .82 for the TLOL-1200. Given these values, the model would state that the TLOL and PAT injectors have the same wall environment when the PAT mixture ratio is reduced by a factor of .73/.82 = .89. When this is done to the data of Figure 31, the 27.9 cm (11 in.) chamber data are found to correlate very well, i.e., the PAT and TLOL data are coincident. However, this correlation over-corrects the 37.5 cm (15 in.) chamber length data.

The compatibility-mixture ratio relationship can be examined with this model. The PAT-2000 was tested in the 37.5 cm (15-in.) chamber with hot fuel at a mixture ratio of 4.14, the highest mixture ratio tested. This is the only point which seems to be beyond the peak heat flux mixture ratio which appears to occur around 3.9 with the PAT-2000 injector. The corresponding PAT-2000 wall mixture ratio at the peak heat flux is 2.85, i.e., .73 x 3.9, which is consistent with analytical predictions.

4. Observations

The heat transfer data generated in this program contained some fairly significant "surprises." These unanticipated results, the possible mechanisms which produce them, and a condensed discussion of each are summarized in Table XI.

The high heat fluxes in the throat region are probably due to the combined effects of soot deposit roughness, chemical reactions in the boundary layer, and lower-than-predicted flow acceleration. As noted previously, the C_g data of Figure 38 are for a 30° convergent angle; they exhibit a large C_g depression in the throat region due to flow acceleration. A smaller C_g depression can be expected for the 13° convergent angle tested in this program and would explain the presence of the peak heat flux at the throat instead of the upstream location predicted.

A plot of $D^{1.8}$ (q/A), which eliminates the diameter effect from the heat flux, is shaped like the C_g curve of Figure 39 and indicates a region of high relative heat flux upstream of the throat. It is of interest to note that the start of this region corresponds closely to the intersection

TABLE XI. - POSSIBLE MECHANISMS INFLUENCING HEAT TRANSFER

UNPREDICTED TEST RESULT	HYPOTHETICAL MECHANISM	DISCUSSION	POTENTIAL EFFECT
High q/A in throat region	(1) Carbon deposit increases surface roughness	Surface roughness increases h_g assume 200-300 % in.	20-30%
	(2) Chemical reactions in the boundary layer	Use enthalpy differential to predict heat flux	40%
	(4) Flow acceleration effects reduced; little or no η_g dip	convergence angle 13° vs 30° for η_g data. Max q/A at throat instead of upstream	40%
	(4) High energy release in convergent section due to intraelement mixing	Data indicate $D^{1.8}$ (q/A) high downstream of outer element ψ intersection with wall	25%
	(5) Carbon particle penetration of boundary layer in convergent section	low particle velocity and 13 wall angle minimize effect	15%
	(6) γ/B flow effects negligible at throat	I_{sp} and η_{c^*} increased for F-F vs F-O flow	7%
	(7) Radiation	Carbon particle temperatures not high enough to be significant	3%
Throat q/A dependent on O/F	(1) Wall O/F low due to poor mixing. Adiabatic wall temperature increases with wall O/F	$(O/F)_w = f_m (O/F)_{overall}$ at throat based on existing mixing model	Approximates data variation
Low q/A at head end of chamber	(1) Fuel film cooling of a very fuel rich barrier	consistent with injector element configuration. Carbon deposits at head end promoted by low temps.	Agreement with data
	(2) Reduced [illegible] mass velocity	Swirl flow not included in predictions.	25-30% 3 in. from injector
	(3) Carbon [illegible] at head end	Physical carbon ejection at head end	N.A
	(4) [illegible] due to low fuel [illegible]	Inconsistent with observed [illegible] effects	N.A
Decreasing L* from 2.9 cm to 1.5 cm (for F-O) reduced total [illegible]	(1) Less mixing effect exists further into convergent section of shorter chamber	Demonstrated by heat profile or calorimeter chamber. Predicted 20% reduction with no effect on convergent section.	0-100% of observed effect

with the wall of a line drawn parallel to the axis from the center of the outer injector elements. A region of increased wall mixture ratio can be expected downstream of this intersection if the outboard fuel flow tends to mix with the entire oxidizer flow from these elements. Since the wall mixture ratio in other axial regions is considered to be fuel-rich, as discussed previously, a local perturbation in mixture ratio as postulated here can increase the heat flux. The potential 25% effect noted in Table XI is based on varying the wall mixture ratio from the 2.04 (see below) to that which gives the maximum heat flux for an overall O/F of 2.8; this effect is significantly larger than the observed increase in $D^{1.8}$ (q/A).

Carbon particle impingement, two-dimensional flow uncertainties, and radiation are not considered to be significant factors in explaining the high convergent section heat fluxes. Particle impingement data directly applicable to nozzle convergent sections are not available. Low particle velocities and the small convergence angle should minimize particle impingement effects.

A significant reduction in all heat fluxes is observed in Figure 37 as the test mixture ratio was reduced from 2.8 to 1.9. The percentage reduction in throat flux can be predicted if the wall mixture ratio is considered to be fuel-rich consistent with the injector element orientation and the mixing efficiency, E_m, is inferred from the performance data. As noted previously, the combustion and thermal compatibility model developed for mixing-limited propellant systems on Contract NAS 3-14379* indicates that the wall mixture ratio at the throat can be calculated as follows:

$$(O/F)_{wall} = E_m\,(O/F)_{overall}$$

Since the PAT-2000 performance data yield an E_m of 0.73, the wall mixture ratios at the throat for the calorimeter chamber tests range from 1.39 to 2.04. Predicted heat fluxes for this range increase significantly with mixture ratio because of the large increase in adiabatic wall temperature. This is illustrated in Figure 40. This figure also shows that the effect of mixture ratio on heat flux cannot be predicted with an E_m of unity.

*Calhoon, D.F., Ito, J.I. and Kors, D.L., "Investigation of Gaseous Propellant Combustion and Associated Injector/Chamber Design Guidelines," (Final Report) and "Handbook for Design of Gaseous Propellant Injectors and Combustion Chambers," NASA CR-121234, 31 July 1973.

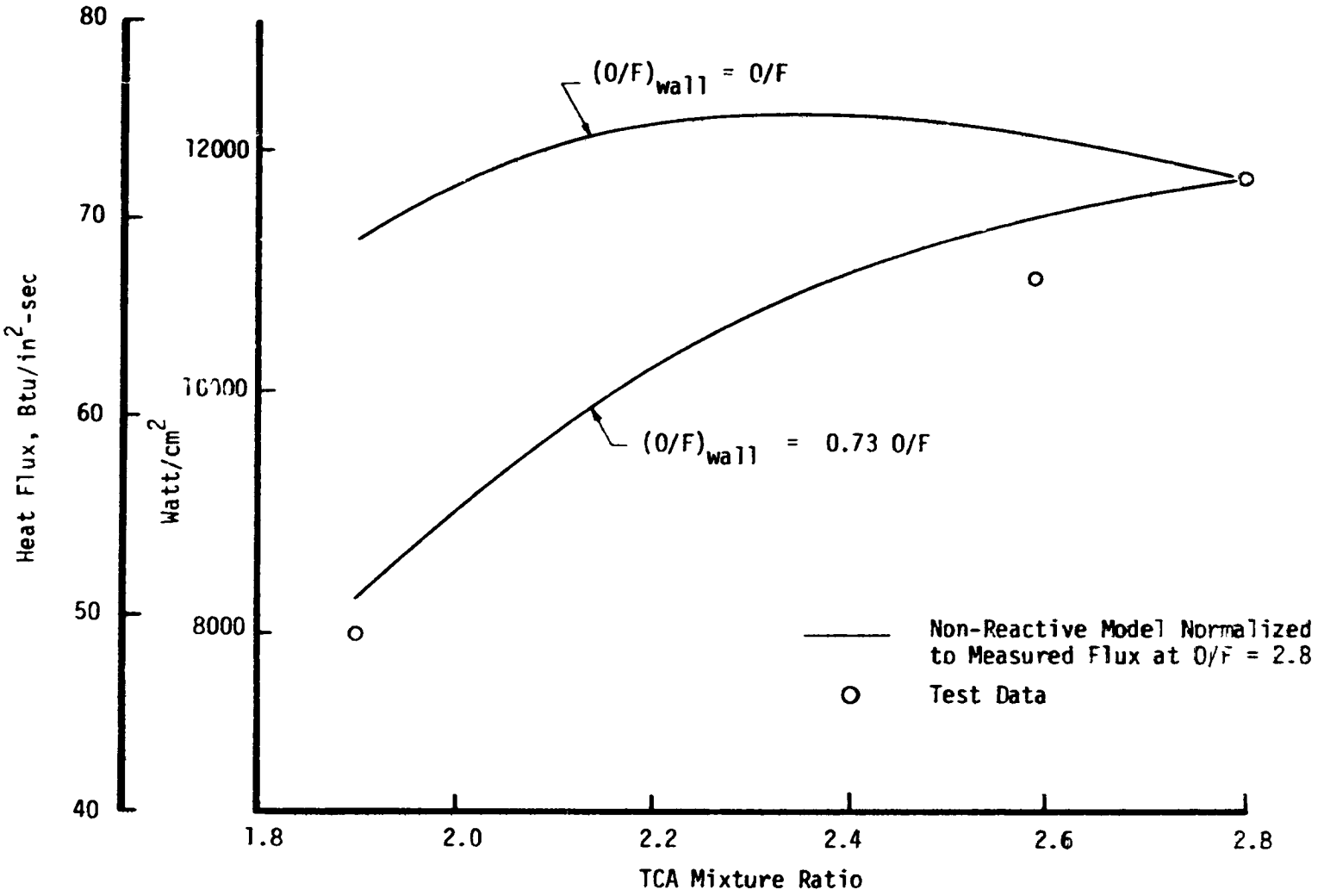

Figure 40. Effect of Mixture Ratio on Throat Heat Flux

The key observation in Table XI is that all heat flux and total heat load trends can be explained by the presence of a fuel-rich zone along the wall, analogous to having fuel film cooling at the injector end, with a gradual axial increase in wall mixture ratio as the propellants mix. In addition to explaining the mixture ratio trends observed at all stations in the calorimeter chamber, this hypothesis accounts for the large axial variations in heat flux relative to predictions for a uniform mixture ratio. Since the wall mixture ratios would be reduced in the convergent section of a shorter chamber, the large reductions in heat load with decreasing L' (Figure 33) are also explained.

The validity of the hypothesis that the thermal results, to a large extent, reflect the propellant mixing profile can be assessed using the experimental heat flux data. Figure 41 shows the axial variation of the wall mixture ratio inferred from the heat flux data for a test mixture ratio of 2.8, assuming a uniform C_g with the wall mixture ratio at the throat equal to 2.04 as defined above. Wall mixture ratios below 1.2 were not calculated because of the need to account for kinetic effects in the thermochemistry model. The first part of this mixture ratio axial profile is consistent with the film cooling model of Rousar and Ewen* assuming the film coolant is the fuel flow from the peripheral fuel orifices plus a small fraction of the outer element oxidizer, thereby lending credibility to the mixing/heat transfer relationship hypothesis. Increased mixing rates and a wall mixture ratio perturbation are observed in the region noted previously where the oxidizer flow from the outer row of elements can impinge on the wall. This perturbation in inferred mixture ratio would be eliminated if a small C_g depression were assumed in the throat region. The thermal model used in Figures 40 and 41 defines the gas-side heat transfer coefficient as before, but all properties are now evaluated at the wall mixture ratio as follows:

$$h_g = C_g\,(Z)\quad DB_f\,(MR_w)\,\frac{1}{D^{1.8}}\left(W_T\,F_{2D}\,\frac{MW_w}{MW_e}\,\frac{T_e}{T_f}\right)^{0.8} \qquad \text{(Eq. 1)}$$

In addition, the adiabatic wall temperature is that associated with the wall mixture ratio. Figure 42 shows the variation of DB and adiabatic wall temperature with mixture ratio.

Low effective mass velocities due to the finite atomization and vaporization rates of the propellants also contribute to the reduction in heat fluxes over the first 10.2-12.7 cm (4-5 in.) of the chamber. This effect was analyzed early in the program but was not included in the heat flux predictions.

5. Soot

The existence of a soot or carbon layer on the hot-gas chamber surface of hydrocarbon-fueled liquid rocket engines has been

*Rousar, D.C. and Ewen, R.L., "Combustion Effects on Film Cooling," NASA CR-135052, 24 February 1977.

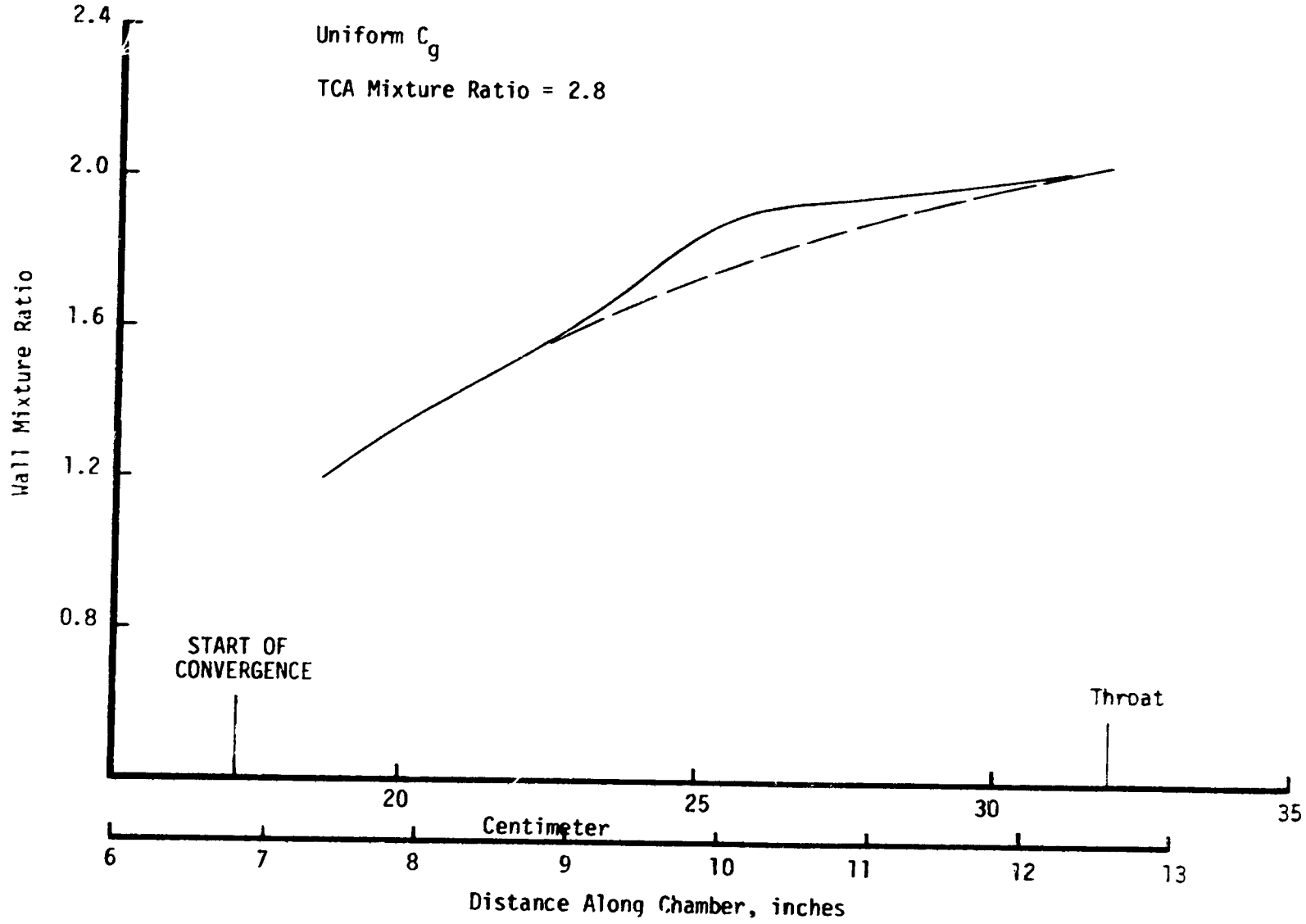

Figure 41. Wall Mixture Ratio Profile Inferred From Heat Flux Data

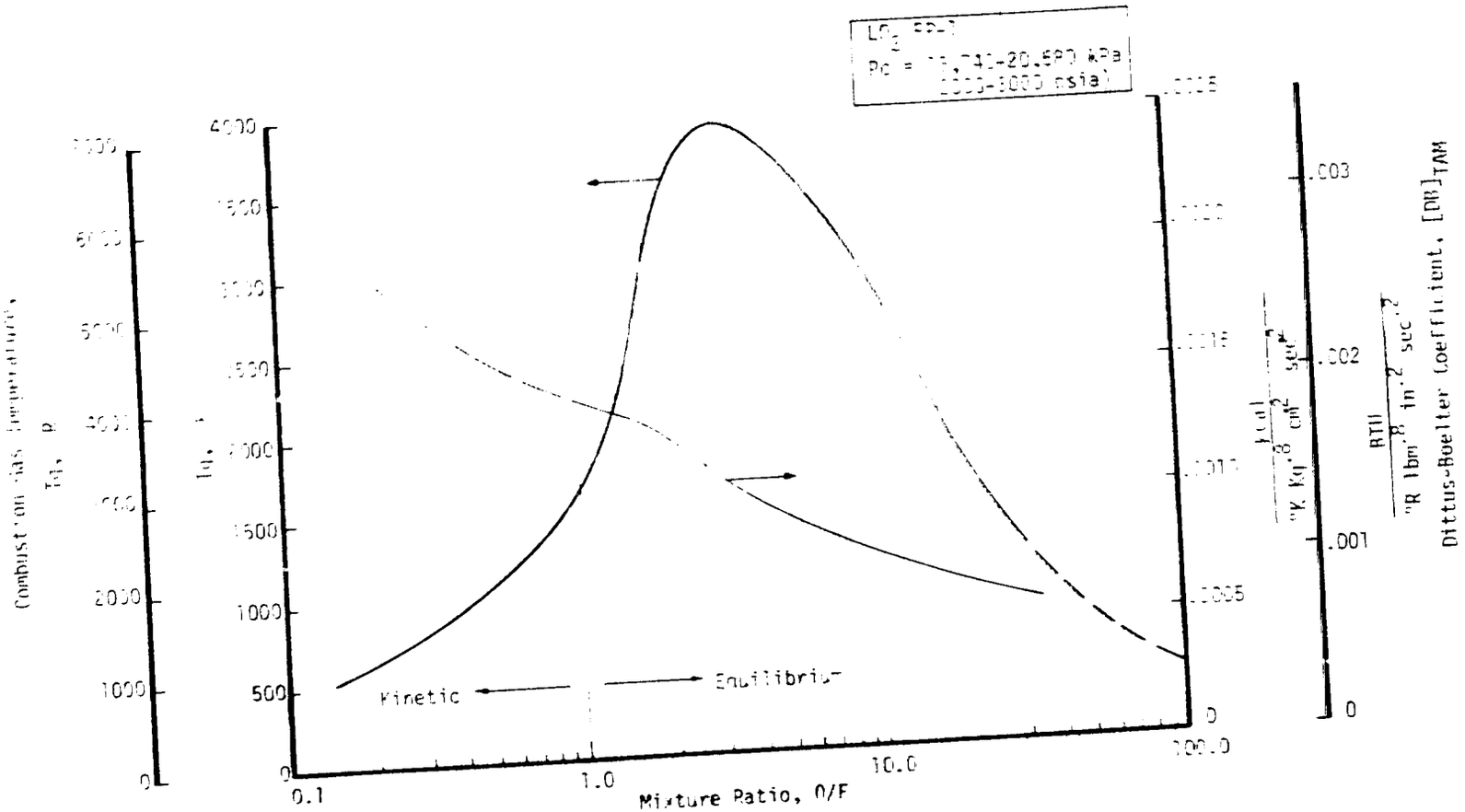

Figure 42. LO_2/RP-1 Thermal Transient Properties are Mixture Ratio Dependent

generally accepted. This soot layer is thought to act as a thermal barrier, reducing the heat flow into the wall. Wall surface thermocouples have measured oscillatory surface temperatures which have been explained as the buildup and spalling-off of a carbon layer. Correlations (such as that given in Figure 43) have been developed which relate the soot layer resistance to the combustion stream properties. Historically, the key question for the rocket chamber thermal designer has not been the existence of a soot layer, but, rather, its thermal resistance and how this resistance might be considered in the chamber thermal design.

One of the goals of this program was to investigate the effect of soot. The data from this program indicate no soot thermal barrier developed, even in tests up to 32 seconds duration. As noted previously, only in the cylindrical section of the chamber was the heat flux lower than the predicted clean wall flux, and this was the portion of the chamber with the thinnest soot deposit. With both the converging section and throat heat fluxes higher than predicted, it is difficult to hypothesize any appreciable thermal barrier being present.

The test data were also reviewed to determine if they contained any time dependence which might suggest either a buildup or buildup and loss of a soot layer. No such time dependence was found. Both the chamber as a whole and the individual circuits quickly established a steady-state condition which changed only when the operating mixture ratio changed.

Soot layer changes could, of course, have been occurring on a very localized basis which would not be detectable by coolant temperature rise measurements if the localized areas were small and occurred at random locations on the chamber wall.

As part of Contract NAS 3-21381*, relationships were developed which expressed the soot layer thermal resistance as a function of the combustion gas properties. The equation for LOX/RP-1 at a mixture ratio of 2.8 is as follows:

$$\frac{X}{K} = e^{9.0 - .51G}$$

where:

$\frac{X}{K}$ = soot resistance (in.^{2}-sec-°R/BTU)

G = gas stream mass flux (lbm/in.^{2}-sec)

*"Investigation of Advanced Cooling Technique for High-Pressure Hydrocarbon-Fueled Engines," NAS 3-21381.

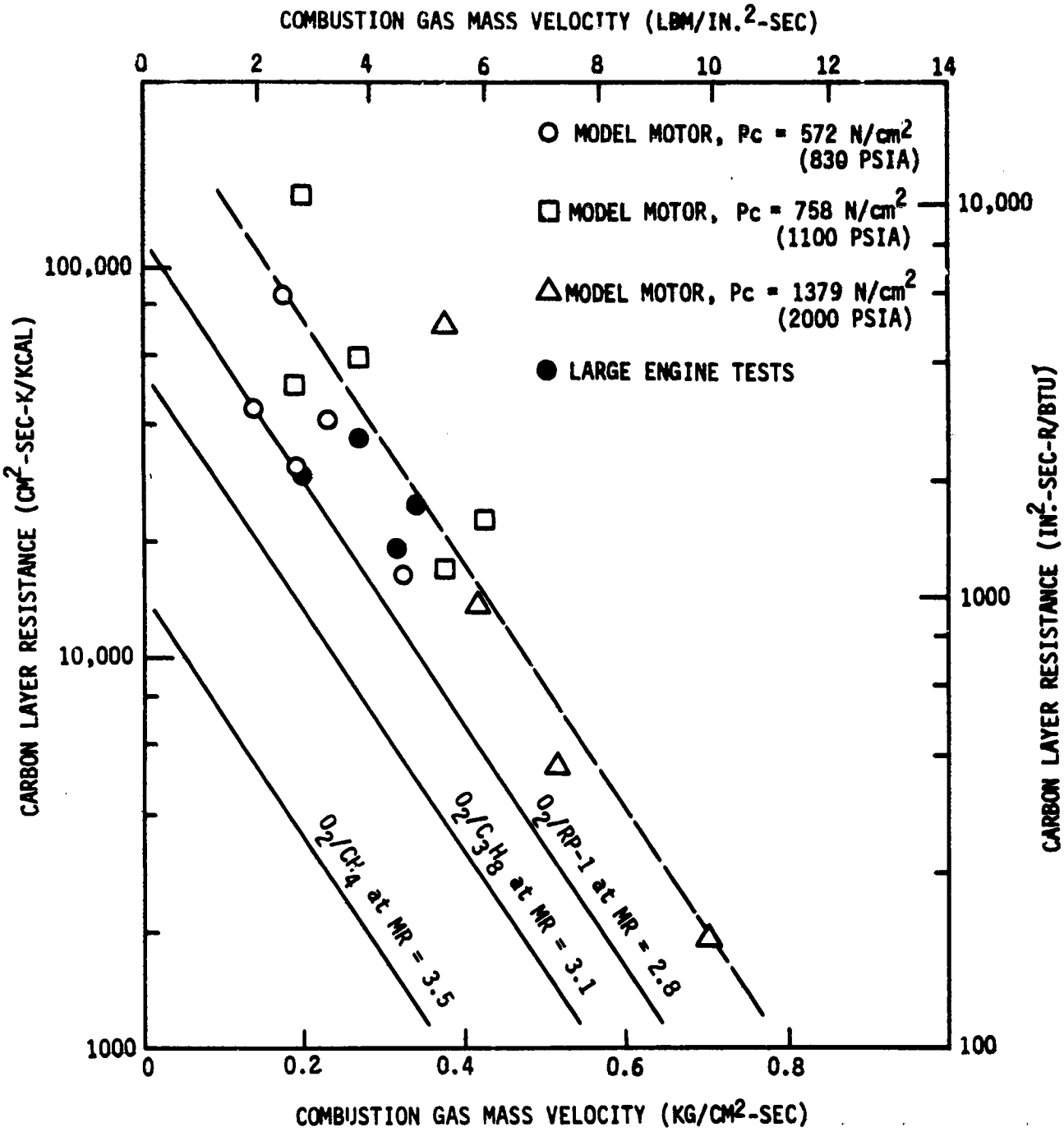

Figure 43. Carbon Layer Resistance Correlations

This equation was used to predict soot layer resistance for the calorimeter chamber. In addition, the total thermal resistance (defined as the combined resistance of the hot-gas film, the wall, and the coolant film) for a number of locations on the chamber was calculated from the test data. The results are given in Figure 44. They show that, with the exception of a very small region by the throat, the predicted resistance for the soot layer is significantly greater than the experimentally determined total wall resistance. Obviously, if there is any soot barrier at all, its resistance is substantially less than predicted.

There may be a very good reason for the experimental data from this program being at variance with the soot resistance correlation and the data from other programs. The soot resistance correlation is largely, and perhaps entirely, based on results obtained from engines with fuel film cooling. The same statement can be made relative to the sooting experience of other programs. The results of this program, however, were obtained without any film cooling although the patterns were designed to provide a fuel-rich orientation at the wall. Consequently, the environment at the wall in this program was likely to be less fuel-rich than that of the early programs, with less soot anticipated. More importantly, the results of this program show the wall flux to be very mixture-ratio-sensitive. The introduction of fuel film cooling could be expected to produce a significant reduction in heat flux, part of which might correctly or incorrectly be attributed to soot resistance.

F. COMBUSTION STABILITY

The investigation of combustion stability was not a primary objective of this program. Rather, the intent was to achieve stable combustion so that valid performance and heat transfer data could be obtained. As a result, no bomb testing was undertaken during the program and there were no tests designed to assess stability margin. If an instability was encountered, the goal was to eliminate it as expeditiously as possible.

1. Test History

A listing of the combustion stability results from the entire program is given in Table VI. The hardware assembly and the location and shape of the acoustic cavities are illustrated in Figures 8 and 9. High-frequency instrumentation was used on every test, and the data were reviewed to provide a stability assessment of each firing. The only mode of instability observed during the program was the first tangential (1-T). Both the TLOL-1200 and TLOL-2000 were unstable in this mode. The observed 1-T frequency was in the range of 3700 to 4400 Hz, which is essentially equal to the analytically predicted 1-T frequency for these chambers. The PAT-2000 injector was found to be stable in all modes in all tests.

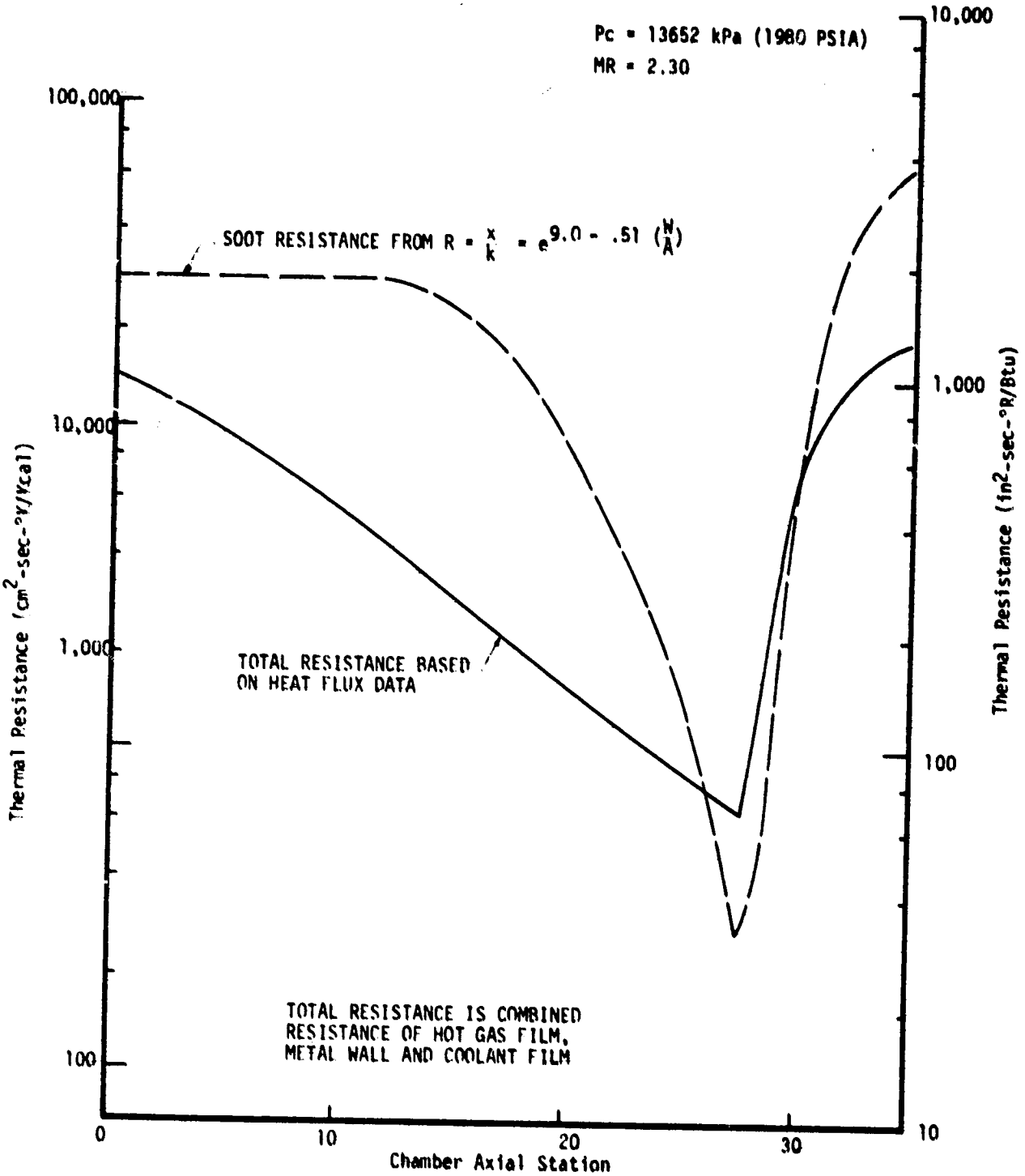

Figure 44. Comparison of Measured Total Resistance and Predicted Soot Resistance

IV, F, Combustion Stability (cont.)

The stability history of the TLOL-1200 indicates it to be very marginal from a stability viewpoint. Seemingly small changes in configuration or operating conditions could move it from stable to unstable. The first test (Test 040) with this unit resulted in a spontaneous 1-T instability 0.4 seconds into the firing. The acoustic cavity configuration for this test consisted of 6 1.78-cm (0.7-in.) deep 1-T cavities and 6 0.0 cm (0.0-in.) deep 2-T cavities. (The cavity depths are measured from the injector face plane.) The total cavity open area on this and all other tests was nominally 33% of the injector face area. Following the 1-T instability on Test 040, the resonator was retuned to 2.03 cm (0.8 in.) deep (6 cavities) and 0.51 cm (0.2 in.) deep (6 cavities). This retuning was undertaken to achieve better 1-T damping. With the retuned cavities, the next 2 tests (046, 047) with this injector were stable.

The TLOL-1200 was tested later (Test 073) with the 27.9 cm (11 in.) long NASA water-cooled chamber, the cooled resonator, and hot fuel. The water-cooled resonator had been machined to provide 8 1-T cavities which were 2.03 cm (0.8 in.) deep and 4 2-T cavities 0.51 cm (0.2 in.) deep. This configuration had been selected for two reasons. First, the cavity depths were consistent with those which had previously been successful on Tests 046 and 047. In addition, biasing the number of cavities in favor of 1-T (i.e., 8 1-T, 4 2-T vs 6 1-T, 6 2-T) appeared reasonable in light of the apparent sensitivity of the TLOL injectors to the 1-T mode. Test 073 was a long-duration, multi-data-point firing. After almost 16 seconds of stable operation, the TLOL-1200 went into a 1-T instability while running at a mixture ratio of 2.6. Earlier in the test, it had operated stably at O/F's of 2.5, 2.7, and 3.1. It was not apparent what the cause of the instability might have been. As this was the first test of the TLOL with heated fuel, the use of heated fuel was considered to be a significant factor contributing to the instability. Other possible factors were the slightly different geometry of the cooled cavities relative to the uncooled cavities and the use of the 27.9 cm (11 in.) chamber.

Test 074, also with the TLOL-1200 injector, was a repeat of the unstable Test 073 but with 311°K (100°F) fuel and the 37.5 cm (15 in.) NASA chamber. This 30-second duration test was stable.

Test 075 was a repeat of Test 074 but with the 27.9 cm (11 in.) NASA chamber and 294°K (70°F) cooler fuel. The injector went unstable 16 seconds into the firing as the mixture ratio was being lowered from 2.8. Although the TLOL-1200 was in good condition at this point, it was not fired again due to the almost random character of the instabilities. It would appear that even in those tests which were stable, the TLOL-1200 must have had a minimal margin of stability in that the differences between stable and unstable operating conditions were small. Bomb testing with a variable tune resonator would be recommended to establish a stable operating configuration and determine the limits of stability with that configuration.

The TLOL-2000 injector did not operate stably. It was tested 4 times and went into a 1-T instability each time the design chamber pressure was reached. Perhaps the most striking result with this injector was the difference in outcome between Tests 057 and 059. In Test 057, there was a problem with the combustion stability monitor which allowed the engine to operate for more than 4 seconds at 12,548 kPa (1820 psi) with a well-developed 4137 kPa (600 psi) peak-to-peak 1-T instability. There was no visible hardware damage on this test. Test 059 was run with the same hardware, operated unstably for 0.3 sec, and produced very severe injector face erosion. The only significant difference between these tests was engine O/F. Test 057, which produced no hardware damage, was run at an O/F of 2.4, while Test 059, which produced the face erosion, was at an O/F of 2.8.

2. Observations

Based on the combustion stability design analyses and the post-fire data analyses, the following observations have been made:

(a) The PAT pattern was stable. In the limited stability testing conducted during the program, the stability of the TLOL-1200 was improved and a marginal stability condition was achieved by a cavity retune.

(b) The experimentally observed value of the combustion pressure interaction index (n) is higher than had been predicted on the basis of historical data.

n Predicted = 0.66

n Experimental = 0.72

(c) The experimentally observed values of sensitive time lags are larger than had been predicted. One possible cause which has been hypothesized for the large delay times is slower than predicted initial droplet vaporization rates resulting from lower than stoichiometric gas temperatures near the injector. The predicted and observed time lags are as follows:

Injector	Original Prediction	Experimentally Observed
TLOL-1200	τ_{ox} = 0.044 ms	$\tau \approx$ 0.135 ms
	τ_f = 0.087 ms	
TLOL-2000	τ_{ox} = 0.041 ms	$\tau \approx$ 0.135 ms
	τ_f = 0.101 ms	
PAT-1200	τ_{ox} = 0.041 ms	Not Determined
	τ_f = 0.067 ms	
PAT-2000	τ_{ox} = 0.031	Not Determined
	τ_f = 0.052	

(d) The experimentally observed 1-L stability agreed fairly well with the prediction for the TLOL injector but poorly with that for the PAT injector. A comparison of the predicted and measured 1-L stability results is given in Table XII. During the start transient, the injectors generally passed through a short period of 1-L instability as they were coming up to the steady-state chamber pressure. The pressure at which the 1-L instability ceased was used to define the boundary between stable and unstable operation as given in the table. A 1-L stability analysis was conducted by ALRC on an OFO triplet LOX/RP-1 injector which was being tested by NASA/LeRC 4137 kPa (600 psia) at the time of this program. The results of that analysis and test program are also given in the table.

G. DATA APPLICATION

The intent of this program was to extend the technology base of LOX/RP-1 to higher pressures. In several areas the experimental results were considerably different from what had been anticipated in the design phase. Although this new data base is relatively narrow and perhaps strictly valid only for the specific hardware tested it still should be considered in subsequent high pressure LOX/RP-1 design activities. The following two subsections present modifications to the injector and chamber design procedures which would be recommended based on the results of this program.

1. Recommended Injector Design Analysis Procedure

Based on the results of this program the first two steps in the injector design analysis (i.e., determination of the reference drop size and the injecjtor induced mass and mixture ratio distribution) would remain unchanged. The modifications suggested by the data from this program show up in the vaporization analysis.

TABLE XII. - COMPARISON OF PREDICTED AND MEASURED 1-L STABILITY

INJECTOR	L' cm (in)	PREDICTED STABILITY	MEASURED STABILITY
TLOL - 1200	37.6 (14.4)	Stable Above Pc = 5516 kPa (800 psia)	Stable Above Pc = 6481 kPa (940 psia)
TLOL - 1200	40.1 (15.8)	No Prediction	Stable Above Pc = 5723 kPa (830 psia)
TLOL - 2000	40.1 (15.8)	Unstable At Pc = 13790 kPa (2000 psia)	Stable Above Pc = 12066 kPa (1750 psia)
PAT - 2000	30.0 (11.4)	Stable At Pc = 13790 kPa (2000 psia)	Stable Above Pc = 9653 kPa (1400 psia)
PAT - 2000	39.1 (15.4)	Unstable	Stable
NASA-OFO 4137 kPa (600 psia)	40.6 (16)	Stable	Stable
	55.9 (22)	Unstable	Unstable

IV, G, Data Application (cont.)

Prior industry analysis practice has been to evaluate the axial chamber droplet vaporization for either just the mass median droplet diameter or for a drop size distribution, but only at the overall injector mixture ratio. This program indicated that in addition one should also consider the simultaneous effects of the initial injector face mixture ratio variation and the axial mixing rate distribution. Thus the droplet size distribution must have its vaporization profile predicted within the most fuel rich stream tube mixture ratio and the most oxidizer rich stream tube mixture ratio at the injector face plane as well as the overall injector O/F. The 3-D Combust subroutine in the JANNAF SDER reference computer program should account for this effect but most users have had technical difficulties operating this subprogram. In lieu thereof, it is recommended that the Stream Tube Combustion (STC) subroutine be run successively at the 3 different zone mixture ratios above. The consequence of this analysis is that the fuel droplet in the oxidizer rich stream tube and the oxidizer droplet in the fuel rich stream tube vaporize at rates comparable to the fuel and oxidizer droplet vaporization rates in the stoichiometric (overall) mixture ratio stream tube. In these cases the opposite propellant vapors are present in sufficient quantity to provide a near stoichiometric gas temperature surrounding each droplet. The simplified Priem Generalized Length model was used to predict these droplet vaporization rates. However, it is hypothesized that the fuel droplets in the most fuel rich stream tube and the oxidizer droplets in the most oxidizer rich stream tubes encounter non-reactive self insulating diluent mixture ratios whose flame temperatures are significantly lower than stoichiometric. To account for this in the analysis, the real fuel droplet vaporization rates are adjusted downward by

$$\frac{d\,\dot{W}_{VAP}\ (RP\text{-}1)}{dx} = \frac{d\,\dot{W}_{VAP}\ PRIEM}{dx} \times \left[\frac{T_g\ (O/F)_{fuel\ rich} - T_{crit,\ RP\text{-}1}}{5000°R - T_{crit,\ RP\text{-}1}}\right]$$

This adjustment reduced the head end vaporization rate as shown in Figure 45 and provided a good fit of the experimental data. There is no proof that this is the only plausible combustion mechanism possible but it did provide the best differential performance correlation between the short and long chambers. Similarly, substituting LO_2 properties in the most oxidizer rich stream tube reduced the oxidizer vaporization rate compared to similar drop sizes in the stoichiometric or fuel rich streamtubes. However, due to the extreme volatility of cryogenic LO_2, it merely increased the 100% oxidizer vaporization chamber length from half the shortest chamber length to 80% of the shortest chamber length tested. Thus the reduced oxygen droplet heat flux reduced the oxidizer vaporization rate in the oxidizer rich streamtube in the forward end of the chamber but had no net effect upon the throat plane vaporization performance. Such was not the case for the RP-1.

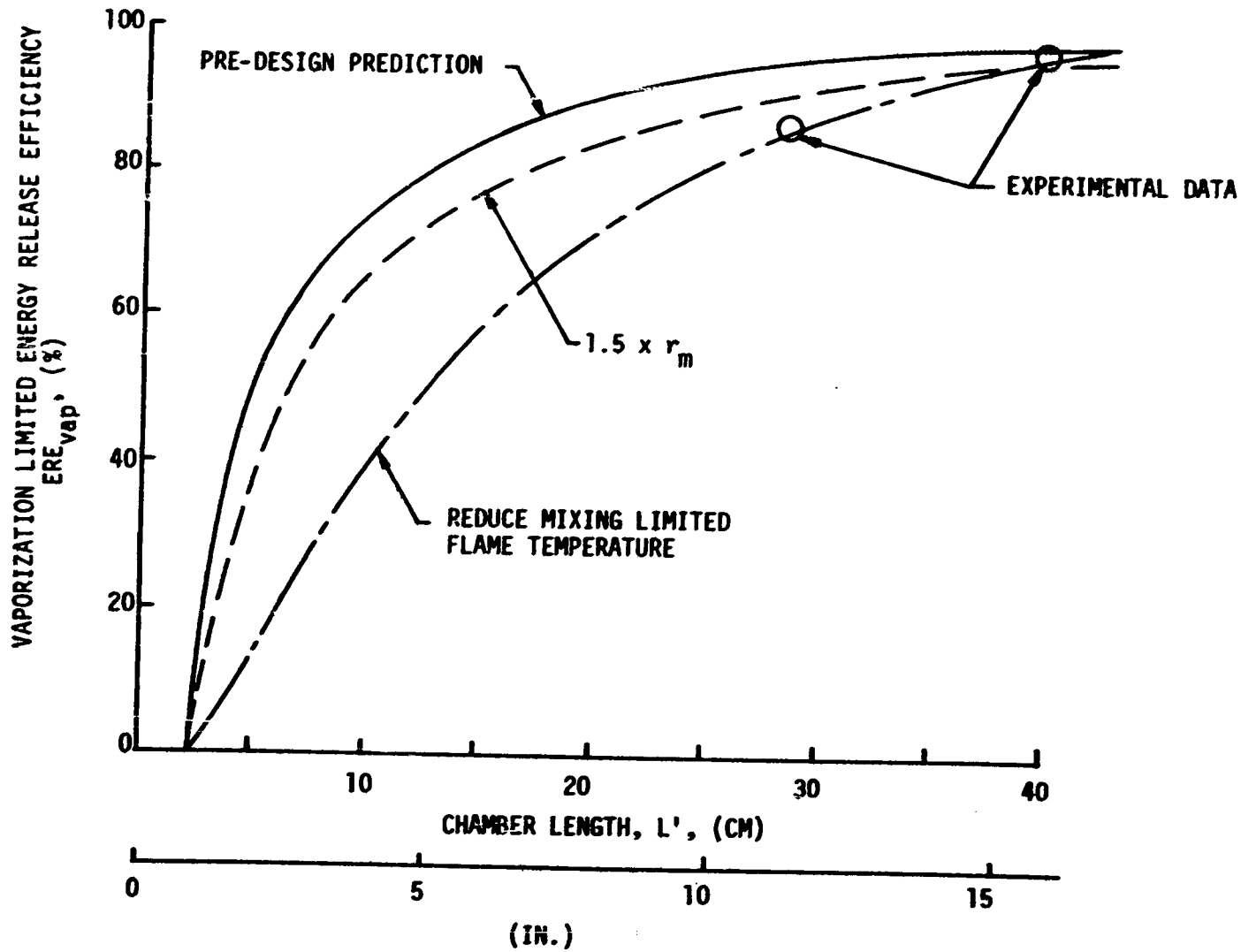

Figure 45. Various Mechanisms were Initially Hypothesized to Rationalize the Low Experimental Fuel Vaporization Efficiency

The most complicating feature of the above recommended vaporization procedure is that the axial stream tube mixture ratio distribution does not remain constant but is a function of the axial mixing rate. The axial mixture ratio profile was determined by comparing the measured heat flux with the predesign prediction and by looking at the throat heat flux corrected for chamber cross sectional area. The axial mixture ratio profile was used to calculate the fuel rich stream tube mixture ratio ($E_m \times (O/F)_{overall}$) and the oxidizer rich stream tube $[(O/F)_{overall}/E_m]$. The E_m profile for the PAT-2000 injector is shown in Figure 46. It is recognized that few programs have calorimeter chamber heat flux data available for determining mixing profile. No analytical models are readily available which are known to accurately predict mixing profiles as a function of design variables or operating parameters. One might consider using available fuel film cooling entrainment models, gas/gas mixing model, eddy viscosity or turbulent kinetic energy mixing models. On severely cost limited design programs, it may be necessary to simply assume a linear increase starting from zero at the injector face to a limiting E_m value (not to exceed 1.0) at the nozzle throat plane.

Having thus predicted the fuel and oxidizer vaporization efficiencies at the nozzle throat plane and the throat E_m mixing parameter the injector energy release performance efficiencies are calculated in the usual manner.

2. Recommended Chamber Design Analysis Procedure

An important factor which must be considered in the thermal design is the makeup of the gas in contact with the wall. The fuel-rich barrier observed in the present tests can be represented for future predictions using the film cooling model of Rousar and Ewen. This model characterizes mixing between the barrier and core flows in terms of an entrainment fraction (defined as the ratio of the mass flux added to the mixing layer to the core axial mass velocity). If the initial barrier mixture ratio is assumed to be 10 percent of the overall mixture ratio and the barrier fuel flow is 20 percent of the total fuel flow*, a cylindrical section entrainment fraction is in excellent agreement with the data presented by Rousar and Ewen. The remainder of Figure 41 can be used to infer an entrainment fraction profile for the convergent section as shown in Figure 47. The increased mixing rates associated with the interaction of the outer row of elements with the converging wall is readily apparent in this figure.

*The fuel flow in the peripheral fuel orifices is 2.5 percent of the total, but that part avoiding spray overlap with the oxidizer is about 19 percent of the total fuel flow.

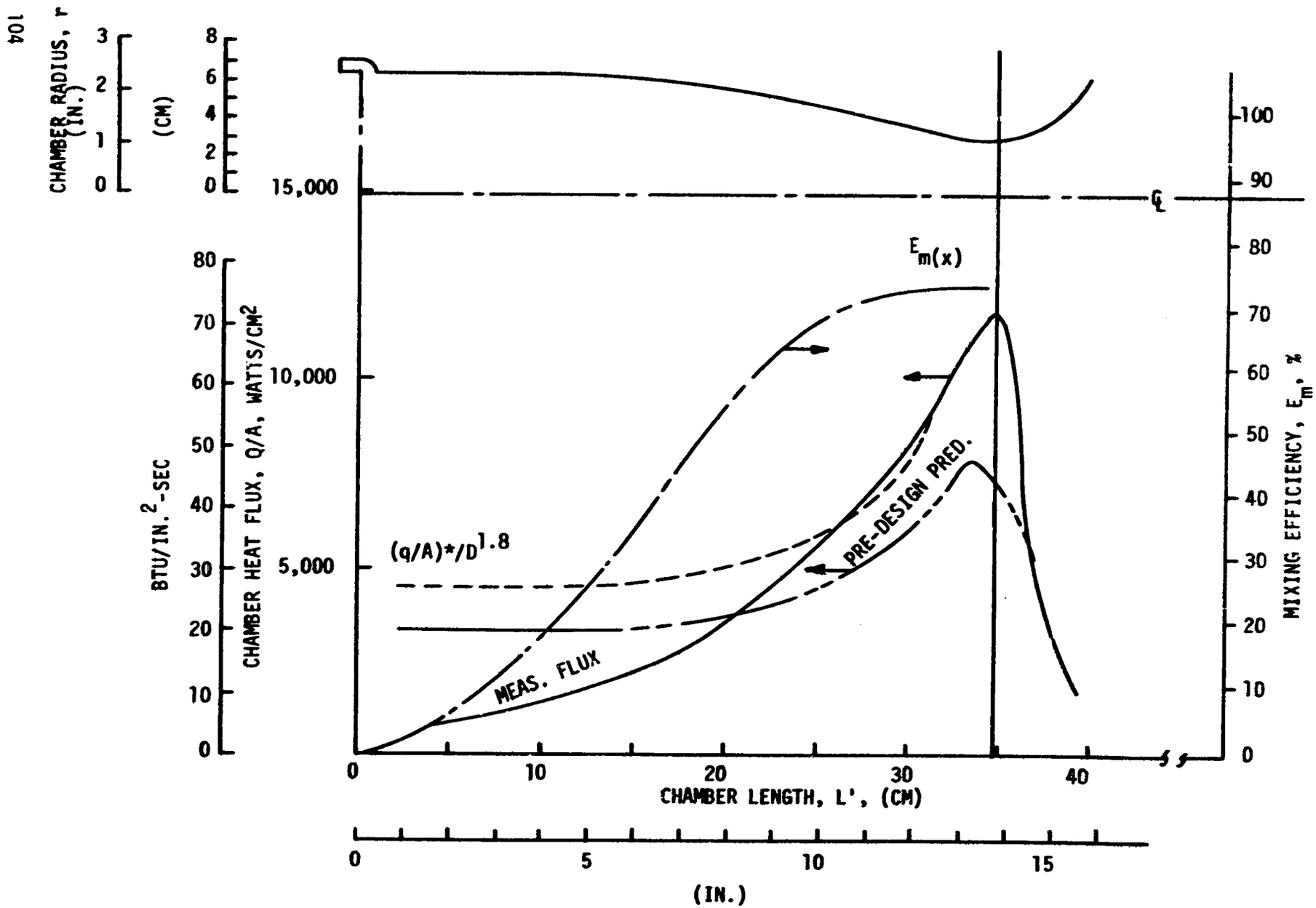

Figure 46. Calorimeter Data Provided Essential Physical Insight which Explains LOX/HDF Combustion Anomalies

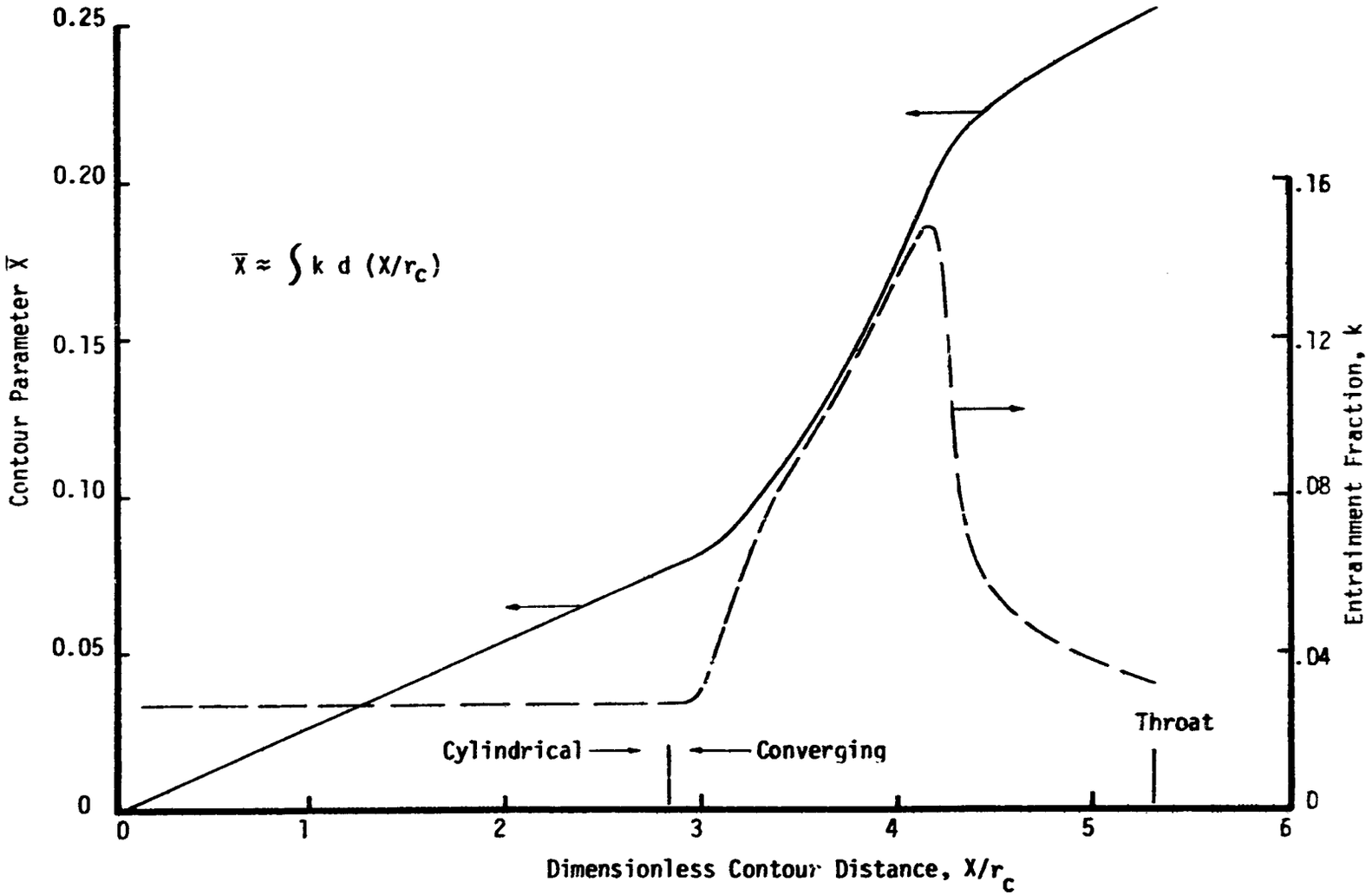

Figure 47. Film Cooling Model Mixing Parameters

IV, G, Data Application (cont.)

The wall mixture ratio is defined in terms of the film coolant effectiveness η as

$$MR_w = \frac{1 + 1.225\ MR}{1 + \eta\left(\frac{1 + 1.225\ MR}{1 + 0.1\ MR} - 1\right)} - 1$$

The film coolant effectiveness is given by

$$\eta = \frac{1}{\theta\left(1 + \frac{W_E}{W_c}\right)}$$

with the shape factor θ shown in Figure 48 and the entrainment flow ratio W_E/W_c calculated as

$$\frac{W_E}{W_c} = \left[5\left(\frac{1 + MR}{1 + 0.1\ MR}\right) - 1\right]\ (2\ \bar{X} - \bar{X}^2)$$

The dimensionless contour parameter $\bar{X}$ is included in Figure 47.

Using the mixture ratio profiles defined [illegible] heat fluxes from the injector to the throat of the calorimeter chamber can be predicted as follows:

$$q/A = h_g\ [T_{aw}\ (MR_w) - T_w] \left[\frac{h_{aw} - H_w}{Cp_f\ (T_{aw} - T_w)}\right]_{\text{throat, MR}}$$

in which h_g is the conventional heat transfer coefficient defined by Equation (1) using a uniform C_g of 0.89. For steeper convergence angles a C_g profile with a flow acceleration dip is recommended. The reactive boundary layer correction in the heat flux equation is evaluated at the throat using the overall mixture ratio. Application of a local reactive correction at the wall mixture ratio does not correlate the data presumably since an equilibrium wall enthalpy is not appropriate at low mixture ratios.

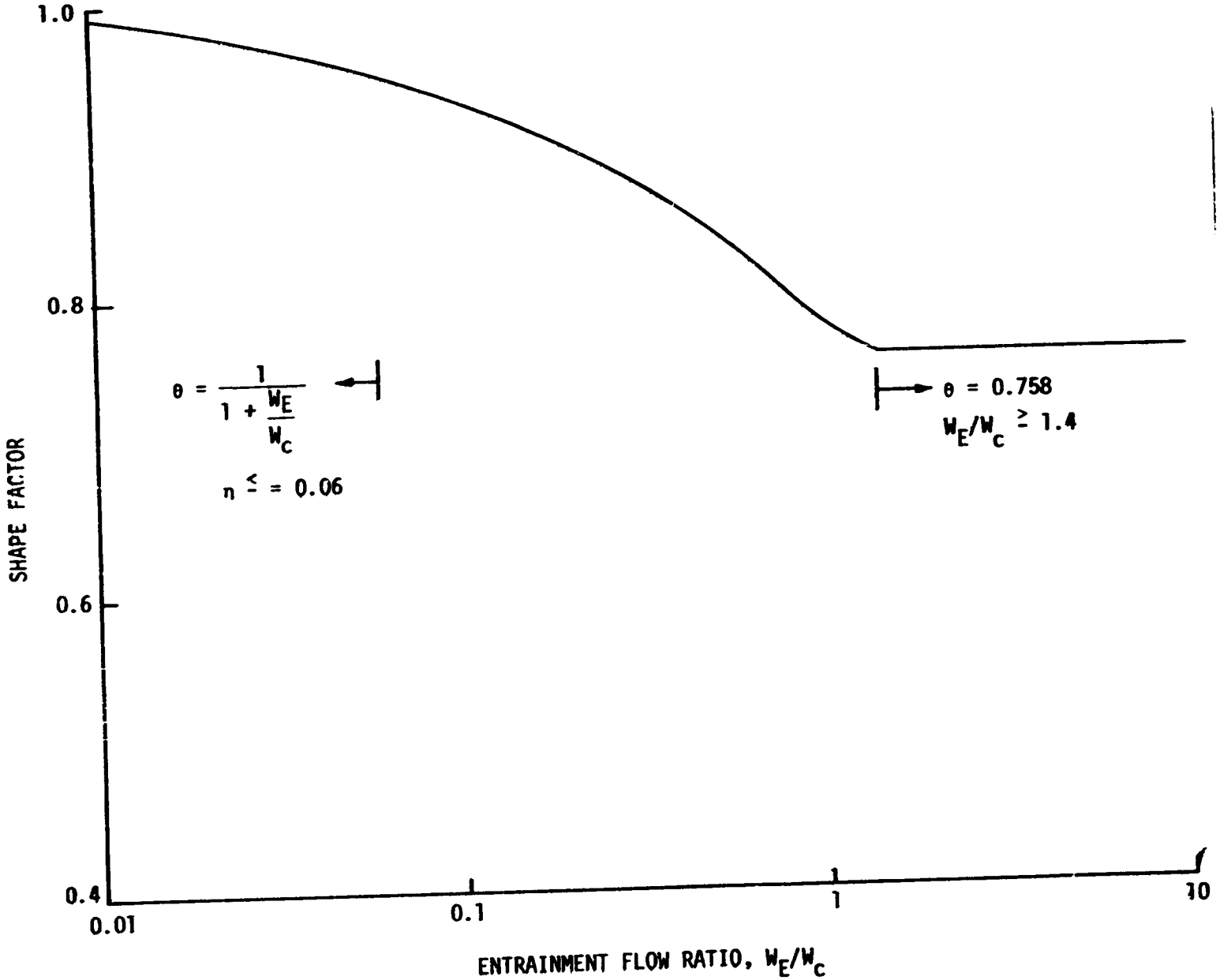

Figure 48. Mixing Layer Profile Shape Factor